2011

Advances in Fiber Reinforced Polymer Repair Incorporating Cathodic Protection

Julio Ivan Aguilar
University of South Florida, julioaguilar85@hotmail.com

Advances in Fiber Reinforced Polymer Repair Incorporating Cathodic Protection

by

Julio Ivan Aguilar

A dissertation submitted in partial fulfillment
of the requirements for the degree of
Doctor of Philosophy
Department of Civil and Environmental Engineering
College of Engineering
University of South Florida

Co-Major Professor: Rajan Sen, Ph.D.
Co-Major Professor: A. Gray Mullins, Ph.D.
Alberto Sagüés, Ph.D.
Autar Kaw, Ph.D.
Kandethody Ramachandran, Ph.D.

Date of Approval:
November 9, 2011

Keywords: Underwater Repair, Fiberglass, Underwater Epoxy, Embedded Anodes, Remote Monitoring

Dedication

To my parents, who told me to go as far as I wanted.

Acknowledgements

I would like to thank my Major Professors, Dr. Rajan Sen and Dr. Gray Mullins, and my committee members, Dr. Alberto Sagüés, Dr. Autar Kaw, and Dr. Kandethody Ramachandran for all of their guidance throughout the formation of this dissertation. I would also like to thank all of the funding agencies: NCHRP's IDEA program, Hillsborough County, Vector Corrosion, Fyfeco, Air Logistics, and the Florida Department of Transportation for making this possible.

I would also like to personally acknowledge every member of the Structural Research group at the University of South Florida: Mr. Danny Winters, Dr. Mike Stoke, Dr. Kingsley Lau, Mr. Jonathan Collins, Mr. Purvik Patel, Mr. Raymond Penn, Mr. Vladimir Simonovski, Mr. Jonathan Gill, Mrs. Whitney Maynard, Ms. Nicole Pauly, Mr. Christopher Alexander, Mr. James Appler, Mr. Deon Burton, Mr. Peter Martin, Mr. Miles Mullins, Mr. Kyle Yeasting, Mr. Kevin Johnson, Mr. Jordan Ekhlassi, and Mr. Mathew Durshimer.

Finally, I'd like to thank Ms. Mersedeh Akoondan for her irreplaceable help at a critical stage.

Table of Contents

List of Tables

List of Figures

Abstract

This dissertation presents findings from two disparate research projects relating to the cathodic protection (CP) of piles supporting bridge elements. The first was a proof of concept study for developing a new hybrid pile repair system incorporating embedded sacrificial zinc anodes within a fiber reinforced polymer (FRP) wrap. The second was to develop and remotely monitor the performance of magnesium anodes protecting steel H-piles supporting two bridges in Florida.

The hybrid FRP-CP system involved a proof-of-concept laboratory study to refine pressure / vacuum bagging systems for pile repair and to quantify the improvement in the FRP concrete bond. Two different FRP systems, one epoxy based and the other urethane based, were evaluated. Improvement in bond was determined through destructive pullout tests conducted on full-size pile specimens that were wrapped while partially submerged in a fresh water tank. The results showed that pressure led to significant improvement in FRP-concrete bond. Pressure was optimal for the epoxy-based system, while vacuum proved better for the urethane-based system. The pressure system was subsequently used to install FRP over embedded anodes in a field demonstration project where four corroding piles were repaired using the hybrid FRP-CP system. Cathodic protection was provided by embedding eight zinc anodes in each concrete pile. Protection below the water line was provided by bulk anodes. Reference electrodes were installed to monitor the performance of the CP system and data loggers were used to monitor the anodic current. Results from over 12 months of monitoring showed that the hybrid FRP-CP

system worked and the current demand of the steel was lower in the FRP wrapped piles compared to the unwrapped control.

Numerical simulations were carried out to determine how the hybrid FRP-CP system could be improved. Initially the investigation focused on determining if bulk anodes alone could be used to provide the required protection. Results showed that while bulk anodes were more effective in FRP wrapped piles, they could not provide adequate protection over the entire splash-zone. In view of this, a preliminary three dimensional finite element analysis was carried out using commercially available software. The analysis showed that anode strips embedded in the pile just beneath the surface may provide adequate protection. Such anodes would be easier to install and are an improvement over the system investigated.

The second project involved the development of a remote monitoring system to assess the performance of a sacrificial anode cathodic protection system used for steel piles on two bridges along I-75 in Florida. The problem was the inexplicable consumption rate of the magnesium anodes. Commercially available systems and sensors were used to successfully monitor the environment and the anodic current of the CP system for over 12 months. A solution for the excess magnesium consumption was proposed through the incorporation of an in-circuit variable resistor that could regulate the current draw from the anode. The system was implemented but its performance will be monitored by the Florida Department of Transportation who assumed responsibility for the equipment. Initial results were promising.

1 Introduction

The damage caused by corrosion is estimated to have a direct cost on the domestic economy of 3% of the gross national product and up to 5% abroad [1.1]. Some have estimated that the indirect cost due to loss of productivity can be upwards of ten times that amount. This was exemplified in 2007 when the I-35W bridge over the Mississippi river collapsed in Minneapolis, MN killing thirteen and costing over $400,000 per day until it was rebuilt and reopened 13 months later [1.2]. Many of the problems plaguing the global infrastructure are due to either poor construction practices or by simply ignoring the potential for corrosion damage at the time of construction. Unfortunately, corrosion is a process which takes decades to occur, therefore by the time the problem is evident, preventative measures are not applicable.

When corrosion occurs on large engineering structures, e.g. bridges and large buildings, there is even greater concern, as there are issues of public safety and cost which must be addressed. Often these structures are of such high importance that demolition is unacceptable and replacement is impractical. The result of this is that repair measures must be undertaken in an attempt to extend the usable service life of these structures.

The most problematic form of corrosion addressed by civil engineers is electro chemical corrosion, whereby structural steel is eroded by chemical reactions, resulting in a reduced cross sectional area and therefore a reduction in the capacity of the structure. This dissertation is focused primarily on chloride induced corrosion of steel in concrete,

and advances in the means of repairing and extending the usable service life of these structures.

When chlorides penetrate concrete and corrode the steel reinforcement, the resulting product (rust) expands to approximately six times the original volume. This generates tension in the concrete and eventually leads to cracking and then spalling. Traditionally, this is addressed by the "chip and patch" method, whereby all loose concrete is removed and the section re-formed with new concrete to cover the affected areas. Unfortunately, by the time cracking and spalling have occurred, the chlorides have usually penetrated far beyond the location of the reinforcement and therefore will continue to corrode the structure after it has been repaired.

The poor performance of the chip and patch method (which can fail in as little as two years) has sparked renewed interest in fiber reinforced polymers (FRP) for structural repairs over the past decade. The high strength and corrosion resistance of FRP has made it an ideal material for replacing the strength lost to corrosion. When a concrete element is repaired with FRP, it has the potential to perform as well - if not better - than the original structure, provided there is adequate bond between the FRP and the concrete. Additionally, if bonded correctly, the FRP can act as a barrier layer, preventing the further intrusion of chlorides and limiting the availability of oxygen needed for the chemical corrosion process.

While FRP does have the ability to reduce the rate of corrosion, it is unable to prevent it once it has initiated. The only proven means of achieving this is cathodic protection, where electrons are provided to the reinforcement, either through an impressed current or by sacrificial means from another metallic element.

This dissertation is a compilation of five independent studies that were performed regarding the repair or maintenance of bridge substructure elements. Because of this, there may be several instances where references or figures are repeated; this was done solely to maintain the ability of the works to maintain their integrity as individual projects. As a result the dissertation has been divided into six ensuing chapters that present each of the five topics and one chapter that summarizes the dissertation findings and conclusions.

Chapter 2 focuses on the overall advances made in corrosion repair using FRP for the past decade, including means of ensuring adequate bond through pressure bagging, the incorporation of cathodic protection, as well the tools and techniques used for installation.

Chapter 3 presents the findings of a laboratory study where the effects of externally applied pressure to curing FRP on concrete are documented. External pressure systems consisted of both external pressure bag and vacuum bag systems. In this chapter, the FRP-concrete bond is evaluated using both destructive and non-destructive methods, and recommendations are made as to which system should be used for bond improvement.

Chapter 4 presents a field study where a bond improved FRP system was combined with an embedded anode CP system to demonstrate how the presence of the FRP can affect the rate at which a structure is corroding.

Chapter 5 highlights the findings of a field study where a remote monitoring and control system was used to monitor CP performance while also providing logic and regulation circuitry to tailor the protection system to the environmental conditions.

Chapter 6 describes a computer model developed based on the CP system described in Chapter 3 of this dissertation. The system was compared to one that was proposed as a means of reducing the cost and therefore improving the practicality of the CP system.

Chapter 7 highlights the most significant contributions from each study undertaken.

Chapter 8 is a description of recommended future work that could be performed in an attempt to make the system even more efficient.

Finally, five appendices supply additional information pertaining to the topics discussed in the dissertation.

2 Advances in Corrosion Repair of Piles Using FRP

The poor performance of conventional chip and patch methods for repairing corrosion damaged piles has led to renewed interest in the use of fiber reinforced polymers (FRP). Over the past decade, laboratory research complemented by numerous field demonstration projects has led to improvements in the design, construction and monitoring of FRP pile repair. The two principal areas of advancement were in the development of techniques borrowed from the composites industry for improving FRP-concrete bond and in the incorporation of a sacrificial anode cathodic protection system within a FRP wrap. Both developments enhance the competitiveness of FRP pile repair. This chapter provides an overview of laboratory and field demonstration studies in recent years that led to these advancements.

2.1 Introduction

Reinforced and prestressed concrete piles are vulnerable to corrosion in tidal waters in sub-tropical regions world-wide. Despite the use of low permeability concretes, chloride ions in seawater can penetrate to the level of the reinforcement and destroy the passive layer that normally protects steel. A recent survey by the Florida Department of Transportation (FDOT) showed that only 2% of 47 "good" bridge repairs survived for more than three years [2.1].

The cost of pile repair is significant; recent data [2.2] from FDOT indicates that the cost of jacketed repairs varies from $400 to $800 per linear ft ($437-$874/m); when

repairs incorporate cathodic protection, they increase to $1,442/ft ($1,577/m) for *non-structural* and $1,728/ft ($1,990/m) for *structural repairs.* These costs do not include mobilization and other overhead charges. Thus, the total cost of the repair is much higher.

Fiber reinforced polymers (FRP) have the potential for lowering the cost of pile repair. Its lightweight, high strength and corrosion resistance presents natural advantages. In fabric form, it offers unprecedented flexibility in construction. Moreover, as fibers can be oriented as required they can provide strength in any desired direction. Numerous research studies undertaken to evaluate the performance of FRP in corrosion repair are summarized in a state-of-the-art paper [2.3]. They all demonstrated that while FRP slowed down corrosion, it could not stop it.

Over the past few years, the University of South Florida has conducted several studies to advance the use of FRP for repairing piles. Specifically, they have explored the feasibility of employing techniques such as pressure / vacuum bagging used by the composites industry for improving FRP-concrete bond [2.4-2.6]. More recently, they developed a sacrificial anode cathodic protection system that can be incorporated within the FRP [2.7] wrap. This chapter provides a brief overview of these developments and highlights some of the more important lessons learnt relating to FRP repair of partially submerged piles.

2.2 Research Significance

The high cost and the lack of durability of conventional chip and patch methods for repairing piles makes FRP an obvious candidate for conducting such repairs. This chapter highlights important advances made over the past five years that will be of

particular interest to both engineers and decision makers faced with mounting budget shortfalls compounded by deteriorating infrastructure.

2.3 Background

Piles driven in tidal waters typically corrode in the "splash zone" a region that is subjected to periodic wetting and drying. The extent of the damage is therefore a function of the actual tides that vary with geographic location. The highest is in the Bay of Fundy, Nova Scotia where tide ranges exceeding 50 ft (15m) have been observed while in some places in the Mediterranean and the South Pacific it never exceeds 2 ft (0.6 m) [2.8]. In Florida the splash zone is taken as 5.5 ft (1.7 m).

Since the FRP must be applied to a surface that is partially wet or fully submerged, special hydro-phobic resins are required. These became available in the 1990's when the first pile repair was undertaken at the SK Refinery Co. in Ulsan, Korea in 1995 [2.9]. In this application, a special epoxy resin was used to repair 20 in. (51 cm) diameter piles using two vertical and one transverse layer of glass fiber material. Trained divers were used for quality assurance. Subsequently, a urethane-based resin was developed and used for the repair of three corrosion-damaged 12 in x 12 in (30 cm x 30 cm) reinforced concrete piles supporting a bridge near Wilmington, North Carolina [2.10] in 2002. In this case too, no coffer dam construction was needed but divers were used to assure quality. In 2007, CFRP was used for the repair of partially submerged piles in Fort Lauderdale in which the same resin was used [2.11]. In 2009, 18 corroding piles supporting the Grove Island Bridge [2.12], Miami were repaired using GFRP and an

epoxy resin. In this case, the entire submerged depth of the pile was wrapped using two GFRP layers – one transverse and the other longitudinal.

Aside from these commercial applications, several demonstration research projects were also undertaken [2.13-2.15]. In these studies, piles at three different sites in the Tampa Bay area were repaired and an innovative scaffolding system used that eliminated the need for underwater divers. An important element in all these repairs was the use of instrumentation to monitor the performance of the FRP in slowing down corrosion. Data from field measurements confirmed laboratory findings that FRP slowed down the corrosion rate [2.15]. The findings also showed that the FRP-concrete bond in these repairs was dependent on the type of resin. In general, bond was better with epoxy resins [2.6].

While the confirmation that FRP slowed down corrosion was encouraging, studies were undertaken to determine if a sacrificial anode cathodic protection system could be incorporated within the FRP wrap. Such a development would allow FRP systems to compete effectively against comparable Life Jacket systems incorporating cathodic protection [2.16].

2.4 Improving FRP-Concrete Bond

Research [2.17] has shown that the effectiveness of FRP in corrosion repair is contingent on the FRP-concrete bond. Advice on "good" bond is given in the ACI 546 guide [2.18] for the selection of repair materials. Though intended for materials used to repair concrete, its recommendations are equally valid for FRP since it performs a similar function. According to these guidelines, direct tension bond values below 100 psi (0.69

MPa) “most likely indicate a serious problem with the repair material bond” while values approaching 200 (1.4 MPa) are comparable to the tensile strength of the concrete substrate and set a limiting value. A tensile bond value of 150 psi (1.05MPa) was suggested as representative of good bond.

Surface preparation is the key to good bond. However, even if the recommendations in guidelines [2.19] are met, bond can be poor unless there is continuous, intimate contact of the saturated FRP material and the substrate during curing. Such contact may be lost in repairs involving vertical elements such as columns or the horizontal soffits of slabs, because gravity effects create tendencies for the resin-saturated FRP to separate from its concrete substrate. In the case of vertical elements, current practice is to use plastic shrink wrap (Fig. 2.1) that is manually wrapped over the FRP repair. Normal stresses introduced by this process create frictional resistance that opposes downward movement due to its weight. However, tests[4] have shown that bond is variable possibly because of non-uniformity in the normal pressures induced by the shrink wrap (Fig. 2.2).

Figure 2.1 FRP repair kept in place by plastic shrink wrap.

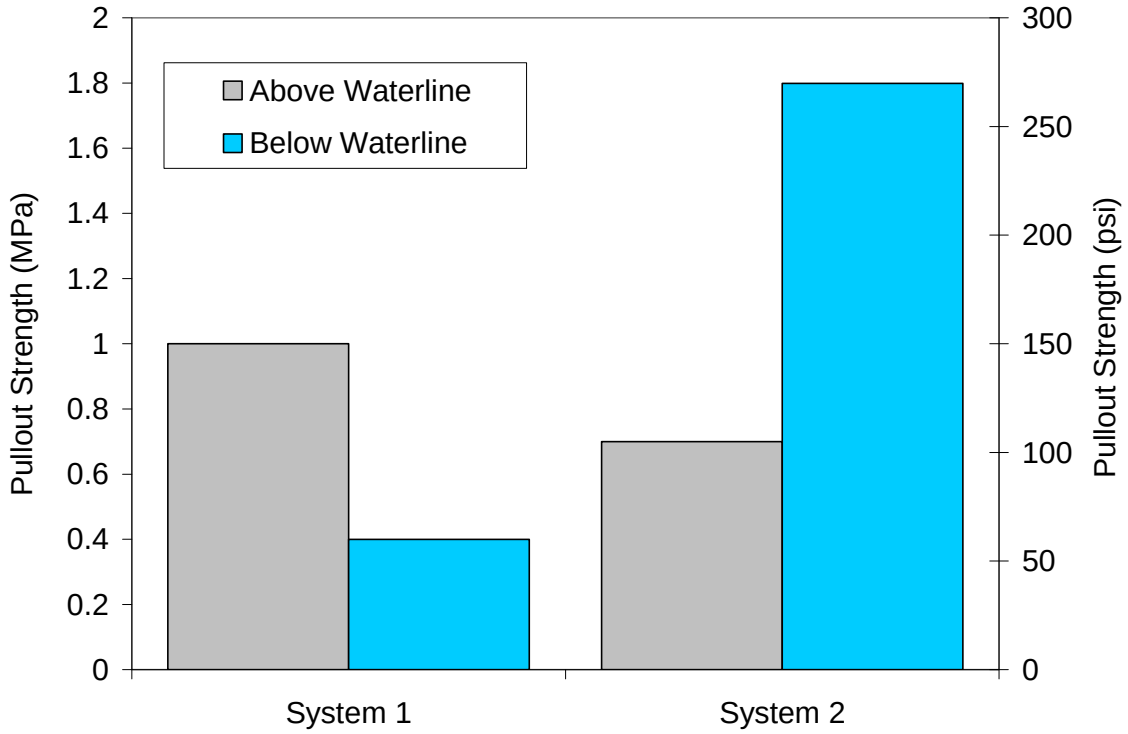

Figure 2.2 Pullout strength of stretch wrapped repair systems.

2.5 Development of Pressure Bagging for Pile Repair

Pressure bagging and vacuum bagging have long been used by the composites industry for fabricating FRP elements. Their extension for enhancing FRP-concrete bond in infrastructure applications has been limited [2.20-2.22]. Since cracked piles are in need of repair, vacuum bagging is not suitable because of the obvious difficulties in achieving an air-tight seal. Nonetheless, a prototype system was successfully developed [2.22].

2.5.1 Pressure Bagging

Pressure bagging FRP repairs for vertical elements such as piles or columns is relatively simple in concept and in application. The pressure bag is comprised of two parts, and outer bag, and an inner bag. The outer bag used in this study was made from

rubberized nylon and was 4 ft 9 in (1.45 m) long and 3 ft 9 in (1.14 m) wide (Fig. 2.3) The design incorporated double stiched edges, a zipper enclosure, cinch straps and a reinforced region for the flange.

Figure 2.3 Outer bag.

The inner bag was an air bladder created using 0.008 in (0.2 mm) thick clear PVC. The bladder was oversized to ensure full expansion when placed and inflated in the outer bag. A 144 in (3.66 m) x 54 in (1.37 m) PVC sheet was cut, folded crosswise, then glued with a 6 in (0.15 m) overlap to produce a 54 in (1.37 m) wide ring (Fig. 2.4a). The ring was then laid flat, and prior to sealing the edges, a metal flange was installed to provide a means of attaching a hose and inflating the bag (Fig. 2.4b and 2.4c). The edges were sealed, folded inward, and taped, resulting in a bag that was 69 in (1.75 m) x 54 in (1.37 m). The bladder was placed inside the outer bag and held using Velcro strips (Fig. 2.4d). The Velcro maintained the proper orientation of the bladder within the outer bag to prevent bunching prior to inflation.

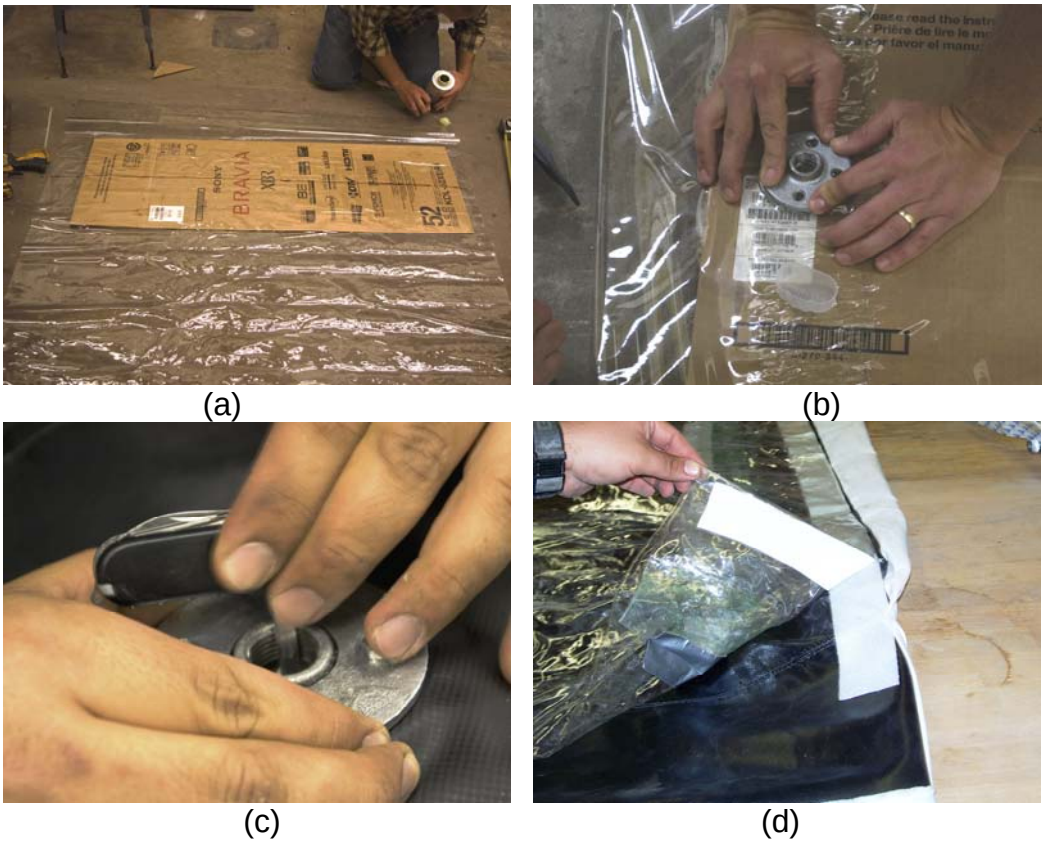

Figure 2.4 (a) 6 in overlap being glued; (b) Flange being installed; (c) Pressure bag being cut in location of flange; (d) Attaching internal bladder with Velcro.

2.5.2 Application of Pressure Bagging for Pile Repair

The effectiveness of pressure bagging in underwater pile repair using FRP was tested in a laboratory experiment using six, 12 in (0.305 m) square pre-stressed concrete piles (2 controls, 4 pressure bagged). The piles were placed in a tank which was partially filled with water so that half of the wrapped region would be completely dry, and the other half submerged. Figure 2.5 shows a pressure bag applied to a laboratory specimen.

Figure 2.5 Pressure bagged pile.

2.6 Results of Pressure Bagging for Pile Repair

Two different FRP systems were evaluated, an epoxy-based and an urethane-based system. In both cases, two glass layers were used and placed using two different schemes. In system 1, the first FRP layer was positioned longitudinally and the second layer wrapped transversely over it; in the second system, both layers were placed transversely.

Pullout tests were conducted using an Elcometer 106 adhesion tester. After the resin had completely cured, the specimens were removed from the tank and pullout testing conducted at node points on a 3 x 12 grid drawn on the FRP surface. Thus, a total

of 36 tests could be conducted on a particular surface - 18 related to the completely submerged section and 18 for the section that was completely dry. With six specimens, it was therefore possible to conduct a maximum of 216 tests. The actual number was fewer because the wrap surface near the bottom was uneven in places. As a result, a total of 210 tests were conducted. The results of the pullouts tests are shown in Figures 2.6 and 2.7.

Figure 2.6 shows that although both scheme 1 and 2 had significantly improved bond for the dry region (111% and 194% respectively) using wrapping system 1 (1 layer transverse and one longitudinal), the urethane-based system only had a 5% increase below the waterline, compared to the 545% increase for the epoxy-based system.

Figure 2.7 shows that the application of pressure has a less dramatic effect on bond in the dry region (17% for the urethane system and 42% for the epoxy system) for system 2 in which both layers are applied transversely. However, both systems have sizeable improvements in the underwater bond (42% for the urethane and 31% for the epoxy-based system).

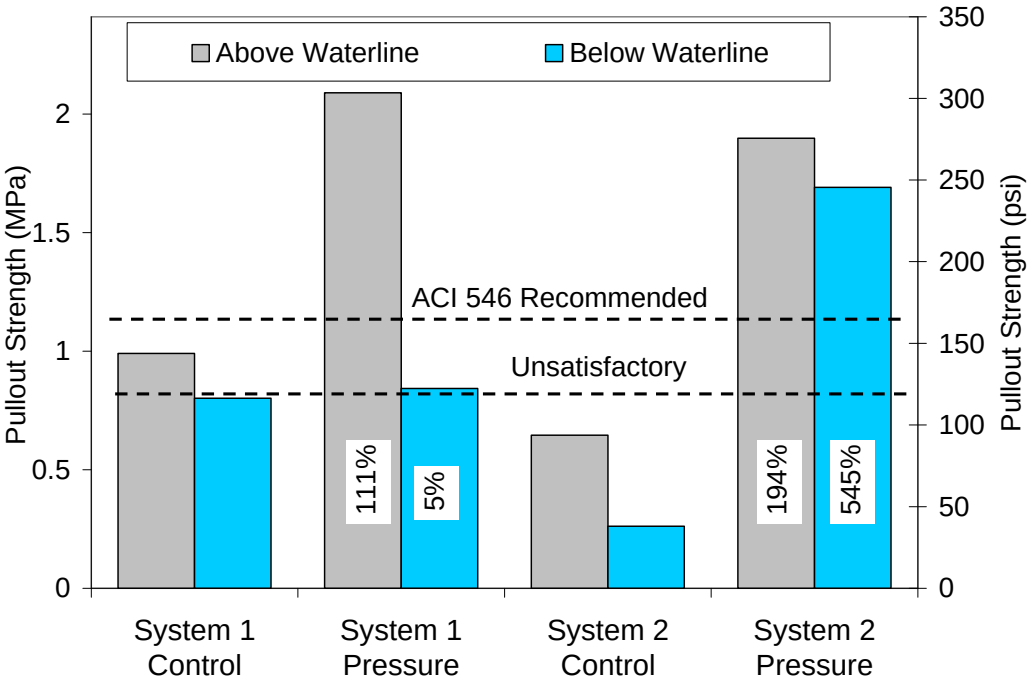

Figure 2.6 Average pullout test results for scheme 1.

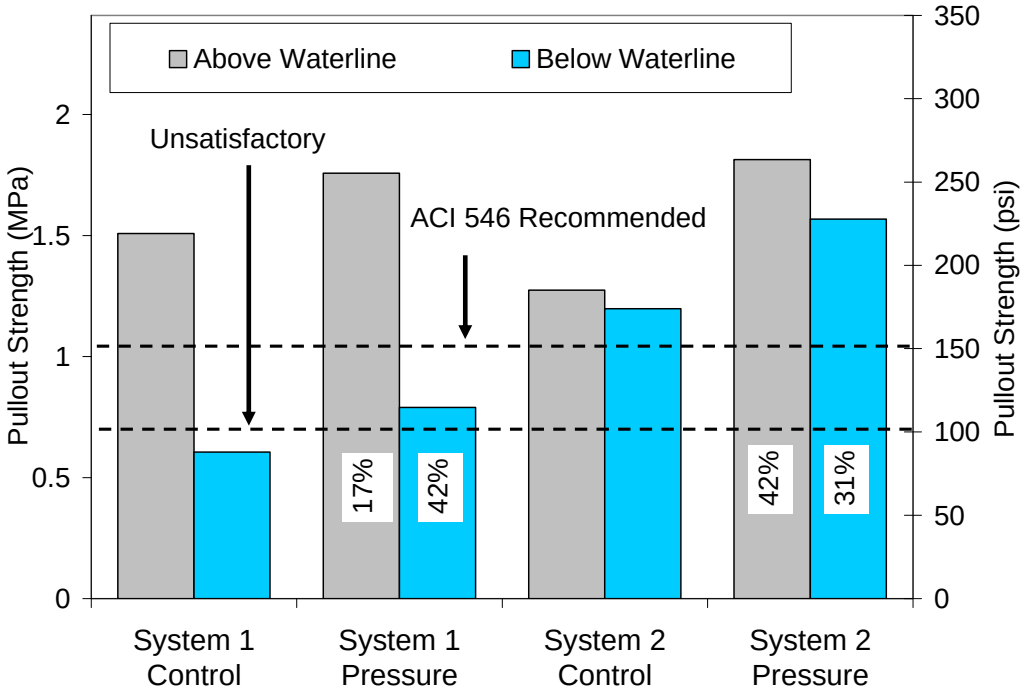

Figure 2.7 Averaged pullout test results for scheme 2.

Thus, the extent of improvement is dependent on both the type of resin and the fiber architecture. Urethane resins (System 1) discharge carbon dioxide during curing; the application of pressure displaces the gas but cannot remove it. As a result, air pockets develop that reduce bond. This is not an issue for the epoxy-based system which do not emit gases and therefore suffers no similar adverse effects from pressure.

An unexpected finding from the study was the noticeably better bond achieved using scheme 2 in which successive FRP layers are applied transversely. This is because it is easier to exert pressure during manual installation for this scheme. Thus, if external pressure cannot be used, it is best to place the FRP material in the transverse direction. In such cases, bi-directional material must be used if longitudinal strengthening is required.

2.7 Sacrificial Anode Cathodic Protection System

Cathodic protection (CP) is an electrochemical technique that is widely used to control corrosion by the offshore industry. CALTRANS was the first to use it to protect bridge structures in the early 1970's [2.23]. Subsequently, its application has extended to substructure elements [2.24]. CP is acknowledged to be the only system capable of stopping corrosion at high chloride concentrations or even when deterioration is at an advanced state.

Two methods (1) impressed current, and (2) sacrificial anode cathodic protection systems are used. In both systems a protective current is applied either from an external source (impressed current system) or by connecting the steel to a more 'active' metal that corrodes preferentially. The current density (applied current divided by the reacting

surface area of the bar) varies from 0.09-0.18 mA/ft^2 (1-2 mA/m^2) for cathodic prevention to 0.48-1.79 mA/ft^2 (5-20mA/m^2) for cathodic protection [2.25].

The sacrificial anode cathodic protection system is more suitable for marine structures because changes in concrete resistivity due to tidal cycles make it more difficult to regulate the impressed current. This can be particularly problematic for prestressed concrete structures due to the risk of hydrogen embrittlement in the high strength steel.

The effectiveness of a CP system is evaluated by the measurement of the protective current and the shift in the potential of the reinforcement in the depolarized state (when the current is temporarily stopped). This requires appropriate wiring and instrumentation that is described later.

2.7.1 Discrete Anode Sacrificial Protection System

Early attempts [2.26] to cathodically protect piles with an FRP wrap employed expanded zinc mesh anodes (Fig. 2.8) of the type developed by FDOT for their Life Jacket system. However, as the FRP is not directly bonded to the concrete surface, it cannot provide any strengthening. This problem can be overcome by using embedded anodes.

Figure 2.8 Expanded zinc anode in FRP pile repair.

In this study, special chemically-treated embedded zinc anodes were used. The chemical treatment was to ensure that they remained active [2.22] and was achieved by maintaining a high pH (14 to 14.5) environment around the zinc.

2.8 Field Demonstration

The Friendship Trail Bridge was selected for evaluating the embedded anode CP system. The piles repaired were 20 in. (0.508 m) square piles reinforced by eight #8 [25] bars. A total of five piles in two different bents (103 and 104) were part of the investigation. Baseline measurements showed that the chloride content at the level of the steel exceeded the threshold limit for corrosion of steel. This was confirmed by half-cell potential readings performed in accordance with ASTM C876 [2.27] that indicated a 90%

probability of corrosion. The performance of two of the piles, a control (104D) and a FRP wrapped pile (104 C) are the subject of this chapter. Both piles were cathodically protected in the identical manner.

Based on an assumed protective design current of 0.25mA/ft^2 (2.80 mA/m^2) it was determined that eight 0.47 lb (0.21 kg) anodes would be required to protect the steel for a 30 year design life. Additionally, a 48 lb (22 kg) bulk anode was used to protect the region below the water line. The layout of the anodes relative to the wrap and reference electrodes is shown in Figure 2.9. The anodes are positioned symmetrically over the 6 ft (1.8 m) wrap depth to ensure efficient distribution of the anodic current. A submerged bulk anode is positioned 2.5 ft (0.73 m) below the mean low water line.

2.8.1 Installation of Embedded Anodes

In an embedded FRP-CP system, the CP system has to be installed first followed by the FRP wrap. This required eight holes sufficient in length to allow horizontal placement of the 14 in. (0.36 m) long anodes. The anodes were placed in accordance with the instructions stipulated by their manufacturer. Additionally, two silver-silver chloride reference electrodes were installed in horizontally drilled holes and positioned as shown in Figure 2.9.

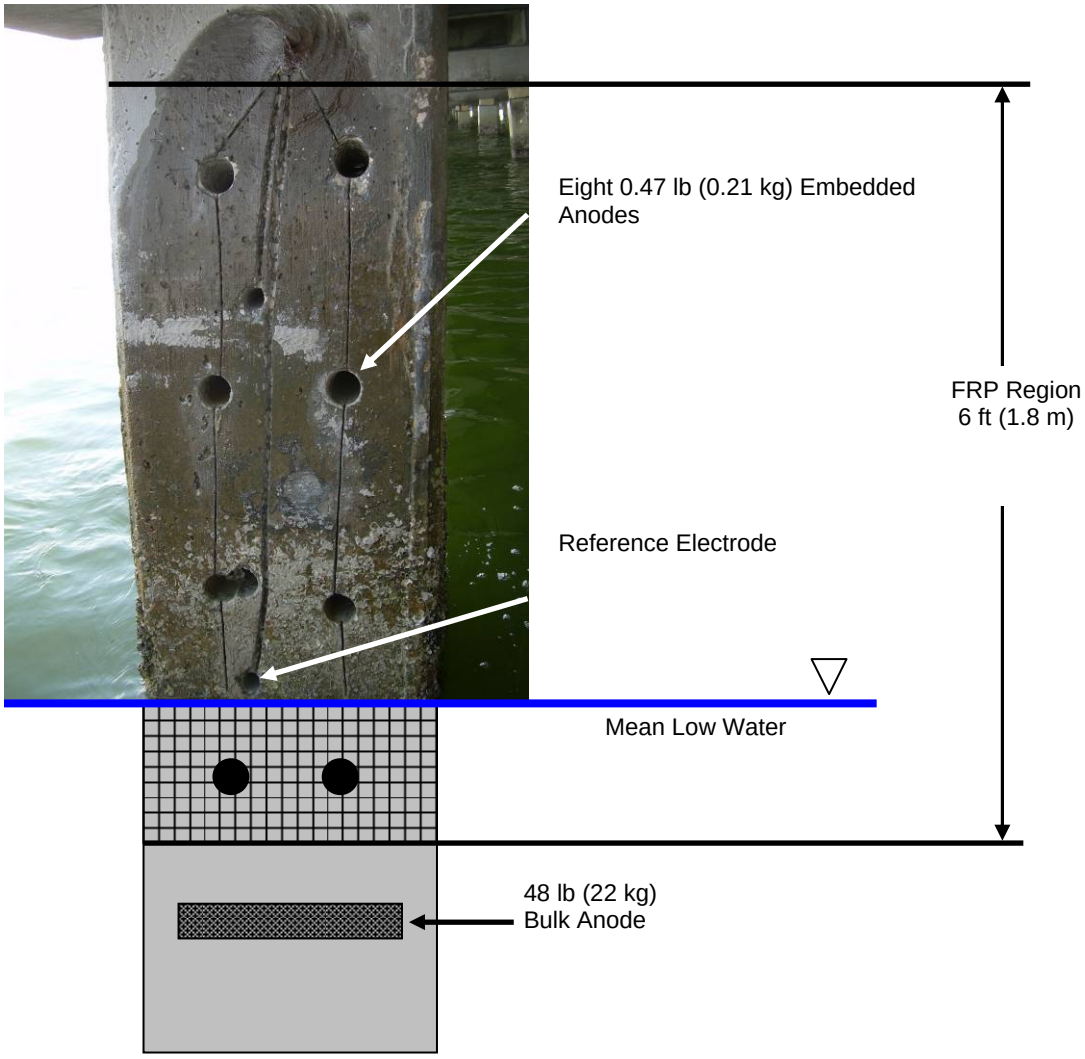

Figure 2.9 Layout of CP system.

Following their installation, the eight embedded anodes were joined using a single continuous wire that was connected to each anode via a stainless steel bolt. The wire was routed into grooves cut in the concrete and covered with grout for protection and connected to a data logger mounted at the top of each pile in a junction box. The two Ag/AgCl reference electrodes were similarly routed into grooves, covered with grout and connected to the data logger. The 48 lb (21.9kg) bulk anode was bolted to the pile and also electrically connected prior to wrapping with FRP. It was bolted to the pile 2.5 ft (0.73 m) below mean low water.

2.8.2 FRP Wrapping

The piles were wrapped after the CP system had been in place for over two months to allow the system to stabilize. Preparation for the wrap began by scraping off all marine growth within the targeted 6 ft (1.8 m) region. Subsequently, the pile surfaces were ground smooth and all edges rounded to a 2 in. (51 mm) radius using a grinder. The surface was then cleaned with fresh water using a 3000 psi (21 MPa) pressure washer to remove all of the debris generated by the grinding process.

Two glass fiber reinforced layers (GFRP) each 0.05 in. (1.27 mm) thick were applied to the prepared concrete surface. The 6 ft (1.8 m) wrap extended 1 ft (30 cm) below the mean low water line (Fig. 2.9). After the GFRP was in place, a pressure bag was placed around the pile and inflated to provide a uniform 2 psi (14 kPa) pressure (Fig. 2.10a). Photos of the piles after removal of the pressure bags are shown in Figure 2.10b.

Figure 2.10 (a) Pressure bag on FRP wrapped pile; (b) Completed piles in bent.

2.8.3 Data Collection

Anodic current information was recorded using commercially available data loggers. All readings were time-stamped and therefore the exact time when anodes were

connected or disconnected for the NACE (Standard RP0290-2000 Item No. 21043) test was known. To determine the role of the bulk anodes in Pile 104 C and the unwrapped control 104D, they were wired to separate data loggers.

2.9 Results

The two measures used to determine the effectiveness of a CP system are (1) "instant-off" test and (2) measurement of the anodic current.

2.9.1 Instant-off Test

Since cathodic protection essentially supplies electrons to the steel reinforcement, its potential becomes "more" negative ("polarized") with respect to a reference electrode as long as the anode remains connected. Temporary (typically 24 hour) disconnection stops the supply of electrons; as a result the steel becomes "less negative" ("de-polarized").

Each "instant off" test therefore entails potential measurements on two consecutive days. On the first day, the anode is disconnected and an "instant off" potential reading taken. On the following day, the potential is read once again and the anode re-connected.

Six series of "instant off" tests conducted over a one-year period after 26, 53, 65, 183, 211 and 335 days are reported. Results corresponding to both the top and the bottom reference electrodes are summarized in Table 2.1.

According to the NACE (Standard RP0290-2000 Item No. 21043) test, a cathodic protection system is effective if the potential decay exceeds 100mV with respect to a

reference electrode. This criterion was met by the FRP wrapped pile (after 183 days) but no reading for the unwrapped control met this requirement at the time of the last test. Since both piles were in a comparable corrosion state initially, these results indicate that the current demand is much higher for the control than the FRP wrapped pile.

Table 2.1 Summary of depolarization "instant-off" tests.

Pile	Days	Top			Bottom		
		Off (V)	24 hr. (V)	Decay (mV)	Off (V)	24 hr. (V)	Decay (mV)
Control (104D)	26	-0.720	-0.714	6	-1.116	-1.078	38
	53	-0.703	-0.694	9	-1.137	-1.120	17
	65	-0.726	-0.692	34	-1.144	-1.093	51
	183	-0.743	-0.705	38	-1.132	-1.044	88
	211	-0.753	-0.690	63	-1.105	-1.028	77
	335	-0.689	-0.669	20	-1.120	-0.978	142
Wrapped (104C)	26	-0.776	-0.711	65	-1.014	-0.956	58
	53	-0.741	-0.665	76	-1.015	-0.924	91
	65	-0.748	-0.651	97	-1.023	-0.859	164
	183	-0.802	-0.664	138	-0.900	-0.791	109
	211	-0.837	-0.743	94	-0.671	-0.603	68
	335	-0.787	-0.647	140	-0.131	-0.649	-

2.9.2 Galvanic Current

The anodic current was automatically recorded by the data loggers and the saved data was periodically downloaded from the bridge site. The current density was calculated by dividing the measured current by the theoretical area of steel protected 13.75 ft^2 (1.28 m^2) (Full calculations can be found in appendix A). As noted earlier, the anodic current varies with concrete resistivity. This in turn is influenced by temperature and tide change. Wet concrete has a lower resistivity compared to dry concrete.

Figures 2.11 and 2.12 plot the variation in current density with time for the control (104D) and its GFRP wrapped counterpart (104C) respectively. The plot shows the history of the recorded data starting with the connection of embedded anodes prior to wrapping (day 0), connection of the bulk anode (day 20) until day 475. Small upward pointing arrows (seven in total) indicate days on which "instant-off" tests were conducted whereby the anodes were temporarily disconnected (Table 2.1). The ordinate axis plots the total current density obtained by adding the separate contributions of the embedded and bulk anodes. Whereas this combined current is shown for the control, because of data logger failure after 183 days (discussed later), the values following this point reported for the GFRP wrapped pile only correspond to the current provided by the embedded anodes. The same plots also show the assumed design protection current of 0.25 mA/ft^2 (2.80 mA/m^2) that is shown as a dotted line.

The results for the control and the GFRP pile can be directly compared for the first 183 days (Figures 2.11 and 2.12). This clearly shows that the protective current required is much smaller for the GFRP wrapped pile. More detailed analysis shows that it is in excess of 20%. No similar comparisons can be made for the subsequent period because of failure of the connection between the bulk anode and the data logger. Nonetheless, there is a clear drop-off in the current demand from the embedded anodes for the GFRP wrapped pile that is not evident in its control counterpart (from day 344 onwards).

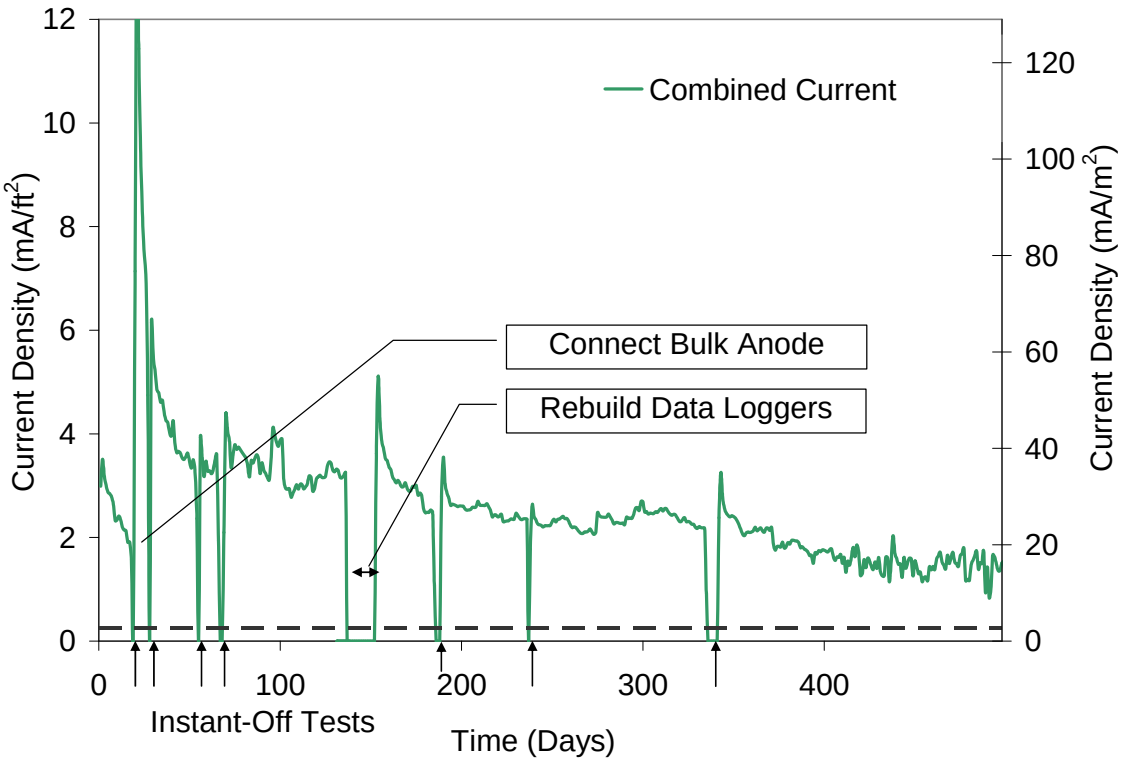

Figure 2.11 Current density for unwrapped control (104D).

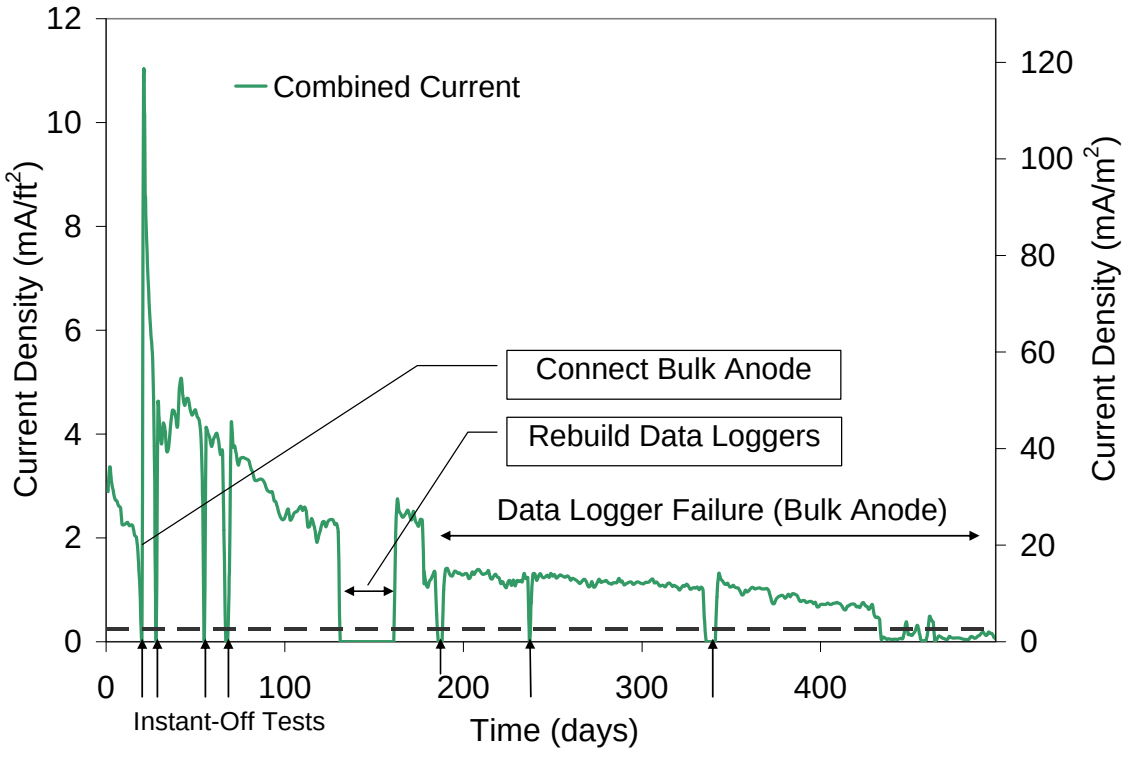

Figure 2.12 Current density for GFRP Pile (104C).

2.10 Discussion

The results from the study clearly indicate that the CP system installed within the GFRP is working. NACE's depolarization criterion was met (Table 2.1) and the progressive reduction in current densities illustrates the contribution of GFRP in slowing the corrosion rate as has been repeatedly demonstrated in independent experimental studies[3].

These tests were performed on only two piles with different chloride contents, and while the data is in itself promising, many more tests should be performed under varying concrete conditions prior to making any definitive statement suggesting that the CP system will be effective in all circumstances.

As mentioned already, not all the data was recorded because of failure of the data loggers due to water intrusion. The data loggers that were used were donated by the manufacturers of the anodes and were not designed for Florida's extremely aggressive environment. Following the first failure after 130 days, replacement data loggers were purchased and placed in individual environmental enclosures. Silicone was generously applied to ensure water-tight integrity. Despite these extraordinary measures some of the data loggers still failed and data was lost. This highlights the need for a more robust system that is placed in a more protected location in aggressive environments.

2.11 Lessons Learned

Since the first demonstration of underwater pile repair there have been significant advancements in the design, construction, and application of FRP that make the system more versatile and cost effective. Some of the important lessons that the researchers learnt are given below.

2.11.1 Power Tools for Surface Preparation

The pile to be wrapped typically has to be cleared of marine growth, surfaces have to be smoothened and corners rounded both above and below the water-line. Initially, electrical grinders were used (this is can only be performed above water), subsequently, pneumatic grinders (poor underwater performance) and finally hydraulically-powered grinders that proved to be the most versatile. Surface preparation is greatly expedited when hydraulically-powered grinders are used.

2.11.2 Wet Layup FRP Application

The first attempts at utilizing a wet layup involved "rolling" the epoxy onto the FRP using a roller (Fig. 2.13a). Although this system worked, there were many drawbacks, namely that the system was heavy, and therefore difficult to transport to the bridge site; and the time taken to saturate the fabric. In the end, this system was abandoned, and replaced by simply laying out the fabric on the ground and rolling epoxy into it (Fig. 2.13b). A more efficient method has yet to be found.

(a) (b)

Figure 2.13 (a) Rolling epoxy onto FRP mechanically; (b) Rolling epoxy manually.

2.11.3 Pressure Bag

The first attempt at utilizing a pressure bag for bond improvement was with a bag fabricated by the research team. This bag was made from nylon and was 7ft x 6.5 ft. (2.13 m x 1.98 m). It used toggles to secure the bag around the pile (Fig. 2.14a). This system was effective, however the toggles proved cumbersome when a full sized bag was being used.

The bag currently being used for FRP installation is a modified version of the original pressure bag (Fig. 2.14b). The new bag is built with using rubberized nylon, and has similar dimensions to the original bag. The new bag uses a zipper as well as buckles to secure it to the pile. The zipper is much easier to use than the toggles, and the buckles can be used to secure the bag in position prior to inflation and provide additional hoop strength during pressurization. These modifications have greatly increased the ease with which the pressure bags are installed.

(a) (b)

Figure 2.14 (a) Pressure bag with toggles; (b) Modified pressure bag.

2.11.4 Complications of Embedded Anodes

The installation of embedded anodes requires a tremendous amount of drilling. Drilling eight holes in the splash zone can take several days, since the lower portions of the pile may be submerged for all but a few hours of the day and hydraulically powered tools were not available. This makes the operation cumbersome. Alternative systems are needed that are easier to install.

A preliminary study was conducted to determine the extent of protection that could be afforded by the bulk anodes alone. Previous studies[25] have shown that extent of this protection is a function of resistivity of the concrete; the lower the resistivity the greater the region that can be protected.

Probes (Fig 2.15a) were used to measure the resistivity of the concrete in the wrapped region (Fig. 2.15b). The results of this can be found in Table 2.3. The

measurements indicated that the bulk anode would not be able to provide the minimum level of protection for more than 1.5 ft (0.457 m) beyond its physical location. This represents a much shorter length than is required - 5.5 ft (1.68 m). More studies are underway to explore this approach.

Table 2.2 Summary of pile resistivity values.

Pile name	Description	Distance From Pile Cap (in)	Readings (Ω-cm)					
			1	2	3	4	Average	Std Dev.
103	Unwrapped control	16	115000	102000	109000	115000	110250	6185
		24	115000	115000	121000	121000	118000	3464
104 A	Wrapped Dec 2008	24	15000	14000	15000	14000	14500	577
104 C	Wrapped Dec 2008	24	24000	25000	25000	25000	24750	500
101 C	Wrapped Summer 2005)	16	48000	54000	51000	48000	50250	2872
		24	26000	25000	26000	25000	25500	577

(a) (b)

Figure 2.15 (a) Resistivity probe; (b) Holes in FRP for concrete resistivity testing.

2.12 Summary

This chapter summarizes results of research undertaken to advance the application of FRP for the corrosion repair of piles. Based on the data presented, the following conclusions may be drawn:

(1) A new pressure bagging system has been developed that can lead to significant improvement in the FRP-Concrete bond. The extent of the improvement at the pressure tested depended on the type of resin. Improvement was best for epoxy-based resins where no gases are generated during curing (Figs. 2.6,2.7).

(2) If no external pressure is applied, bond is improved if a purely transverse lay-up is used.

(3) An embedded sacrificial anode cathodic protection system was designed and implemented. Instant-off tests (Table 2.1) show that the CP system appears to be effective for this type of reinforced concrete pile. Data collected over 15 months shows that the protective currents were higher in the unwrapped control compared to the FRP wrapped piles (Figs. 2.11, 2.12). This indicates lower corrosion rates in the FRP wrapped piles and confirms findings from laboratory studies that have consistently shown that FRP tended to slow down the corrosion rate. Lower currents imply less anode consumption and therefore longer service life for the anodes in the FRP wrapped piles.

3 Improvement in FRP-Concrete Bond by External Pressure

This chapter presents results from an experimental study that evaluated the improvement in the FRP-concrete bond to dry and wet substrates due to applied pressure. In the study, twelve full-sized pile specimens including four controls were wrapped using two different GFRP systems, a pre-preg and a wet layup, and two different layouts typically used for uni-directional and bi-directional fibers. Wrapping was conducted inside a partially filled tank to ensure that the bonded areas of the dry and wet regions were identical. Sustained pressure was maintained during curing by using pressure / vacuum bagging. Bond improvement was evaluated from over 400 pullout tests. Results showed that external pressure led to improved bond in both the dry and submerged regions. However, vacuum bagging was better for pre-preg systems while pressure bagging was better for wet lay-ups. Transverse fiber layout typically used with bi-directional fibers gave better bond in controls where no external pressure was applied.

3.1 Introduction

Tests have shown [3.1] that external pressure significantly improves the FRP-concrete bond. In general, the bond attained without pressure is satisfactory and external pressure unnecessary. However, where gravity effects of the resin-saturated fibers have to be countered, external pressure is required. Thus, in the repair of vertical elements such as columns or piles, a plastic shrink material is tightly wound over the curing FRP in the transverse direction (Fig. 1). The normal force applied by the plastic shrink material

introduces normal stresses that confine the wet fabric and set up the necessary frictional resistance to offset gravity effects. But in non-circular cross-sections, confining pressures are non-uniform; they are higher on the rounded edges than on the flat surface. This is the most likely reason why field pullout tests have found the FRP-concrete bond to be variable [3.2] in piles repaired in this manner.

Uniform pressures can be imposed by using *pressure bagging* or *vacuum bagging*. These established techniques are routinely used by the automotive and aerospace industries for fabricating FRP components. Their application for infrastructure repair has been limited and few studies reported. Stallings et al. 2000 [3.3] mentioned using vacuum bagging for repairing a bridge slab while Nazier et al. 2005 [3.4] used vacuum bagging for repairing a pile cap. The latter paper provides detailed information on the vacuum bagging technique used but no quantitative data on the improvement in the FRP-concrete bond.

More recently, a simple and inexpensive system was developed to extend the application of vacuum and pressure bagging to pile repair in tidal waters [3.5]. Though attempts were made to quantify improvement in the FRP-concrete bond, results were inconclusive. This stemmed in part because the repaired surface under water was uneven in places and direct tensile loads could not always be applied.

This chapter presents results from a comprehensive study undertaken to evaluate the impact of vacuum / pressure bagging on FRP-concrete bond for simulated repair of piles in a tidal zone [3.6]. Results from over 400 pullout tests compared the bond attained in identical pressure / vacuum bagged specimens with those from identical shrink-

wrapped controls in both dry and submerged regions. The study also evaluated the role of two commonly used fiber layout schemes on the FRP-concrete bond.

3.2 Background

3.2.1 Pressure Bagging

Pressure bagging is similar in concept to a blood pressure cuff used in medical practice. An air-tight bladder is incorporated within a flexible or rigid restraining structure that is wrapped around the element to be repaired. Flexible restraints are preferred as they can be fitted and adapted as needed. This method requires the material of both the air-tight bladder and the restraining structure to be designed to withstand the hoop tension stress arising from the applied external pressure.

In applications, the pressure bag with the air bladder inside is positioned around the pile or column after the FRP and shrink wrap have been applied in the usual manner. The pressure bag is secured around the pile using fastenings and compressed air used to inflate the bladder to the desired pressure. This is sustained until the resin has cured. Figure 3.1 shows a photo of shrink-wrapped (two on the left) and pressure-bagged piles (two on the right).

Figure 3.1 Control and pressure bagged piles.

3.2.2 Vacuum Bagging

Vacuum bagging applies pressure by creating a vacuum (limited to a maximum of 1 atmosphere, 30 in. (760 mm) of mercury). The essential components of a vacuum bagging system are a vacuum bag, a vacuum pump capable of creating a significant vacuum and a sealing system to ensure no leaks develop (Fig. 3.2). Additionally, there needs to be a "breather layer" to provide a pathway for vacuum to all areas under the bag without blockage. Compared to pressure bagging, higher pressures can be readily applied since the material does not have to resist hoop tensile stresses. The disadvantage is the need to maintain an airtight seal around the perimeter of the wrapped region. This can be problematic especially for concrete elements that are cracked. The vacuum bag piles can be seen in Figure 3.3.

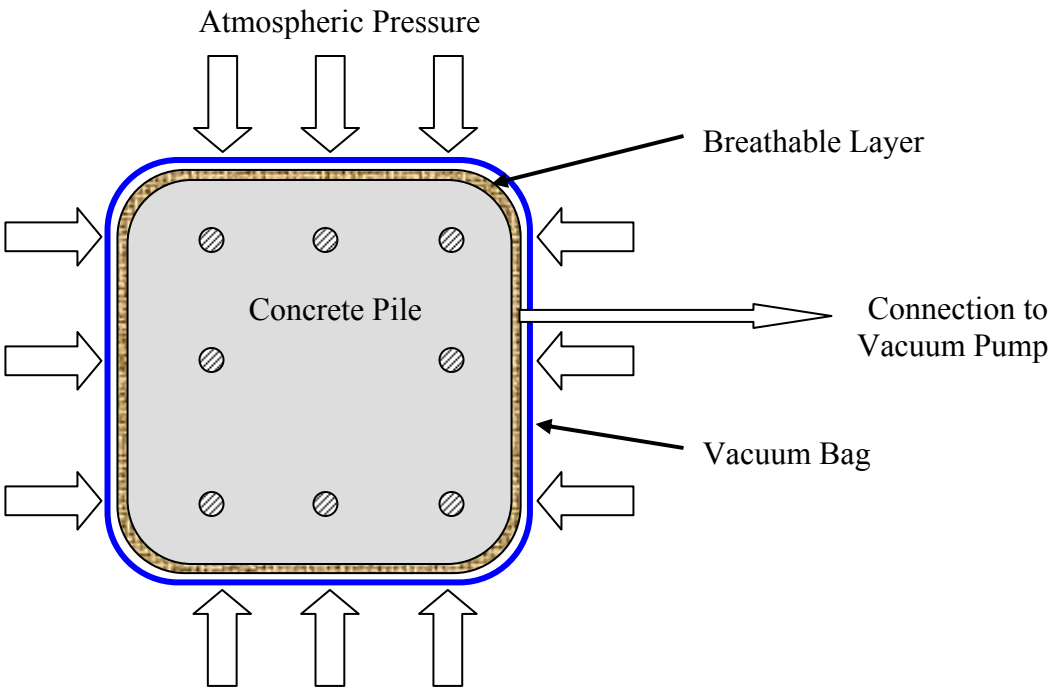

Figure 3.2 Vacuum bag schematic.

Figure 3.3 Vacuum bagged repaired piles.

3.2.3 External Pressure

The literature [3.1] indicates that pressures higher than a minimum 1.5 psi (10 kPa) ensure good bond for surfaces that are horizontal. However, vertical surfaces require

higher pressures because of the need to offset gravity effects discussed earlier. In an earlier study pressures ranging from 3-15 psi (20-100 kPa) were used [3.5] and the bond was qualitatively found to be satisfactory. The same range was retained in this study. The intent was to use 10 psi (69 kPa) for both systems; however, as pressures of only 7 psi (48 kPa) were found to be safe for the material used to make the pressure bag, this lower pressure was used for the pressure bagged system. The gage pressure for the vacuum bag system was maintained at 11 psi (76 kPa).

3.3 Experimental Program

The goal of the test program was to quantify improvement in bond arising from the application of pressure bagging and vacuum bagging over traditional shrink-wrapped control specimens. Since the manner in which the fibers are laid out, that is, transversely or longitudinally, affect the contact pressure between the resin-saturated fibers and the concrete substrate in vertical elements, two different schemes were evaluated. These are identified as '*Scheme 1*' and '*Scheme 2*' in the chapter.

In *Scheme 1*, fibers are first laid longitudinally and then wrapped over transversely. In *Scheme 2*, the fibers are only applied in the transverse direction. Originally, it was envisaged that uni-directional materials will be tested using scheme 1 and bi-directional materials using scheme 2 as is customary. Unfortunately, all the available pre-preg material was bi-directional. Therefore, for the pre-preg system, bi-directional material was used for both schemes 1 and 2.

3.3.1 Specimen Details

Sixteen 5 ft (1.53 m) long, 12 in x 12 in (300 x 300 mm) prestressed pile sections were earmarked for the study. They were obtained by cutting 20 ft (6.1 m) length piles prestressed by four ½ in (12.7 mm) diameter Grade 270 strands into 5 ft (1.53 m) lengths (Fig. 3). The average compressive strength was estimated to be around 4400 psi (30.3 MPa) from non-destructive testing.

Of the sixteen specimens, twelve were used in the study with the remaining four set aside as "spares". The sixteen were split equally between the pre-preg (A1 to A8) and the wet lay up systems (F1 to F8). The corners of each specimen were rounded to a 1½ in. (40 mm) radius using a concrete router with a Secco wet grinder equipped with a 1½ in. (40 mm) half bullnose granite routing bit. Any irregularities were patch filled with hydraulic cement. All specimens were pressure washed immediately prior to wrapping.

3.3.2 Tidal Wrap Simulation

FRP wrapping was conducted inside a 10 ft x 6 ft x 4 ft (3 m x 1.83 m x 1.22 m) deep tank filled with potable water. The depth of the water inside the tank was kept such that exactly half of the wrap length (18 in.(457 mm)) would be under water and half (18 in.(457 mm)) above (Fig. 3.1-3.2). This was to ensure that the same number tests could be carried out to evaluate the bond that developed in both the dry and wet regions.

3.3.3 Material Properties

Two contrasting FRP systems used in previous field demonstration studies [3.7-3.9] were evaluated. These are a pre-preg system developed by Air Logistics (with only

bi-directional fibers) and a wet lay up system developed by Fyfe (with both uni-directional and bi-directional fibers). Since the goal of the study was to investigate improvement in bond, only lower cost glass fiber was tested.

3.3.4 Pre-Preg System

The pre-preg system uses a unique water-activated urethane resin in conjunction with a custom woven fabric. Because it is water-activated, the FRP material must be pre-impregnated with resin and sent to the site in hermetically sealed foil pouches. The pouches are opened just prior to application to prevent premature curing from atmospheric moisture. The properties of the bi-directional fibers as provided by the manufacturer are summarized in Table 3.1 [3.10]. In this table, along with all subsequent tables, the "Tensile Modulus" refers to the amount of stress required for the fibers to deform with a corresponding unit of strain, the "Ultimate Elongation" describes the % increase in length before failure, and the "Laminate Thickness" is the thickness of one layer of epoxy saturated fibers.

Table 3.1 Properties of Air Logistics Aquawrap® fabric.

Property	Value
Tensile Strength	54,000 psi (372 MPa)
Tensile Modulus	3.24×10^6 psi (22.3 GPa)
Ultimate Elongation	1.67%
Laminate Thickness	0.026 in (0.66 mm)
Dry fiber weight per sq. yd.	24 oz (813 g/m^3)

3.3.5 Wet Layup System

Fyfe's Tyfo® SEH-51A is a custom-weave, uni-directional glass fabric while Fyfe Tyfo WEB is a custom 0/90 bi-directional weave. They are usually used with Tyfo-S Epoxy. However, for underwater application, Tyfo® SW-1 underwater epoxy is used

instead. The FRP fabric must be impregnated on-site just prior to use. Properties of these materials as provided by the manufacturer are summarized in Table 3.2 [3.11].

Table 3.2 Properties of Fyfe Tyfo® fabrics.

Tyfo® Composite	Property	Value
SEH-51	Tensile Strength	66,720 psi (460 MPa)
	Tensile Modulus	3.03 x 10^6 psi (20.9 Gpa)
	Ultimate Elongation	2.20%
	Laminate Thickness	0.05 in (1.3 mm)
	Dry fiber weight per sq yd.	27 oz (915 g/m^2)
WEB	Tensile Strength	35,840 psi (247 MPa)
	Tensile Modulus	2.24 x 10^6 psi (15.4 GPa)
	Ultimate Elongation	1.60%
	Laminate Thickness	0.01 in (0.25 mm)
	Dry fiber weight per sq yd.	8.7 oz (295 g/m^2)

3.3.6 Wrapping Details

The twelve piles were wrapped in three separate operations with four piles wrapped on each occasion. In the first two operations, the pre-preg and the wet lay up systems were used to wrap four controls and four pressure bagged piles. In the final operation two piles from each of these systems were vacuum bagged in the same tank (Fig. 3.2).

3.3.7 Pre-Preg System

In the pre-preg system, a base primer coating is first applied to the 3 ft (0.91 m) region of the pile that is wrapped. In *Scheme 1* (control pile A5 and pressure bagged pile A7), the material was laid first in the longitudinal direction then wrapped over in the transverse direction with no overlap. In *Scheme 2* (control pile A3 and pressure bagged pile A8), two FRP layers were successively wrapped around the pile in the transverse

direction with no overlap. Following wrapping, a plastic shrink wrap material was placed over the wrapped region in the transverse direction (Fig 3.1). Since the urethane resin gives off carbon dioxide, the surface of this plastic shrink wrap was punctured using a special tool to allow these gases to escape.

Piles A7 (*Scheme 1*) and A8 (*Scheme 2*) were pressure bagged. For this operation, two layers of burlap were placed over the shrink wrap and kept in place with duct tape. The burlap provides a breathable layer between the pile and the un-inflated pressure bag that was subsequently placed around the pile. The two ends of the bag were zip-fastened and a connection made to a air compressor. The pressure was set to 7 psi (48 kPa) where it was maintained for 24 hours.

Piles A6 (*Scheme 1*) and A4 (*Scheme 2*) were vacuum bagged. These were prepared the same way as the pressure bagged piles. Following the installation of the burlap over the shrink wrap, sealing rings were placed above and below the wrap. The vacuum bag was then slipped over the pile and sealing rings and duct tape used to secure it in place. Vacuum was then applied through the connectors integrated in the vacuum bag to a gage pressure of 22 inch (550 mm) of mercury or 11 psi (76 kPa).

3.3.8 Wet Layup System

Unlike the pre-preg system, the piles wrapped in the wet layup system require no base primer prior to the application of the resin saturated fiberglass. However, the resin has to be mixed on site and applied to the fiberglass just prior to wrapping. *Scheme 1* layout used uni-directional Tyfo® SEH-51A fiberglass (F8, F3), while *Scheme 2* layout

used bi-directional Tyfo® WEB fiberglass (F5, F1). The control piles were F8 and F5 while the pressure wrapped piles were F3 and F1.

The procedure for wrapping was identical to that for the pre-preg system excepting that it was not necessary to (1) apply a base resin layer, (2) perforate the shrink wrap and (3) to provide a burlap layer over the shrink wrap. Instead, the pressure bag was placed directly around the shrink wrap and its two ends zipped together. The applied pressure was kept at 7 psi (48 kPa) for 24 hours as for the pre-preg system.

The procedure for installing the vacuum bag for the wet layup system was also identical to that for the pre-preg system. Although there was no need to perforate the plastic shrink wrap to vent gases, it was nonetheless perforated to allow evacuation of any air which may have been trapped between the pile and the FRP. Vacuum was then applied and maintained as before at 11 psi (76 kPa) for 24 hours.

3.4 Evaluation of FRP-Concrete Bond

To compare the relative FRP-concrete bond in the controls, pressure-bagged and vacuum-bagged specimens, all pullout tests were conducted on the same relative pile face and at identical locations in each of the 12 specimens. The face identified as D in Figure 3.4 (side A is the trowel-finished exposed face in the prestressing bed) was selected because its wrapped finish was similar in all the test specimens.

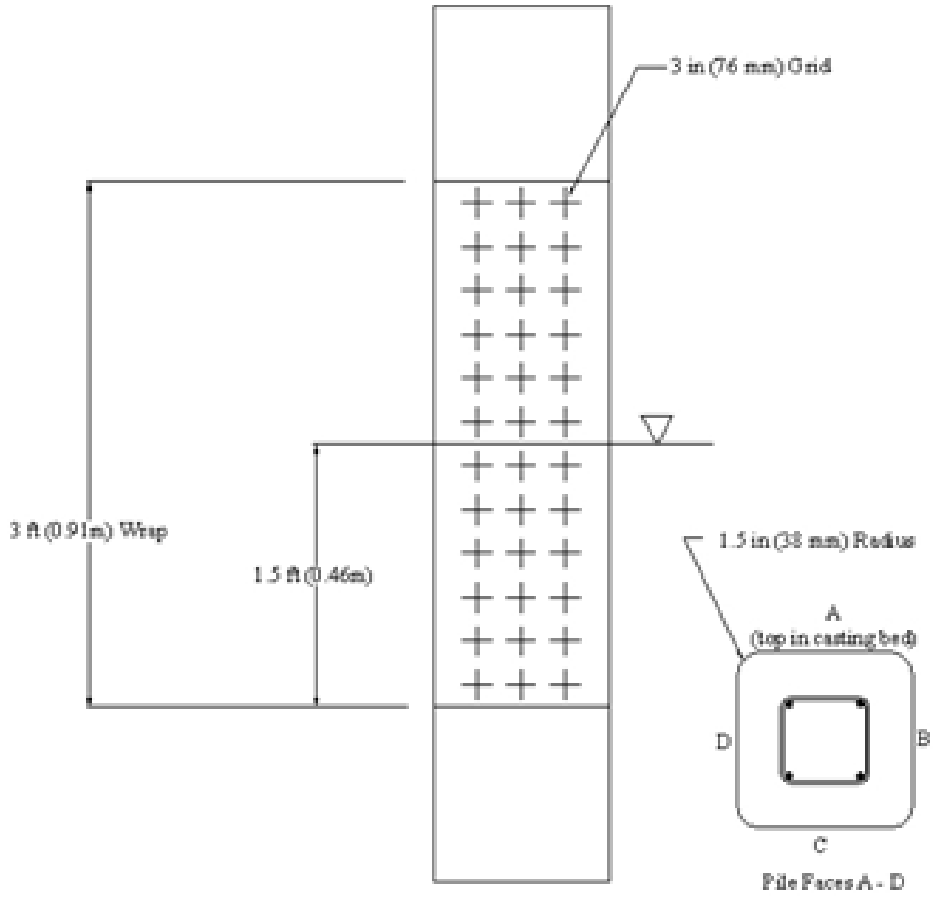

Figure 3.4 Testing grid (left) and definition of "D" face used in pullout test (right).

A 3 in. (76 mm) square grid was drawn over the wrap (Fig. 3.4) and direct tension pullout bond tests conducted at the intersection of the grid lines in accordance with ASTM D4541 [3.12]. In these tests, 1.25 in. (31.8 mm) diameter sand-blasted aluminum disks were bonded to the FRP surface using 3M DP-420 epoxy (Fig. 3.5). This epoxy attains shear strength of 4,500 psi (31 MPa) after 3 days. Tests were conducted after the epoxy had cured for 3 days using an Elcometer 106 adhesion tester.

Figure 3.5 Installation of dollies for pullout test.

3.4.1 Results

Results for a total of 422 pullout tests are presented. For the overwhelming majority, failure was by debonding in which the FRP separated cleanly from the concrete surface. This indicated that the FRP-concrete bond was poorer than the tensile strength of the concrete. There were occasional tensile concrete failures, partial concrete failures, and failure due to separation of the two FRP layers.

A summary of the results is given in Table 3.3, and the full table of results can be found in Appendix B. This shows the variation in the *average* FRP-concrete bond based on every foot (0.3m) length for all piles tested. For each of the two schemes, the results for the shrink wrapped controls and the pressure and vacuum bagged specimens are shown alongside.

Inspection of Table 3.3 confirms that the fiber architecture layout affects FRP-concrete bond. For the shrink-wrapped controls, the bond is generally better for *Scheme 2* (two transverse layers) layout for both the pre-preg and the wet layup systems. Thus, for the wet lay up system, the bond variation with depth for *Scheme 2* layout is 218, 136 and

187 psi (1.5, 0.94, 1.3 MPa) compared to 103, 59 and 36 psi (0.71, 0.41, 0.25 MPa) for *Scheme 1* layout. Similar trends may be noted for the pre-preg system.

Table 3.3 Average pullout stress per wrap width.

System	Distance from top (in)	Distance from top (mm)	Average Pullout Stress, psi (kPa)					
			Scheme 1 Longitudinal + Transverse			Scheme 2 Transverse + Transverse		
Pre- Preg	0-12	0-300	163 (1123)	314 (2165)	255 (1758)	257 (1772)	255 (1758)	293 (2020)
	12-24	300-600	58 (400)	189 (1303)	231 (1593)	112 (772)	174 (1200)	154 (1062)
	24-36	600-900	142 (978)	135 (930)	167 (1151)	92 (634)	118 (813)	199 (1371)
Wet Layup	0-12	0-300	103 (710)	298 (2053)	250 (1723)	218 (1502)	254 (1750)	248 (1709)
	12-24	300-600	59 (407)	218 (1502)	144 (992)	136 (937)	272 (1874)	169 (1164)
	24-36	600-900	36 (248)	266 (1833)	101 (696)	187 (1288)	211 (1454)	97 (668)

An overview of the average pull-out values corresponding to the entire dry and wet regions for *Scheme* 1 and *Scheme 2* layouts for the pre-preg and wet layup systems respectively is shown in Figures 3.6-3.9. The plots that are in the form of bar diagrams provide information on the number of tests conducted (usually 18) and also the relative increase in bond normalized relative to the respective controls above and below the waterline. Thus, the number "2.11" in Figure 3.6 indicates that the bond for pressure bagging is 2.11 times that of the control (or a 111% increase).

Pressure bagging and vacuum bagging tend to improve bond in both the dry and submerged regions. However, pressure bagging worked better with the wet layup system and vacuum bagging better with the pre-preg system. This can be readily seen from Figures 3.6-3.9. For example, for the pre-preg system, vacuum bagging led to increases in the FRP-concrete bond in the submerged region by 45% and 90% compared to 5% and 30% from pressure bagging (Fig. 3.6-3.7). In contrast, for the wet layup system, pressure

was more beneficial. For the same submerged region, pressure led to increases ranging from 31% to 545% compared to a 42% reduction and a 157% increase under vacuum bagging (Fig. 3.8-3.9).

It is believed that this difference arises because of the differing resin chemistry; while the urethane resin used by the pre-preg system releases carbon dioxide during curing, no similar gases are released by the wet layup system. Thus, while pressure helps to force the resin into the concrete pores thereby improving the FRP-concrete bond, it is not as effective in removing any gases generated. In contrast, vacuum helps bond by rapidly evacuating the carbon dioxide for the pre-preg system but is not as effective in maintaining pressure for the wet layup system.

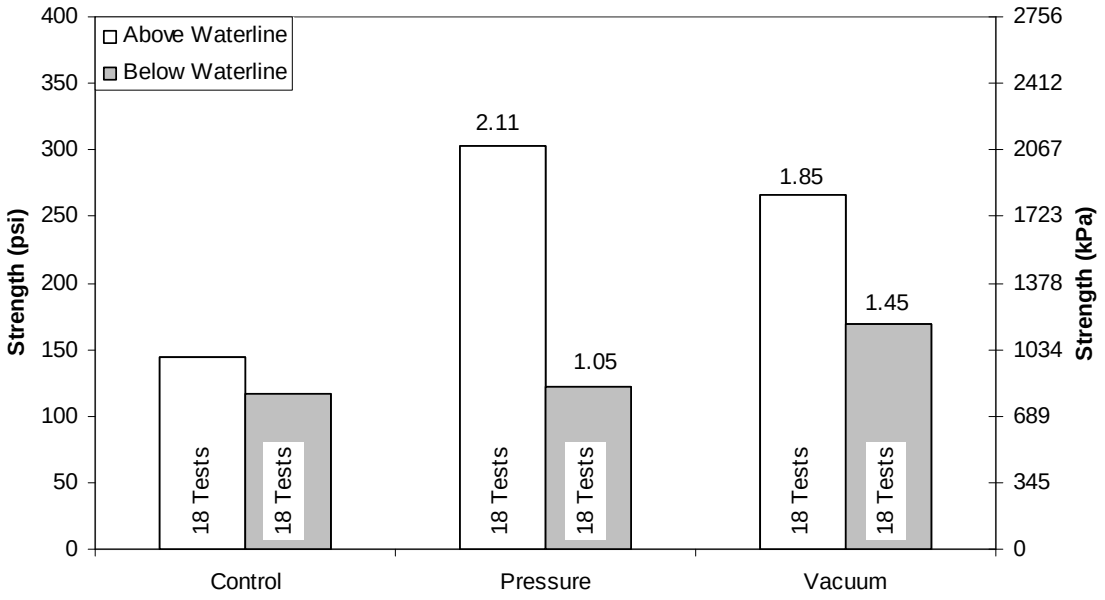

Figure 3.6 Pre-Preg – scheme 1 average strength increase.

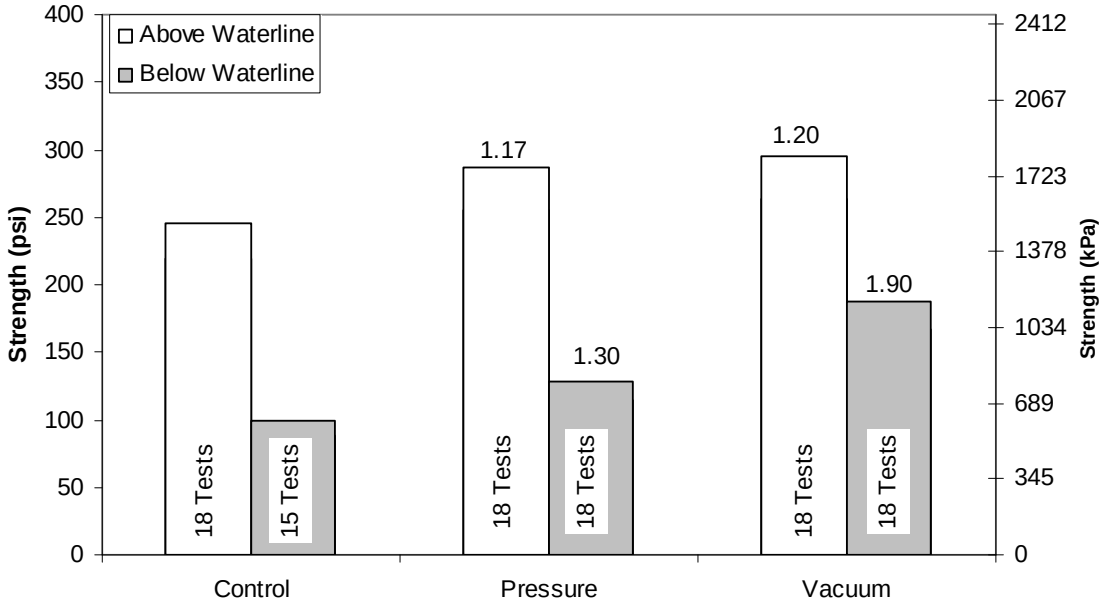

Figure 3.7 Pre-Preg - scheme 2 average strength increase.

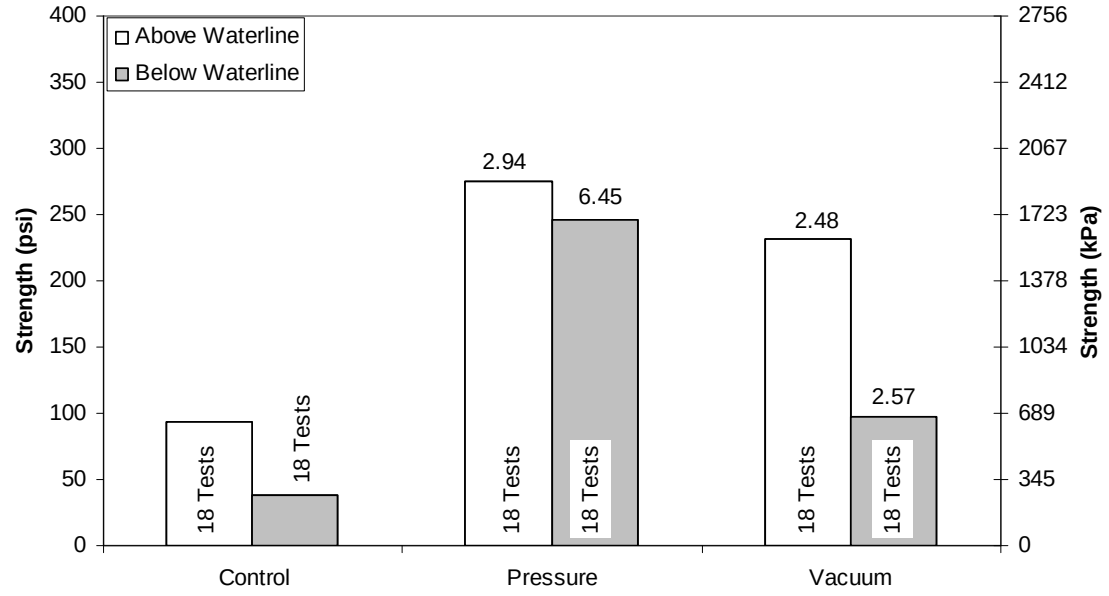

Figure 3.8 Wet Layup - scheme 1 average strength increase.

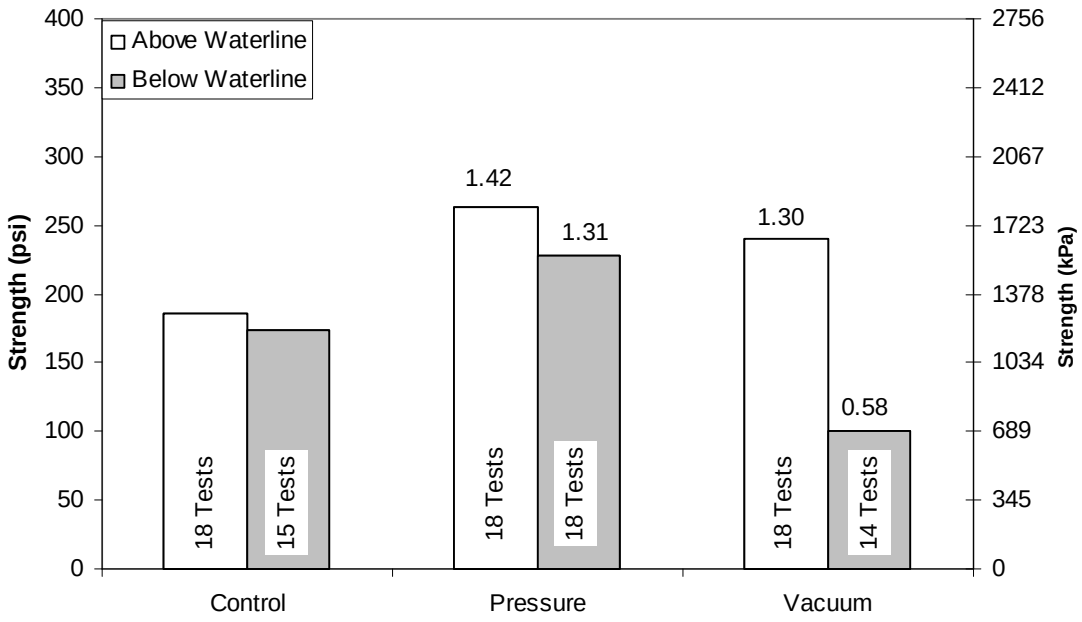

Figure 3.9 Wet Layup – scheme 2 average strength increase.

3.4.2 Contour Plots

The spatial variation in the measured pullout values from the 422 tests are shown as contour plots in Figures 3.10 and 3.11 for the pre-preg and the wet layup systems respectively. These plots were developed by normalizing the pullout values with respect to the direct tensile strength of concrete, f_t, taken as $6\sqrt{f_c'}$ [3.13]. This works out to be about 400 psi (2.76 MPa) for the 4,400 psi (30.3 MPa) average concrete strength.

For the FRP-concrete composite to be effective, it is not necessary for the bond to equal or exceed the direct tensile strength of concrete. For example, the recommended minimum bond for epoxy protecting concrete in a corrosive environment is in the 200-250 psi (1.38-1.72 MPa) range [3.14]. Such a range is equally valid for FRP-concrete systems.

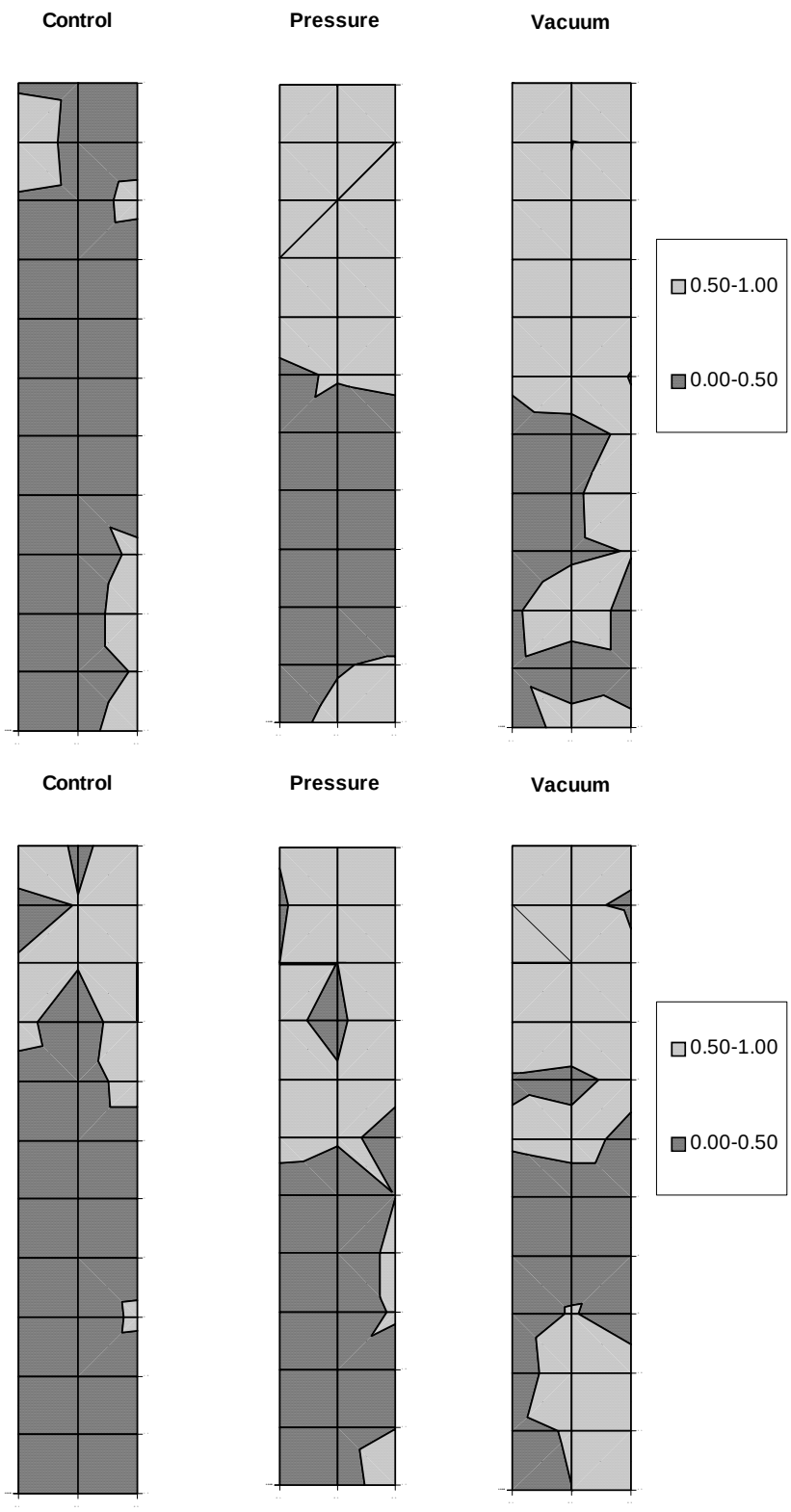

Figure 3.10 Pre-Preg pullout contour maps (top-scheme 1; bottom- scheme 2).

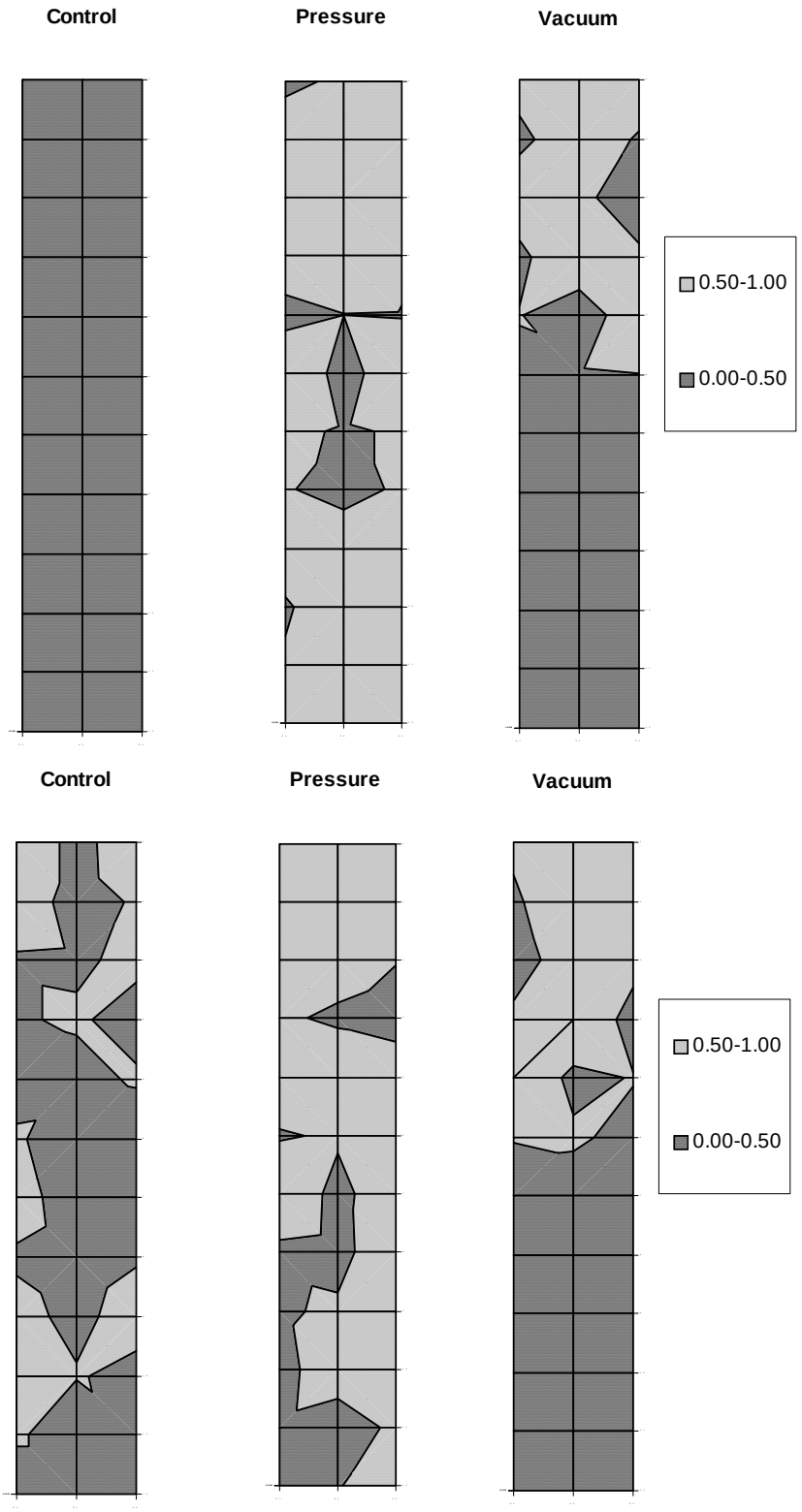

Figure 3.11 Wet Layup pullout contour maps (top-scheme 1; bottom-scheme 2).

The intent of the contours is essentially to demarcate regions of "good" and "bad" bond. Thus, they are plotted for only two ranges (1) Bad bond corresponding to pullout values below $0.5f_t$ or 200 psi (1.38 MPa), shown as a darker shade in Figures 3.10-3.11 and (2) Good bond corresponding to bond values exceeding 200 psi (1.38MPa), shown as a lighter shade.

Inspection of Figures 3.10 and 3.11 show that the bond that develops in controls is generally "bad" and inferior to that obtained by pressure or vacuum bagging. The FRP wrap at the left side of the plots is generally bad in nearly all the cases. This may be because it borders the poorly finished exposed pile surface (face A in Fig. 3.3).

Conclusions reached earlier regarding the benefits of pressure bagging for the wet layup system and vacuum bagging for pre-preg are reiterated by these plots. In general, the bond in the submerged region is poorer compared to that in the dry region. This may be because the concrete pores in the submerged region are saturated by water.

3.5 Discussion

The results presented in Figures 3.6-3.11 show that both pressure bagging and vacuum bagging enhance the FRP-concrete bond. However, despite, the application of sustained uniform pressure there is wide variation in the pullout resistance. This is partly because uniform pressure is superimposed over uneven pressures impressed by the shrink wrap and partly because of the different conditions of the dry and wet surfaces. The chemistry of the resin, the roundedness of the edges plays a role in accentuating these differences.

Though net pressures were higher for vacuum bagging (11 psi (76 kPa)) compared to pressure bagging (7 psi (48 kPa)), its impact could not be differentiated from the tests. This suggests that the lower pressure value will provide similar results. In practice applied pressures between 5-10 psi (34-69 kPa) should suffice to maintain continuous contact between the FRP and concrete while the resin cures. Also, pressures were sustained for 24 hours for convenience. This could be reduced depending on the type of resin and its curing time.

A result that may be of some practical relevance is the role of the fiber layout on bond for the *controls*. In general, the FRP-concrete bond was better for *Scheme 2* (only transverse layers) controls in both the dry and wet regions (Table 3.3). This is probably because higher pressure can be applied where two layers are wrapped over each other in the transverse direction compared to a single transverse layer in the case of *Scheme 1*.

3.6 Summary

This chapter presents results from a comprehensive test program to evaluate the FRP concrete bond in both dry and submerged regions arising from the application of pressure and vacuum bagging. In the tests, the FRP-concrete bond was systematically evaluated using a 3 in. (76 mm) grid over the entire wrapped face (Fig. 3.5). Based on the information presented in the chapter, the following conclusions may be drawn:

(1) Both pressure and vacuum bagging improve the FRP-concrete in both the dry and fully submerged region (Table 3.3, Fig. 3.6-3.11).

(2) Pressure bagging works best with the wet layup system (Fig. 3.8-3.9). Vacuum bagging works best with the pre-preg system (Fig. 3.6-3.7). These contrasting

results arise because of the resin chemistry. In the case of the pre-preg system, carbon dioxide is released during curing that can cause movement of the FRP away from the concrete surface. Such gases are not released from wet layup systems using epoxies.

(3) Fiber layout affects the bond that is achieved in shrink-wrapped controls. Bond was found to be better in layouts using multiple transverse wraps rather than a single transverse wrap. This is because applied pressures are higher when the FRP material is tightly wound transversely around a vertical member for all layers. In field applications, a better bond will be achieved using a transverse layout.

4 FRP Pile Repair Incorporating Cathodic Protection

Fiber reinforced polymers (FRP) are increasingly being used for corrosion repair. As barrier elements FRP can only slow down corrosion. Cathodic protection (CP) is the only proven method for stopping electro-chemical corrosion of steel. This chapter describes a new method for repairing corrosion damage in which a sacrificial cathodic protection system is incorporated within a FRP repair. The system was implemented in a demonstration project in which corroding piles supporting the Friendship Trail Bridge, Tampa Bay were repaired. The repaired piles were instrumented so that the performance of the CP system could be assessed. Results indicate that the CP system is effective in protecting the reinforcing steel. It also shows that corrosion rates are lower in FRP wrapped piles. This can increase the life of the anodes by over 20%.

4.1 Introduction

Several independent studies have conclusively demonstrated that *when bonded correctly,* fiber reinforced polymers (FRP) can significantly reduce the corrosion rate, e.g. [4.1-4.3]. However FRP cannot fully arrest the underlying electro-chemical reactions responsible for corrosion of steel in chloride contaminated concrete. This can only be overcome by incorporating a cathodic protection (CP) system within the FRP wrap.

In the past decade FRP was used for repairing corroding piles in tidal waters in several demonstration projects [4.4-4.6]. The feasibility of incorporating a cathodic protection system within the FRP wrap was also attempted [4.7] influenced by findings

from pioneering research [4.8-4.10] conducted by the Florida Department of Transportation. This research culminated in the development of the Life Jacket system [4.11] for pile repair that uses a combination of mesh anodes bonded to the concrete surface and a bulk anode placed in the salt water.

The earlier attempt at incorporating CP within the FRP wrap (Fig. 4.1) may have been effective as a means for providing cathodic protection. However, the role of FRP in strengthening was compromised since it was no longer bonded to the concrete surface but instead to the cementitious material surrounding the mesh anode. This prevented effective load transfer by shear.

This chapter describes a new FRP-CP system that was developed to overcome this problem. In the application, embedded anodes were used so that the FRP material could be directly bonded to the pile surface. The system was implemented and evaluated in a field demonstration project in which corroding piles supporting the Friendship Trail Bridge in Tampa Bay's estuarine waters were repaired. The FRP wrap was applied using pressure bagging [4.12-4.13] to ensure the integrity of the FRP-concrete bond. The piles were instrumented to allow the performance of the new system to be evaluated using protocol established by NACE [4.14].

Figure 4.1 Sacrificial CP system using a mesh anode [4.7].

4.2 Background

Cathodic protection is an electrochemical technique that is widely used to control corrosion by the offshore industry. CALTRANS was the first to use it to protect bridge structures in the early 1970's [4.15]. Subsequently, its application was extended to substructure elements [4.8-4.10]. CP is acknowledged as the only system capable of stopping corrosion at high chloride concentrations or even when deterioration is at an advanced state.

Two methods (1) impressed current systems (not addressed here), and (2) galvanically coupled systems are used for providing cathodic protection. Galvanically coupled systems, also known as sacrificial anode cathodic protection systems, work on the principle of bimetallic corrosion. This principle states that if two dissimilar metals or alloys are connected in a corrosive electrolyte, the more 'active' metal corrodes preferentially thereby protecting the less active material. Activity is defined with respect to the position of the metal in the electromotive series: the more negative the metal on the electromotive series, the more active it is. Over the years, several galvanic systems, e.g. metalized coatings, zinc-mesh anode, zinc-hydrogel, have evolved. More information on these systems may be found in NACE's state-of-the-art report [4.16].

4.2.1 Requirements for Successful Galvanic Systems

Galvanic systems are effective as long as the sacrificial anode remains active. Passivation can occur if non-soluble corrosion by-products form on the anode surface. In case of zinc, laboratory and field research indicates that salt water, e.g. from periodic

wet-dry cycles, splash, sea water mist, prevents this type of passivation (formation of oxide film) and ensures satisfactory long term performance [4.15].

In the proposed application, embedded zinc anodes are used to minimize the impact on the concrete surface for bonding of the FRP. Zinc anodes used for this type of application are chemically treated to ensure that they remain active [4.17]. The preferred method of activation is maintaining a high pH (14 to 14.5) environment around the zinc with lithium hydroxide that is designed to keep the sacrificial anode active yet not affect the steel.

4.3 Objectives

The goal of this project was to implement a new FRP-CP system for repairing piles and monitor its effectiveness. Since the effectiveness of FRP in slowing down corrosion is contingent on its bond [4.3], the FRP wrap was applied using pressure bagging [4.12-4.13].

4.3.1 Site

Piles selected for the study were those supporting the Friendship Trail Bridge, Tampa Bay that had been used in earlier studies [4.18]. The particular piles selected were on the Hillsborough side of Tampa Bay on bents 103 and 104 each with four piles designated as A-D that appeared to be in a similar state of damage. The site is recognized to be an extremely aggressive environment.

4.3.2 Chloride Analysis

Cores were taken out from the center of the "splash zone" (region subjected to periodic wet/dry cycles) from each of the three piles that are reported in the study. These include an unwrapped control (pile 104D) and two others (103A, 104C) that were identically FRP wrapped.

The chloride content was determined using the ASTM acid soluble method [4.19]. The chloride content at the level of the steel varied from 1.96 lb /cy (1.16 kg/m^3) to 6.1 lb/cy (3.62 kg/m^3). These values fall within, or exceed the accepted conservative threshold limit for corrosion of steel in concrete of 1-2 lb /cy (0.6-1.2 kg/m^3) [4.20] below which there is only a small probability of corrosion.

4.3.3 Half-Cell Potential

The half-cell potential of all three piles was mapped with respect to Cu/CuSO4 electrodes Using ASTM Standard C876 [4.21]. The surface potentials varied from -111 mV to -552 mV in the dry region, and from -192 mV to -629 mV in the "splash" zone. The values of this analysis can be found in Appendix C. This standard suggests that there is a 90% probability of corrosion in regions where readings were more negative than -350mV, however, that applies generally to atmospherically exposed concrete that is not saturated with water. In the case of wet concrete, such as found in this study, the correlation might be different. When the potential data are considered together with the chloride analysis results, however, it may be concluded that there is a high probability that the piles were indeed corroding.

4.3.4 Anode Design

A CP system was designed [4.22] and it was found that eight 0.47 lb (0.21 kg) anodes would be required to protect the steel for a 30 year design life. The anodes were Galvanode DAS – 0.25 lb 99.99% pure zinc/ft anodes [4.23]. Each anode has an initial driving voltage of 200-500 mV, and a polarized driving voltage of 50-200 mV. The layout of the anodes relative to the wrap and reference electrodes is shown in Figure 4.2. The anodes are positioned symmetrically over the 6 ft (1.8m) wrap depth to ensure efficient distribution of the anodic current. A submerged bulk anode is positioned 2.5 ft (0.73 m) below the mean low water line.

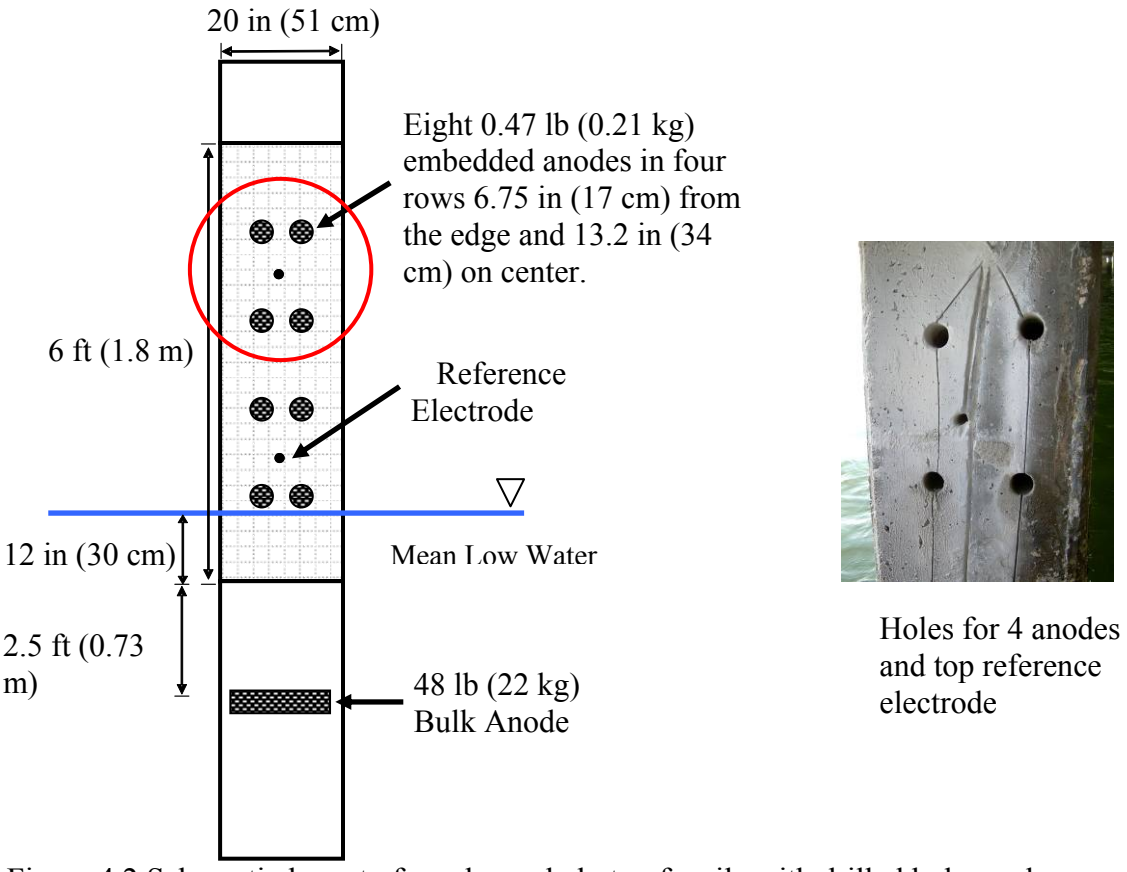

Figure 4.2 Schematic layout of anodes and photo of a pile with drilled holes and grooves.

4.4 Field Implementation

In an embedded FRP-CP system, the CP system has to be installed first followed by the FRP wrap. The installation of the anodes does not require any surface preparation other than removal of obstructive marine growth from the pile surface. Additionally, connections to the reinforcing steel are made near the pile cap.

Of the eight holes that had to be drilled, two are located close to the water line. Therefore, the drilling operation was conducted when low tide was expected. Holes drilled were sufficient in length to allow horizontal placement of the 14 in. (35.6 cm) long anodes. Prior to their placement, the holes were flushed with fresh water and compressed air was then used to blast out any remaining moisture or particulates from within. The holes were then pre-filled with a low resistivity grout (Fig. 4.3) and the anode inserted. After the grout had cured, a high impedance voltmeter was connected between the reinforcing steel and the anode to verify that there was no contact (indicated by a reading exceeding 1mV). If such a voltage was detected, the anode would have to be replaced.

Following installation, the eight embedded anodes were joined using a single continuous wire that was connected to each anode via a stainless steel bolt. A two-part epoxy putty was then placed over the bolt to prevent corrosion of the wire. The wire was then routed into grooves cut in the concrete and covered with grout for protection. Two Ag/AgCl reference electrodes were installed in the same manner in pre-drilled holes and their wires routed into grooves and covered with grout.

(a) (b)

Figure 4.3 (a) Anode being installed in grout filled hole. (b) Anode after installation.

The final step was to install the bulk anodes. These were installed only on two piles – control (104D) and a wrapped pile 104 C. The bulk anodes were 48 lb (21.8 kg) zinc blocks that were bolted to the pile 2.5 ft (0.73 m) below mean low water.

4.4.1 Junction Box

As mentioned earlier, the eight embedded anodes were connected using a single copper wire which created a loop between all of the anodes and the reinforcing cage (Fig. 4.4). The bulk anodes were connected to the reinforcement cage using a separate wire.

The wire leading from the anodes was routed into a junction box where it was connected to the reinforcement cage. This was done so that a switch could be used to disconnect the anodes. The junction box housed the data loggers used for monitoring CP performance. The wires for the reference electrodes were also routed into the junction box so that they were protected from the environment.

4.4.2 Data Collection

Anodic current information was recorded using commercially available data loggers. All readings were time-stamped and therefore the exact time when anodes were connected or disconnected for the NACE tests [4.16] was known. To determine the role of the bulk anodes in Pile 104 C and the unwrapped control 104D, they were wired to separate data loggers.

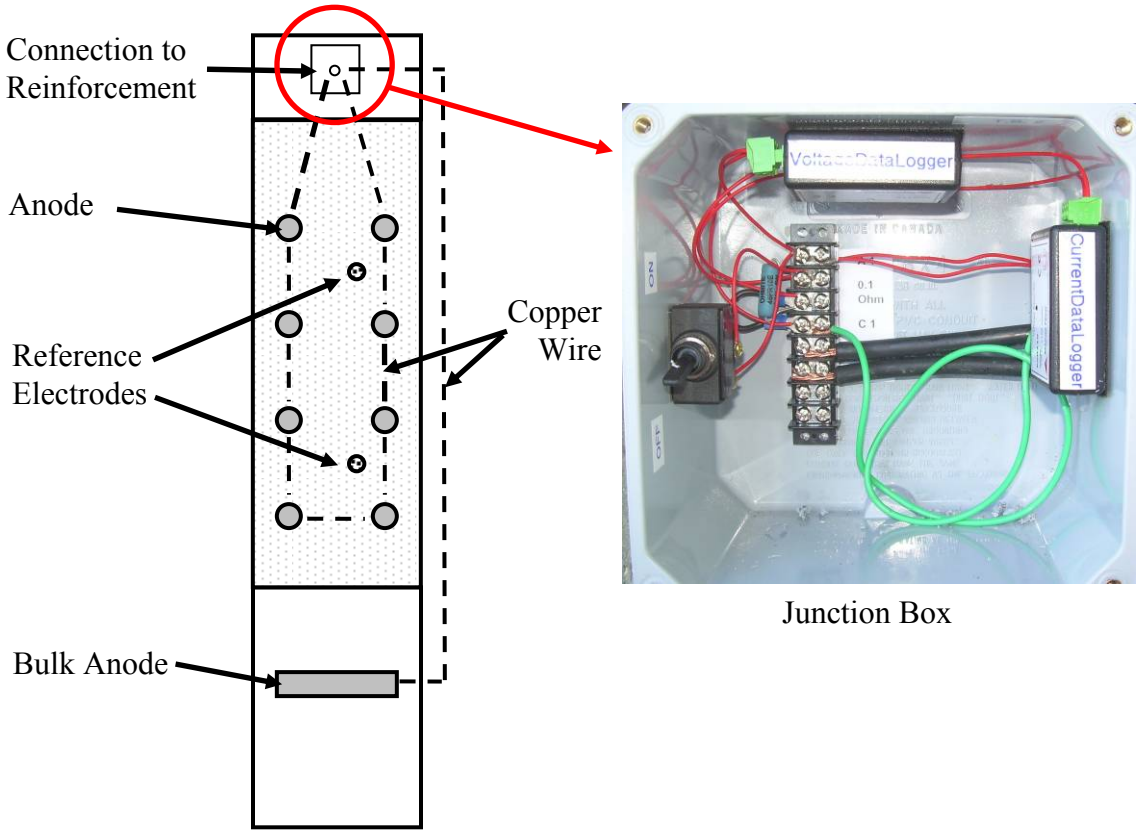

Figure 4.4 Schematic of anode wiring.

4.4.3 FRP Wrapping

The piles were wrapped after the CP system had been in place for over two months. This delay was to allow the system to stabilize. Preparation for the wrap began by scraping off all the marine growth within the targeted 6 ft (1.8m) region. Following

this, the piles were ground smooth and all edges rounded to a 2 in. (51 mm) radius using a grinder. The surface was then cleaned with fresh water using a 3000 psi (21 MPa) pressure washer to remove all of the debris generated by the grinding process.

Two glass fiber reinforced layers (GFRP) each 0.05 in. (1.27 mm) thick were applied to the prepared concrete surface. The 6 ft (1.8m) wrap extended 1 ft (30 cm) below the mean low water line (Fig. 4.2). After the GFRP was in place, a pressure bag was placed around the pile and inflated to provide a uniform 2 psi (14 kPa) pressure (Fig. 4.5a). This offset the tendency of the resin-saturated FRP to slide down the pile surface. Tests had shown that this system significantly improved bond [4.13]. A photo of the piles after removal of the pressure bags is shown in Figure 4.5b.

Figure 4.5 (a) Pressure bag on FRP wrapped pile. (b) Completed piles in bent.

4.4.4 Water Intrusion Damage

The junction boxes housing the data loggers were designed for normal outdoor use. However, conditions proved to be much more severe than anticipated and salt water entered the boxes, damaging some of the data loggers. Since there was no remote monitoring system in place, this damage was not immediately discovered. Following its discovery, a more robust system was designed in which all the data loggers were placed

in watertight enclosures, and all interior components made of stainless steel. Probes were added to the outside of the box so that tests to evaluate the effectiveness of the CP system could be conducted without opening the junction box thereby reducing the risk of water intrusion.

4.5 Results

Results from two series of tests conducted are presented. The first relates to "instant-off" tests conducted to determine the effectiveness of the installed CP system [4.14]. The second relates to the measurement of the anodic current that provides a measure of the level of galvanic protection afforded to the steel.

4.5.1 Instant-off Test

The effectiveness of a CP system is judged by the "instant-off" test in which the connection between the anodes and the reinforcement is temporarily disconnected, typically for 24 hours. Since cathodic protection essentially supplies electrons to the steel reinforcement, its potential becomes "more" negative ("polarized") with respect to a reference electrode as long as the anode remains connected. Temporary disconnection stops the supply of electrons; as a result the steel becomes "less negative" ("de-polarized") over this time frame.

Each "instant off" test therefore entails potential measurements on two consecutive days. On the first day, the anode is disconnected and an "instant off" potential reading taken. On the following day, the potential is read once again and the anode re-connected. Four series of "instant off" tests were conducted to evaluate the

effectiveness of the installed FRP-CP system over a 6 month period. The first test was conducted 26 days after the FRP wrap was in place. Subsequent tests were carried out after 53, 65 and 183 days. Results are summarized in Table 4.1.

Table 4.1 Summary of polarization decays from "instant-off" testing.

Pile	Days	Top			Bottom		
		Off (V)	Stabilized (V)	Decay (mV)	Off (V)	Stabilized (V)	Decay (mV)
Control (104D)	26	-0.720	-0.714	6	-1.116	-1.078	38
	53	-0.703	-0.694	9	-1.137	-1.120	17
	65	-0.726	-0.692	34	-1.144	-1.093	51
	183	-0.743	-0.705	38	-1.132	-1.044	88
FRP + Full CP (104C)	26	-0.776	-0.711	65	-1.014	-0.956	58
	53	-0.741	-0.665	76	-1.015	-0.924	91
	65	-0.748	-0.651	97	-1.023	-0.859	164
	183	-0.802	-0.664	138	-0.900	-0.791	109
FRP + Embedded Anodes (103A)	26	-0.743	-0.629	114	-1.014	-0.875	139
	53	-0.774	-0.622	152	-1.033	-0.850	183
	65	-0.782	-0.590	192	-1.057	-0.760	297
	183	-0.820	-0.579	241	-1.077	-0.734	343

Table 4.1 contains information for (1) the unwrapped control (104D) with both embedded and bulk anodes, (2) the FRP wrapped pile with the embedded and bulk anodes (104C) referred to as "FRP + full CP" and (3) the FRP wrapped pile with embedded anodes only (103A). Since there were two reference electrodes, two sets of "instant-off" tests were conducted for each pile - one with respect to the "top" reference electrode and the other with respect to the bottom reference electrode (Fig. 4.2). Only one of each type of pile was wrapped, as this investigation was a simple proof of concept for the FRP-CP system.

Three sets of measurements are presented from each test; the "instant off" voltage reading taken immediately after the anode is disconnected and the "stabilized" voltage

reading taken the following day approximately 24 hours later. The difference between these two readings is the "decay". All readings taken with respect to the embedded Ag/AgCl electrodes were converted to equivalent $Cu/CuSO_4$ readings by adding 113 mV that represents the difference between both electrodes with respect to the Standard Hydrogen Electrode (SHE).

Inspection of Table 4.1 shows that the potential decay was generally greater at the bottom than at the top. Thus, for the control the maximum decay was 38 mV at the top (after 183 days) compared to the maximum 88 mV (after 183 days) at the bottom. For the pile with the "full CP", the corresponding values were 138mV and 164mV. This trend was also followed by the pile with the embedded anodes (241 mV vs. 343 mV).

According to NACE [4.14], a cathodic protection system is effective if the potential decay exceeds 100mV with respect to a reference electrode. This criteria was met by the FRP wrapped piles (after 26 days by the FRP wrapped pile with the embedded anodes and after 183 days for the pile with FRP + Full CP but not by the control where the maximum decay was 88mV) indicating that the FRP-CP systems in place were effectively protecting the steel.

4.5.2 Galvanic Current

The instant off test indicates whether the CP system is working or not. However, it does not provide any information on the level of protection provided. This is given by the "current density" defined as the quotient of the measured anodic current and the total surface area of the protected steel. For the piles each reinforced by eight #8 bars that was

spirally wrapped by ¼ in (6.35 mm) spiral ties spaced at 9 in (23 cm) on center, the theoretical surface area was calculated as 13.75 ft^2 (1.28 m^2).

The anodic current was automatically recorded by the data loggers and the saved data was periodically downloaded from the bridge site. The current density was calculated by dividing the measured current by the theoretical area of steel protected 13.75 ft^2 (1.28 m^2). The anodic current is not constant but varies with concrete resistivity. This in turn is influenced by tide change. Wet concrete has a lower resistivity compared to dry concrete.

Figure 4.6 plots the variation in current density with time for the control, the FRP + full CP and the FRP with embedded anodes systems. In this plot, the current density is based on the daily average current. Inspection of this plot shows a number of discontinuities arising from the installation of the bulk anode on day 20, four instant-off tests (shown by arrows pointing upwards) and the failure of the data logger for the full FRP + CP pile (103A) due to salt water intrusion in the junction box.

Selected data extracted from Figure 4.6 is summarized in Table 4.2. This contains data for ten sets of measurements over the first 166 days. These are initially reported at 10-day intervals over the first 60 days followed by three readings taken on day 153, 160 and 166. Since the anodes remained connected, the steel continued to be cathodically protected though current readings for pile 103A were not saved. This resumed following replacement of the damaged data loggers by identical units. Thus, there is a discontinuity in the data reported.

Inspection of Table 4.2 shows that the current density is lowest for the pile with only the embedded anodes [1.18 mA/ft^2 to 3.17 mA/ft^2] (12.68 mA/m^2 to 34.17 mA/m^2)

and highest in the unwrapped control [2.3 mA/ft^2 to 12.69mA/ft^2] (24.78 mA/m^2 to 136.64 mA/m^2). For the FRP wrapped pile with the full CP the corresponding range is 2.32mA/ft^2 to 9.53mA/ft^2 (24 mA/m^2 to 102.6 mA/m^2). The peak value corresponds to measurements recorded following the installation of the bulk anode that provided additional current.

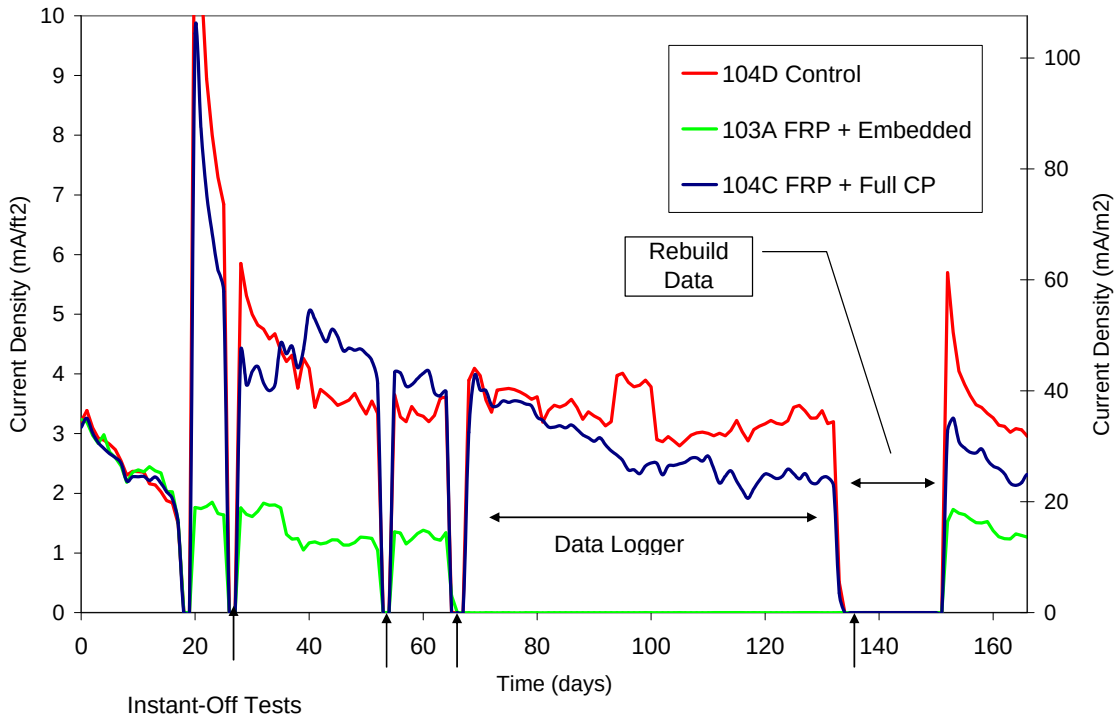

Figure 4.6 Average daily current density of the different systems.

In general, the current and the current density reduced with time from 3.23mA/ft^2 to 2.94mA/ft^2 (34.76 mA/m^2 to 31.67 mA/m^2) for the controls; 3.19mA/ft^2 to 2.32mA/ft^2 (34.29 mA/m^2 to 24 mA/m^2) for the FRP with full CP and 3.17mA/ft^2 to 1.46mA/ft^2 (34.17 mA/m^2 to 15.70 mA/m^2) for FRP with embedded anodes. This is shown more clearly in Figure 4.6 where the variation in current density with time is plotted.

The reduction in current density in the FRP wrapped piles indicates a slower corrosion rate since less current is required to protect the same amount of steel. The lower current draw also indicates that the anodes will be consumed at a lower rate meaning that they will last longer following Faraday's law. The slower corrosion rate again provides field confirmation of laboratory results that indicated that FRP slowed down the corrosion rate [4.1-4.3].

An estimate of the increased life provided by FRP can be made by comparing the anodic current draw for the full FRP-CP system (104C) with the control (104D). In the calculations, the current consumption was taken as 31.9 mA for 104C and 40.5 mA (104D) from Table 4.2 that represents the current consumption after 166 days. Using these values, the incorporation of FRP was found to increase the anode life by 27%. Since the anodic current fluctuates (Table 4.2) such an estimate is clearly an approximation. Nonetheless, it provides a quantitative measure of the benefit of combing cathodic protection with FRP wrapping.

Table 4.2 Current density of the different systems.

Days	Control (104D)			FRP + Full CP (104C)			FRP + Embedded Anodes (103A)		
	Current	Current Density		Current	Current Density		Current	Current Density	
	mA	mA/ft^2	mA/m^2	mA	mA/ft^2	mA/m^2	mA	mA/ft^2	mA/m^2
1	44.4	3.23	34.76	43.8	3.19	34.29	43.65	3.17	34.17
10	31.7	2.3	24.78	32.4	2.35	25.32	32.5	2.36	25.44
20	174.55	12.69	136.64	131.1	9.53	102.63	24.5	1.78	19.14
30	67.95	4.95	53.19	51.9	3.77	40.63	22.9	1.67	17.93
40	70.4	5.12	55.11	71.9	5.23	56.29	16.2	1.18	12.68
50	54.45	3.96	42.63	62.3	4.53	48.77	17.7	1.29	13.86
60	46.55	3.39	36.44	57	4.15	44.62	18.75	1.36	14.67
153	61.3	4.46	47.99	45.05	3.28	35.27	23.35	1.7	18.28
160	46.15	3.36	36.13	33.45	2.43	26.19	18.8	1.37	14.72
166	40.5	2.94	31.67	31.9	2.32	24	20.1	1.46	15.7

4.6 Discussion

This chapter presents results from a field demonstration project in which FRP wrap was combined with an embedded anode CP system to protect piles in tidal waters. The use of embedded anodes meant that the strengthening property of the FRP material was not compromised since it was directly bonded to the concrete surface making load transfer by shear possible. The FRP itself was bonded to the concrete surface using pressure bagging, a newly developed system [4.12-4.13]. Comprehensive laboratory tests have shown that pressure bagging can significantly improve FRP-concrete bond under dry, wet and submerged conditions.

As with any CP installation, the operation involves anode placement, completion of circuitry and connections to the reinforcing steel. All these operations involved drilling the concrete surface that can be time consuming without the right equipment. Additionally, data loggers were installed to allow monitoring of the CP system. These were all located in a protected junction box placed very close to the pile cap that is usually dry. These measures proved inadequate and water intruded into the junction box and damaged the data loggers. A more effective replacement box was designed and installed. Despite the enhanced protection, water intrusion occurred once again. However, silicone seals prevented damage to the data loggers. This experience shows how aggressive the environment is and the need to take extraordinary measures to protect the instrumentation.

The results of the instant-off tests indicate that the CP system is effective in polarizing the steel. However, NACE [4.14] criterion was only met by the FRP wrapped piles, not by the control (Table 4.1). No explanation for this may be found in the

literature. However, since later instant off potentials were more negative than the initial measurements, the CP was effective in polarizing the steel in the control as well.

Current densities calculated showed that the anodic current was lower in the FRP wrapped piles compared to the control indicating reduced corrosion rates (Table 4.2, Fig. 4.6). This confirmed findings from independent laboratory studies [4.1-4.3]. However, the current densities in all three piles met the minimum protection current densities of 0.93 – 1.86 mA/ft^2 (10-20 mA/m^2) [4-22].

In the conventional Life Jacket system, bulk anodes are used to protect the steel in the submerged region [4.11] and also control the anodic current draw during low tide. This reduces costs since it allows for shorter jackets and also increases the life of the anode. In contrast, the cost of extending the FRP wrap below the mean low water line is not as excessive. In this study the FRP wrap extended 1 ft below the mean low water line as shown in Figure 4.2. Preliminary findings from this study indicate that the performance of the FRP wrap without the bulk anodes met all NACE requirements for cathodic protection. This suggests that bulk anodes may not be needed for FRP wraps incorporating embedded anodes that extend below the mean low water line.

As the intent of the research project was to evaluate the feasibility of developing an embedded anode CP system that could be combined with a FRP wrap, it was not possible to conduct alternative investigations that could determine whether bulk anodes by themselves would provide sufficient protection to stop corrosion in steel [4.24]. Such a system would be far easier to install and make FRP even more cost effective.

4.7 Summary

This chapter presents results from a pilot study which explored the effectiveness of an embedded sacrificial anode system inside a FRP wrap for repairing piles in tidal waters. The piles were instrumented to allow the effectiveness of the CP system to be evaluated using established NACE protocol [4.14]. The concept developed is general and can be used for protecting columns in dry regions that are subject to de-icing salt water run-off from bridge expansion joints.

Based on the data presented, the following conclusions may be drawn:

(1) Results of "instant off" tests indicate that the embedded anode system successfully polarized steel inside the FRP wrap (Table 4.1).

(2) Measured protective currents were higher in the unwrapped control compared to the FRP wrapped piles (Table 4.2, Fig. 4.6). This indicates lower corrosion rates and confirms findings from laboratory studies that have shown FRP tended to slow down the corrosion rate. Lower currents imply less anode consumption and therefore longer service life for the anodes in the FRP wrapped piles.

(3) A pile with embedded anodes alone provided similar corrosion protection compared to one with both the embedded and bulk anodes (Table 4.2, Fig. 4.6). This suggests that bulk anodes may not be required if the FRP wrap is extended below the mean low water line.

(4) Special measures are needed to protect all electrical connections inside the junction boxes to prevent damage by salt water intrusion.

5 Remote Monitoring/Control of a Cathodic Protection System

Cathodic protection systems are the only proven means of protecting a structure once corrosion has commenced, and can even supply sufficient current to prevent its initiation. The design of these systems typically revolves around the use of either magnesium or zinc anodes depending on water quality. In areas of highly variable water quality, neither material is ideally suited for year-round usage when implementing a sacrificial anode system. Remote monitoring of cathodic protection systems is one way of assessing performance and can alert responsible parties to problems within hours of a system failure. Additionally, these systems can be used to control and regulate the flow of electrons so that the steel is adequately protected while increasing the useful lifetime of the anodes. This chapter discusses an eighteen month program for two bridges along Interstate 75 where such a system was implemented.

5.1 Introduction

Remote monitoring systems are becoming more popular due to enhancements in technology which have enabled the devices to perform a wide range of tasks previously not possible while maintaining economy. These advancements in technology have also reduced the power demand of the sensors, resulting in systems that can perform adequately despite being in locations where external power sources do not exist.

For bridges, inspections are typically performed according to a set schedule which can range from several months to years unless an incident occurs which would require

special inspection. Between site visits, there are countless undocumented events that can affect the overall structural welfare. Without some means of monitoring these activities, damage to structures can go unnoticed for extended periods of time, possibly compounding the magnitude before the situation is addressed.

In addition to monitoring events, remote monitoring systems are capable of providing a continuous log of data obtained from a variety of sensors (e.g. temperature, strain/load, deflection, etc.). This provides an unprecedented amount of information which can enable interested bodies to better understand the behavior of the environment and the structure. Newer devices are also capable of issuing commands, thereby enabling activities to be initiated and terminated without the need of a technician onsite.

This chapter describes the installation and evaluation of a system designed to monitor the site environmental conditions, anodic current being provided to a structure, and remote control of a system designed to regulate the anodic current. The remote system provided periodic readings (e.g. min, hour, or day) enabling trends to be observed that would not normally be observed using traditional assessment methods

5.2 Background

In the past, remote monitoring was largely focused in two main areas. The first area was in the monitoring of storage devices for nuclear and other hazardous waste products [5.1-5.6]. The US Department of energy was deeply interested in sensors and robots that could be remotely operated to detect faults in storage tanks. These devices greatly reduced the need for human inspections and had a corresponding reduction in the risk to human life from contamination of corroded vessels. The remote sensors ranged

from simple devices to detect cracks in tanks to cameras on fully automated robots that could visually determine if a 55 gallon drum was tipped, dented, or corroded [5.5].

The other area of interest was in the monitoring of pipelines for the chemical industry [5.7-5.13]. These pipeline may extend for hundred of miles, and could transport toxic or explosive chemicals or gasses. The corrosion monitoring devices detected any areas of reduced steel cross section or cracks and made monitoring parties immediately aware of the situation. It is not until recently that remote monitoring has been incorporated into general civil engineering infrastructure.

Studies have shown that more focus has been made on using remote monitoring elements on superstructure elements than on those of the substructure [5.14-5.17]. In its most basic state, remote monitoring involves taking measurements that can be transmitted via cellular, radio, or phone lines to an operations center where the data is analyzed. These systems essentially only vary in the types and number of measurements taken and transmitted. Some measure, store, and send periodically; others measure, send and have no provisions for storage. Few bridge systems, though, involve control systems that physically change functions of on-site devices.

In a previous project [5.18], on-site data loggers were able to provide useful data about the level of cathodic protection provided to the steel reinforcement. Unfortunately, the devices were not robust enough to withstand the elements, and data acquisition still required considerable time and expense to travel to the monitoring site routinely. However, inclement weather sometimes restricted access to the site. Use of a remote monitoring system would have not only have provided continuous access to the data but

also identified problems immediately, instead of months later after the data was acquired and analyzed.

Systems designed to monitor cathodic protection should at a minimum be able to track both the anodic current and steel potential. Therein, criteria for proper cathodic protection usage have been suggested for both current density and steel potential [5.19 and 5.20].

5.2.1 Current Density

One of the means of assessing the effectiveness of a cathodic protection system is the current density or current per unit area of exposed steel. Revie [5.19] states that for steel in "stationary fresh water", a current density of 11 to 56 mA/m^2 (1.02 to 6.05 mA/ft^2) is required. For steel in "moving, oxygenated fresh water", the density range is increased to 54 to 160 mA/m^2 (5.0 to 14.9 mA/ft^2), and for steel in "seawater" this range is typically between 32 and 110 mA/m^2(2.9 to 10.2 mA/ft^2), but can be as high as 160 to 430 mA/m^2 (14.8 to 39.9 mA/ft^2) in "cold and arctic waters."

5.2.2 Steel Polarization

A more common, often easier, means of determining the effectiveness of a system is by measuring the level of polarization achieved by the steel. Criteria have been established based on adequate protection of underground or submerged metallic pipes [5.20]. These criteria are commonly applied to all ferrous structures whereby the polarized potential (in-circuit) is at least 850 mV less than that of a Copper-Copper Sulfate reference electrode (or -754 w.r.t. Ag/AgCl). Alternately, if a structure achieves a

depolarization value of at least 100 mV below the natural potential, when comparing the instant-off (value immediately after the CP system is disconnected) to the natural potential, the system is also deemed to be effective.

5.2.3 Anode Selection

The most common materials used as sacrificial anodes for protecting steel are zinc and magnesium. The selection has traditionally been based on the resistivity of the fluid as shown in Table 5.1 [5.21]. Typical resistivity values for fresh and salt water can be on the order of 3000 Ω-cm and 20 Ω-cm, respectively [5.22]. Hence, zinc anodes are more often used in saltwater, and magnesium typically restricted to freshwater use. Brackish water would therefore be used to define water with a resistivity range between that of fresh and saltwater, and may be better suited to either anode material (site dependent), as low resistivity leads to a high rate of self consumption in magnesium anodes.

This chapter discusses the design and implementation of a remote monitoring/cathodic protection system for a site with variable water conditions wherein the anodic current and steel potential were both monitored for effectiveness and tailored to satisfy the above criteria. Without definitive resistivity measurements for a brackish water site, magnesium anodes provide assurance that both current and potential criteria are met. However, unnecessary reduction in anode life may result from both self consumption and the anodic current provided to the steel. To address this issue, a limited study was also conducted to quantify the role that self consumption plays on the lifetime of magnesium anodes specific to this environment.

Table 5.1 Recommended anodic material based on resistivity [5.21]

Electrolyte Resistivity (Ω-cm)	Effective Anode Material		Degree of Corrosivity
0 – 500	Zn		Very High
500 - 1000			High
1500		Mg	Moderate
2000			
>2000			Mild to Negligible

5.3 Objectives

The main objectives of the study were to design and implement a remote monitoring system to document the effectiveness of cathodic protection systems. The system was further enhanced to regulate/ control both the anodic current and steel potential. To this end, three general tasks were undertaken:

(1) Install water resistivity gages with a basic remotely monitored system.

(2) Install new anodes with current monitoring capabilities.

(3) Devise and demonstrate a current and potential regulation system.

5.4 Case Study

The portion of Interstate 75 used in this study has numerous canals, resulting in many two lane, short span bridges used for crossing these canals. The rainfall varies significantly throughout the year, causing water levels in the canals to fluctuate drastically. This results in commensurate variations in resistivity.

As part of an FDOT funded study, two bridges (herein referred to as Bridge 1 and Bridge 2) were selected for evaluation. Both bridges were similar with three short spans supported by two pile bents (in water) and two end bents (Fig. 5.1). Each pile bent was supported by seven steel H-piles (HP12x84). The upper most portion of the piles was jacketed in concrete down to a height just below the normal water level. Three

magnesium anodes were used to prevent corrosion installed at ¼, ½, and ¾ points between the bottom of the jacket and the mud line.

Figure 5.1 Bridge 1 used for evaluation of systems.

After an extensive underwater survey of the existing anode conditions and scattered debris left from construction, one pile from each of the two bents from Bridge 1 and one pile from Bridge 2 were selected (3 total). These piles measured no electrical connectivity to other piles that might otherwise affect the study findings.

The field installation of the remote monitoring systems was conducted in two phases to measure:

(1) Water resistivity, water and air temperature, and relative humidity.

(2) Additional measurements of water depth, anodic current, and steel potential.

5.4.1 Remote Monitoring System

The essential components of a remote monitoring system are (1) remote monitoring unit(s) (2) a communications network and an (3) operations center [5.23]. The specific system used at a site depends on the type of sensors and data requirements for the project. Some examples of monitoring systems and applications are given in References 5.24 and 5.25.

There were two types of monitoring systems utilized in this project, the first (master) was a unit capable of direct communication with the operations center (Fig. 5.2a). The second, (slave) relied on the master unit for transfer of information (Fig. 5.2b). In addition, the master units also contained all of the devices for environmental monitoring. Both systems utilized components from Campbell Scientific®, with the main difference being that the master units contained CR 1000 data-loggers while the slave units contained CR 800 versions.

(a) (b)

Figure 5.2 Remote monitoring boxes configured as (a) master and (b) slave units.

5.5 Installation

5.5.1 Phase I

In the Phase I installation, a single data logger was mounted on Bridge 1. This device consisted of a data collection unit outfitted with devices for monitoring air temperature, water temperature, and resistivity (Fig. 5.3). After initial installation, it was determined that the original antenna was inadequate for communication with the device

because of its location, therefore that antenna was replaced by an omni-directional unit. Phase 1 monitoring lasted 147 days.

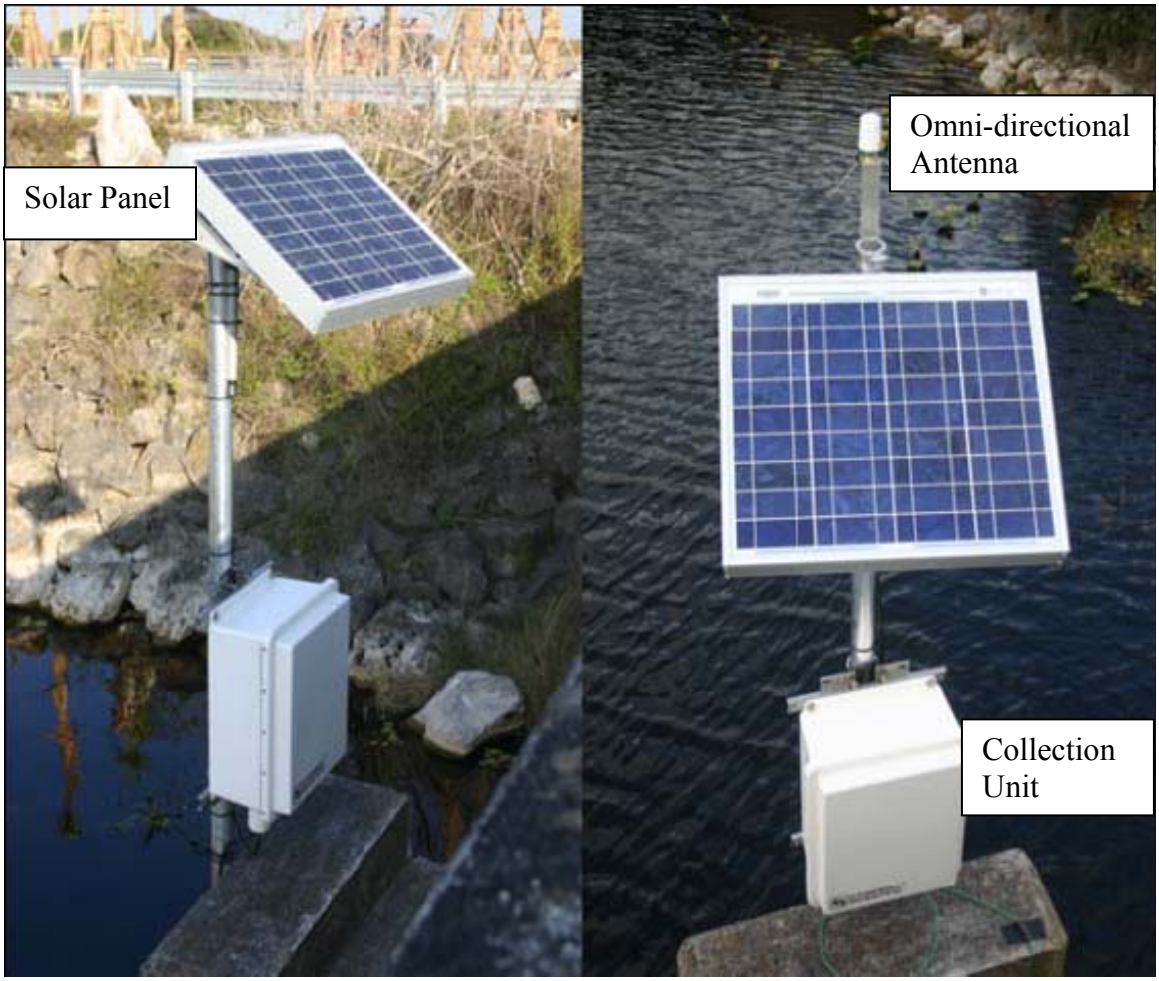

Figure 5.3 Data collection unit as installed (left);
upgraded with omni-directional antenna(right).

5.5.2 Phase II

Following the successful installation of the remote monitoring system in Phase I, the remaining systems were installed. The final instrumentation scheme was established (Table 5.2) and the northern most piles on the bridge were selected for instrumentation.

Each of the three anodes in each pile was connected to its own channel on the data loggers, to determine if any one anode was providing noticeably more current than

another anode on the same pile. Each pile was also connected to an Ag/AgCl reference electrode which was used to establish the level of polarization achieved by the cathodic protection system. In addition, there was a weather station present at both bridge sites which recorded local atmospheric data. As there was no need for multiple weather stations on one site, it can be seen in Table 5.2 that Bridge 2 – Pier 3 did not have any of these systems installed.

Table 5.2 Instrumentation scheme for Bridge 1 and 2 (number of sensors).

Bridge and Pier	Pile no.	Current	Potential	Resistivity	Water Temp	Air Temp	Water Level
1/ Pier 2	7	3	1	1	1	1	1
1/ Pier 3	7	3	1	0	0	0	0
2/ Pier 2	7	3	1	1	1	1	1

5.6 Results

5.6.1 Phase I

The first 147 days of monitoring are reported on a separate graph (Fig. 5.4) that illustrates the variability of conditions of the site over the first five months. During that time, the water temperature varied by over 10 ^{o}C (18 ^{o}F), the air temperature by 30 ^{o}C (54 ^{o}F) and the resistivity ranged from approximately 1400 Ω-cm to 2400 Ω-cm.

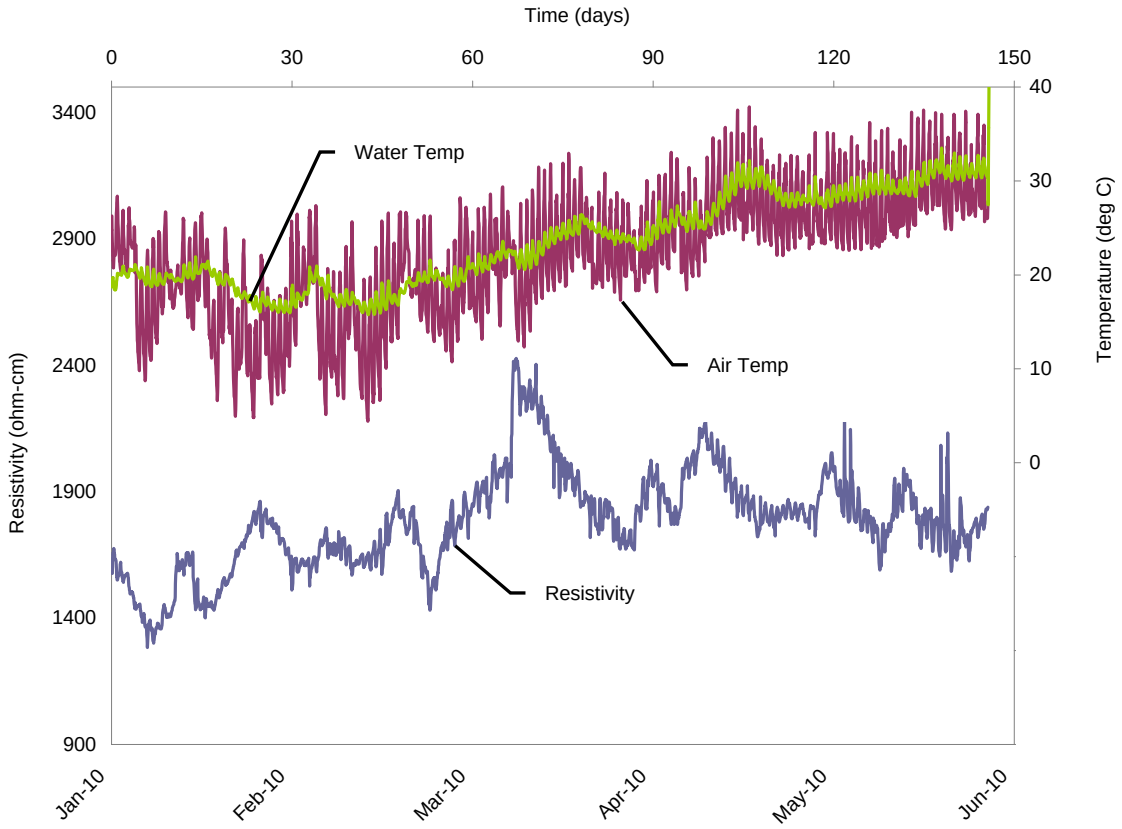

Figure 5.4 Water resistivity and air temperature for Bridge 1.

5.6.2 Phase II

Phase II commenced on day 148 from the initial monitoring date. As the data for all piles on both bridges shows similar trends, the values for Bridge 2 are presented in the graphs below. For this reason, many of the plots show data commencing on day 148 with the exception of plots containing the data from both bridges.

5.6.2.1 Resistivity

The resistivity of both bridges was plotted in Figure 5.5 against the anode applicability criterion from Table 5.1. Inspection of this plot shows that only between the period of ~ Day 350 to 540, corresponding to February to July of 2011, the resistivity of the water was below 1500 Ω-cm, making zinc the preferred anode. Zinc anodes are

generally preferred in saltwater conditions, where the rate of self consumption of magnesium is so great that they are not an ideal anode. The lowest recorded reading from the monitoring period, however, was only 900 Ω-cm, which is 45 times greater than the resistivity of saltwater (~20 Ω-cm). This data suggests that magnesium anodes may be suitable for use year round, if the rate of self consumption during this period of lowest resistivity is not of great concern.

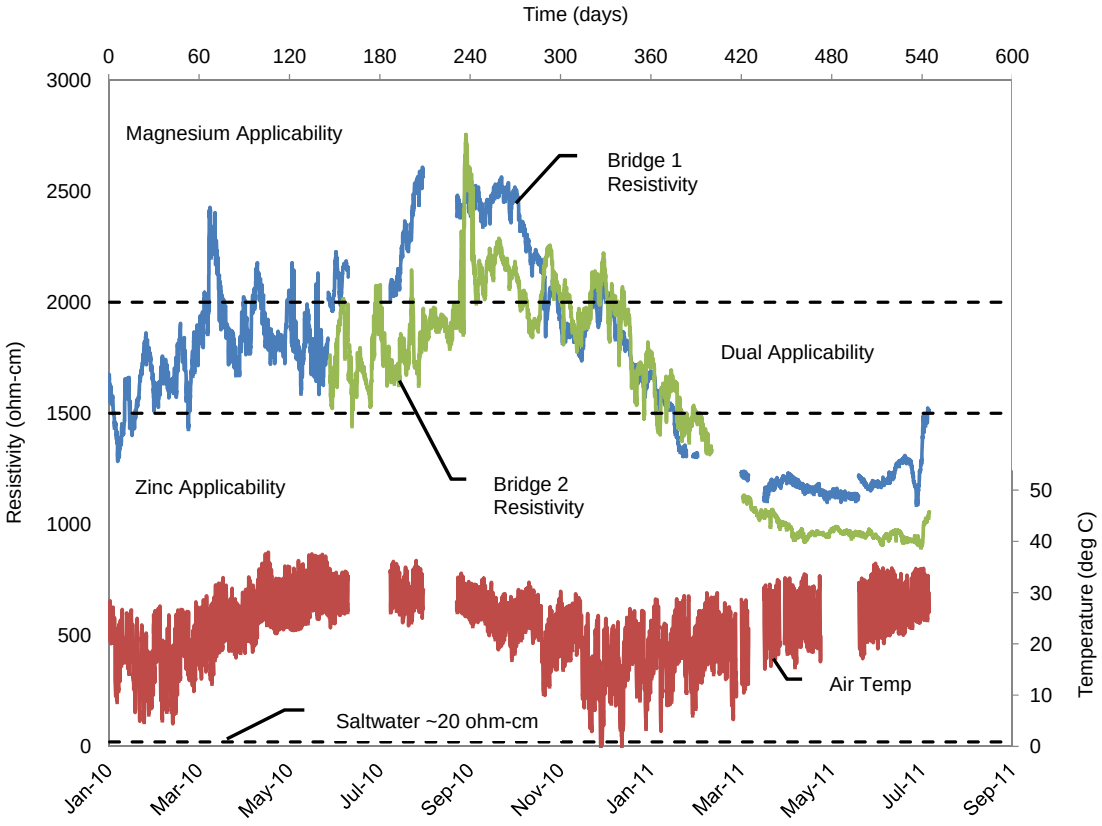

Figure 5.5 Resistivity plot of both bridges along with daily temperature variation.

5.6.2.2 Anodic Current

As mentioned earlier, a current density of 11 to 56 mA/m^2 (1.02 to 6.05 mA/ft^2) is required for steel in *stationary fresh water*. To assess the current being provided by each anode, individual currents were monitored for all anodes on all three piles. The piles were assumed to be HP12x84 1.83 m (6 ft) with approximately 3 m (10 ft) of steel

exposed between the concrete jacket and the mud-line. This meant that for a 3 m (10 ft) length with three anodes, each anode would be responsible for protecting a nominal steel area of 1.9 m^2 (20 ft^2)/anode. All three anodes yielded almost identical data for the three monitored piers, therefore the averaged current data for Bridge 2 is presented in Figure 5.6.

In Figure 5.6, points of interest are identified as "A" to "E" and are defined below in the legend. Of note is that the anodes are providing an average current density far in excess of 11 mA/m^2 (1.02 mA/ft^2) with the exception of the zone labeled as "E", corresponding to polarization investigations explained later. This suggests that current regulation is possible.

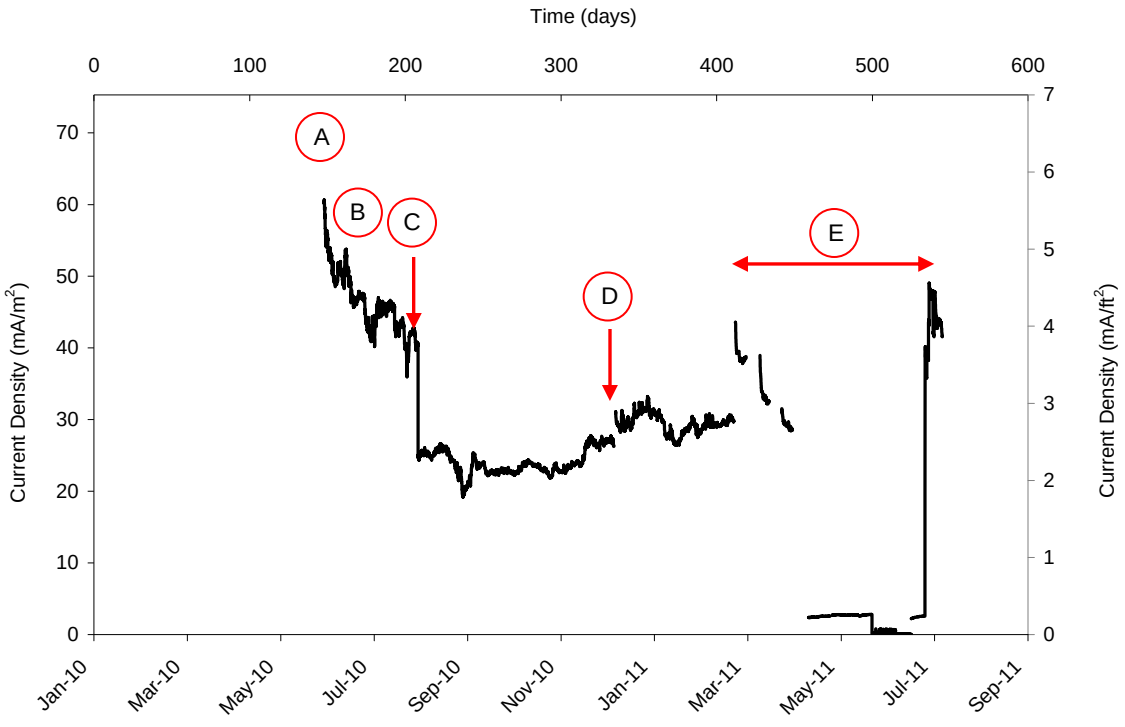

(A)- Anode energizing using 0.3 Ω shunt. Initial current 140 mA (7 mA/ft^2; 75.3 mA/m^2)
(B)- Current variation
(C)- Shunt resistance changed to 4 Ω
(D)- Preliminary instant-off test (December 2010, Shunt resistance changed to 3 Ω
(E)- Instant-off testing commenced on field piles (March 2011)

Figure 5.6 Average anode current for Bridge 2.

5.6.2.3 Steel Polarization

The on potential of the steel can be used as a means for assessing the performance of a CP system. NACE [5.7] requires an on-potential of -850 mV measured with a $Cu/CuSO_4$ reference electrode, considering voltage drops due to external sources. This corresponds to an on-potential of -0.754 mV measured against the Ag/AgCl electrode used in this project. The on-potential for both bridges was recorded hourly. Initially, both bridges had periods where the potential was more negative than 0.754 mV, however as the effect of the ohmic resistance of the fluid was unknown, these values could not be used for proper assessment. In addition, the potential of the steel fluctuated greatly without a corresponding change in the current being provided by the anodes, suggesting that there was an issue with the accuracy of the readings obtained by the electrodes. Depolarization measurements were therefore necessary to provide a more accurate picture of the effectiveness of the system. These tests were performed in the later portions of the study and are responsible for the great fluctuations in steel potential observed between March and July 2011 in Figure 5.7. The depolarization testing is described in the "Current Regulation Procedure" portion of the chapter.

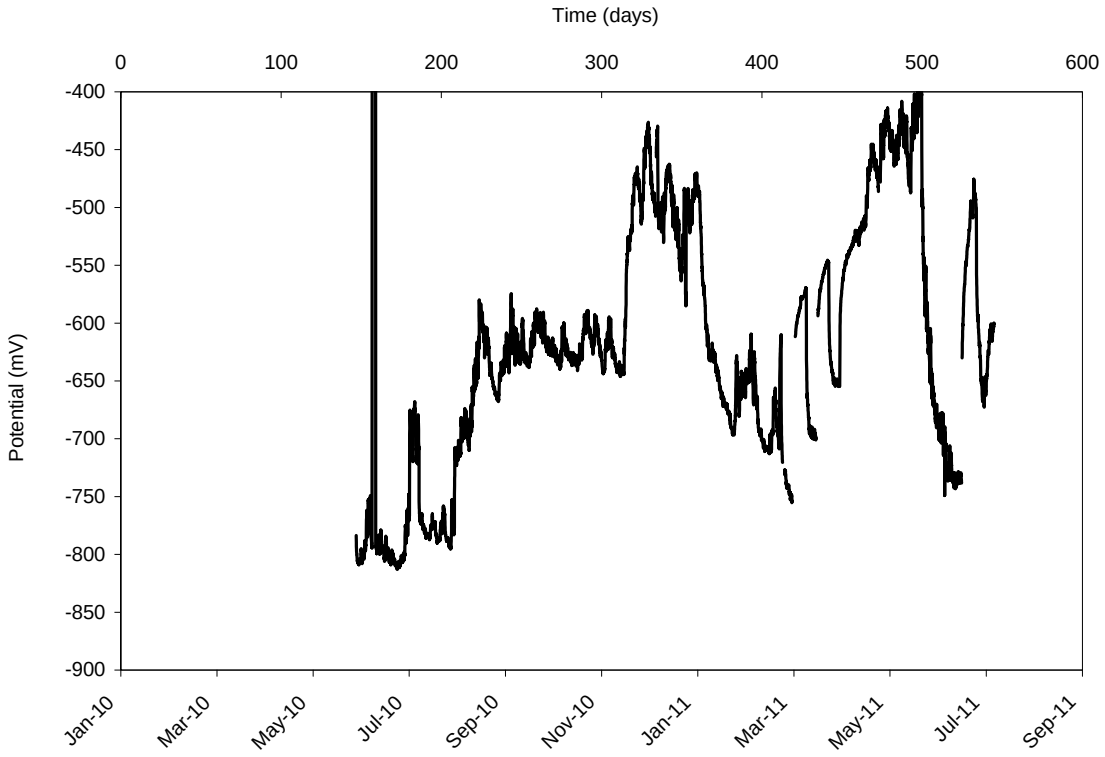

Figure 5.7 Steel potential for Bridge 2.

5.6.2.4 Water Level

The water level of the channel was obtained by measuring the distance from the R50 A-L acoustic sensor to the bottom of the channel. The recorded distance from the acoustic sensor to the water was then subtracted from this value to get the depth of the water in the channel. The depth for Bridge 2 was plotted along with the corresponding water resistivity in Figure 5.8. The figure indicates that there is a loose linear relationship between water elevation and resistivity that was also seen for Bridge 1. This relationship suggests that the water level affects the concentration of the particles held in suspension, meaning that a higher water level represents a lower particle concentration and therefore a higher resistivity. This data also suggests that an indication of the resistivity can be assumed based on the depth of the water in the channel.

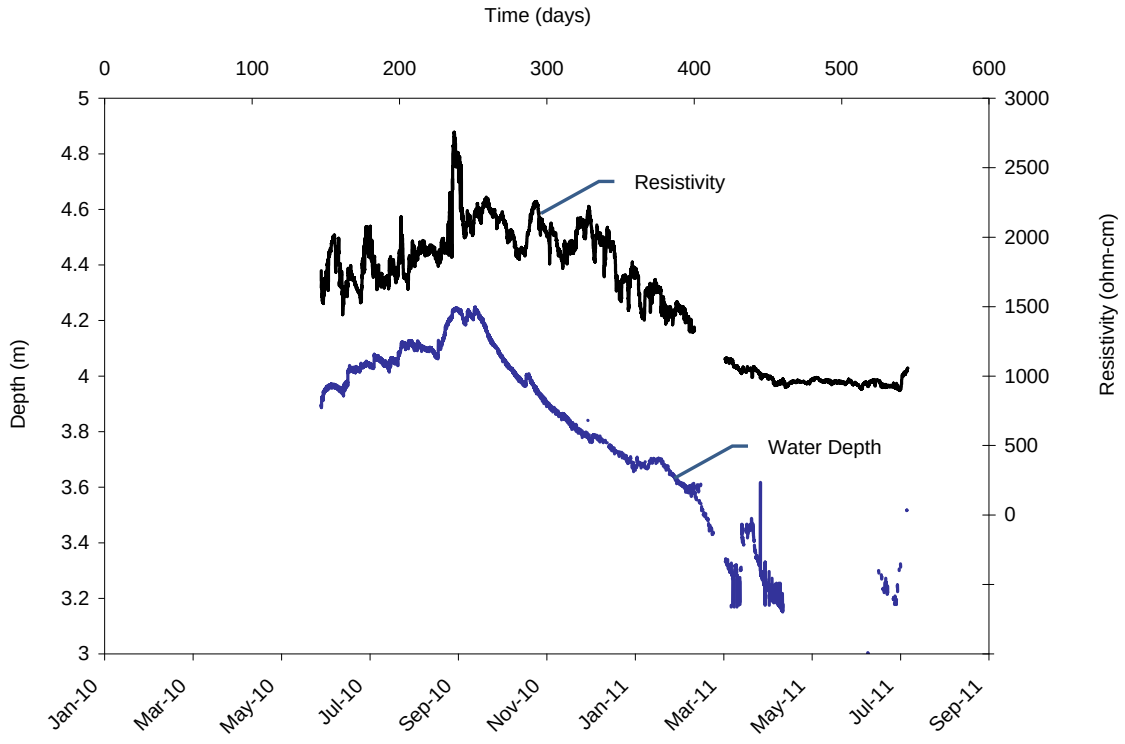

Figure 5.8 Water level and resistivity for Bridge 2.

5.7 Current Regulation Device

A device was designed that could regulate the in-circuit resistance between the anode and the steel. The device created incorporated latching relays to physically engage resistors in parallel, thereby altering the overall resistance. This device used a LM339 comparator to compare an excitation voltage from the data-logger, as specified by the command center, to a pre-set range of voltages. Depending on the intensity of the excitation voltage, the LM339 will engage 1, 2, 3 or all 4 relays, thereby putting the corresponding resistors in circuit parallel to each other. A picture of the device is shown in Figure 5.9.

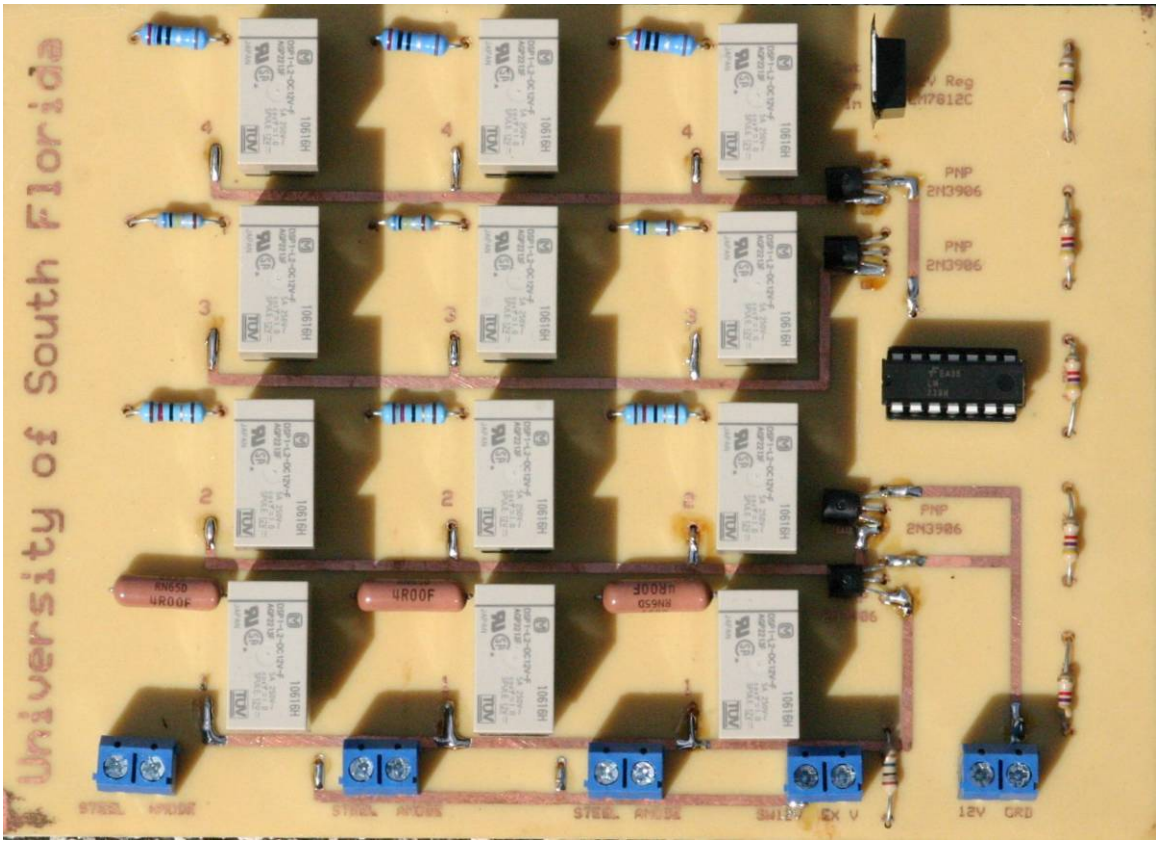

Figure 5.9 Regulating resistor circuit.

5.7.1 Circuit Testing

After the circuit was designed and tested in the laboratory, it was installed on the instrumented pier for Bridge 2. The circuit was installed with a 4 Ω, a 12 Ω, a 6 Ω, and a 2 Ω resistor for each anode; this gave resulting parallel resistances of 4, 3, 2 or 1 Ω for the anodes. The range of 1 Ω to 4 Ω appeared to encompass the full range of resistors that could regulate the anodic current while still providing an adequate density to achieve satisfactory protection. The device was tested over approximately 9 days with different resistances. The results of this are plotted in Figure 5.10.

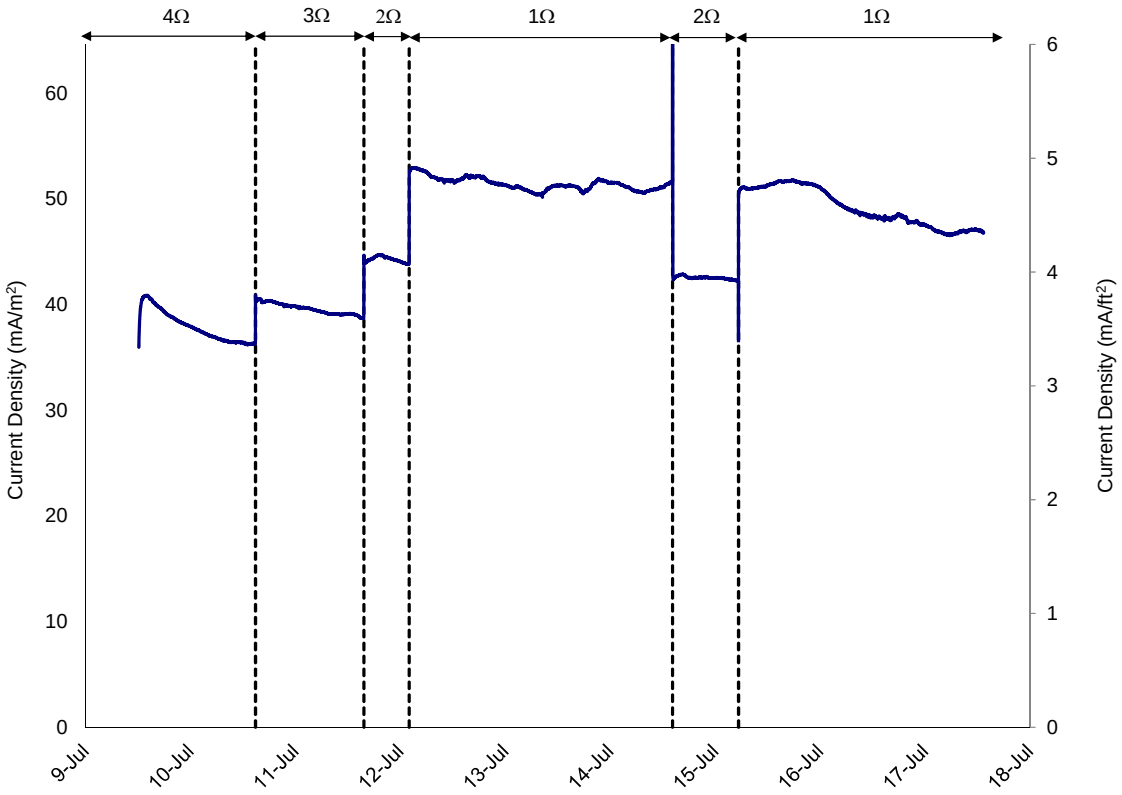

Figure 5.10 Current density using regulating resistance circuit.

The evaluation of the device was done when the resistivity of the water was ~900 Ω-cm, representing the time of highest self consumption. During that period, the 4 Ω resistor provided a current density of over 32.3 mA/m^2 (3 mA/ft^2), almost three times the minimum required. This suggests that the device would be capable, through the use of a lower resistance value, of providing adequate protection when the resistivity of the water is greater.

5.8 Regulation Procedure

While the accuracy of the reference electrodes was questionable throughout the monitoring period (shown by the unexplained and drastic shifts in potential seen in Figure 5.7), the devices were still capable of performing depolarization testing. This is

done by comparing the potential of the steel one second after the anodes are disconnected "instant-off" to the potential after the steel has depolarized. NACE [5.7] Item 6.2.2.1.3 states that a 100 mV depolarization can represent an adequate level of protection. The regulating resistance circuit allowed these tests to be performed by simultaneously disconnecting all three anodes from the circuit. This was done by disengaging all of the resistors in parallel for all the anodes. A relationship between current density, in circuit resistance, and steel depolarization was then developed from this data and plotted in Figure 5.11.

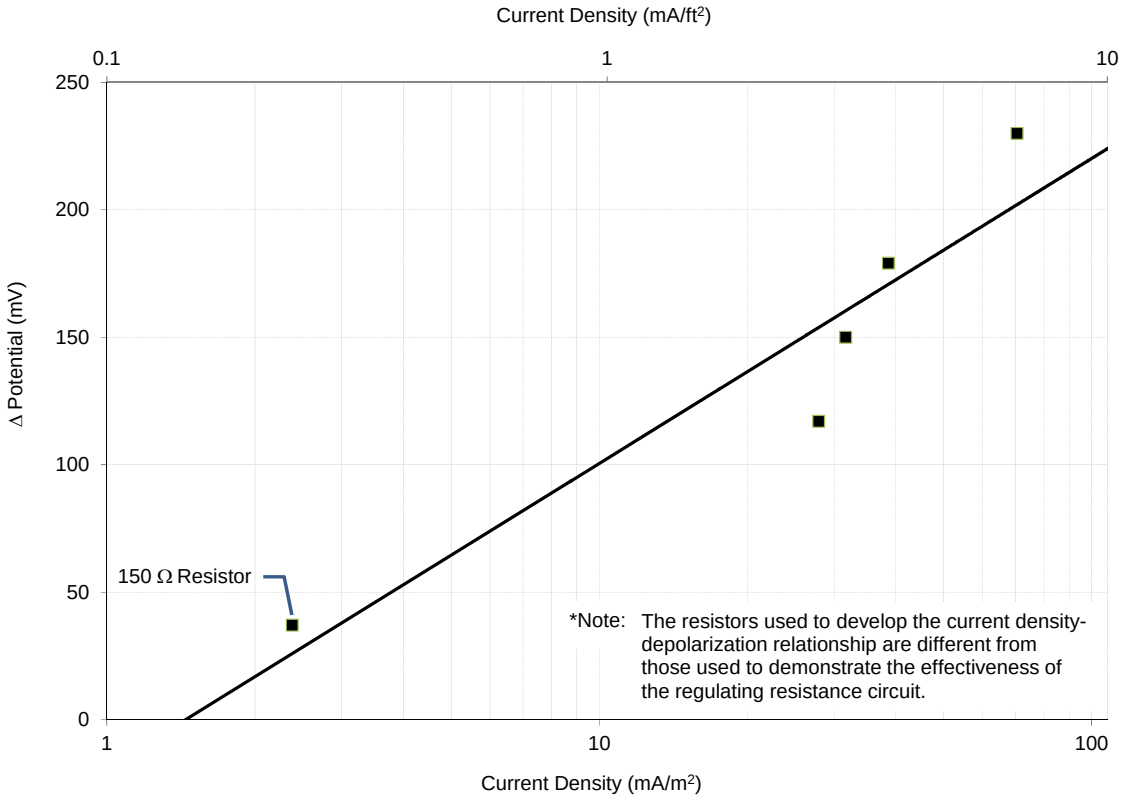

Figure 5.11 Current density-depolarization relationship.

The data plotted in Figure 5.11 indicates that for all of the resistors selected for all three piles, the only time when the depolarization was less than 100 mV was when a 150 Ω resistor were installed. The graph also indicates that a current density of over 21.5

mA/m^2 (2 $mA/ft^{2)}$ will provide an adequate level of polarization in all cases. The procedure for current regulation is therefore simply to alter the in-circuit resistance to limit the current being provided to the anodes while providing a minimum current density of 21.5 mA/m^2 (2 mA/ft^2).

5.8.1 Self Consumption

While not discussed in any great length, the regulation of the anodic current might not truly lengthen the useful service lives of the anodes if the rate of self consumption is high, so this issue needed to be addressed.

Traditionally, the self consumption is factored into a magnesium anode design by using an efficiency factor of approximately 0.5, meaning that only ½ of the useful anode mass will be used to protect the structure while the other portion is lost due to self consumption. Such a correlation would significantly reduce the expected service life of the anodes, and so a determination of the actual conditions at the bridges of interest was deemed necessary to establish if a more precise estimate of the effect of self consumption could be possible.

A limited study were therefore performed during the period when the water resistivity was lowest (~1000 Ω-cm) to evaluate the self consumption of magnesium in this environment. 20.3 cm (8 in) diameter magnesium discs were mounted on stands and electrically isolated from each other shown in Figure 5.12. A total of six specimens were submerged at each of the monitoring sites and one set was recovered periodically until all were retrieved. This mass before and after submersion were recorded, and the difference was divided by the number of days submerged to obtain a value of mass lost per time.

This value was then divided by the surface are of the anodes to obtain a mass lost per unit area per time. This value was then applied to the dimension of the anodes installed on the piles in order to obtain an equivalent rate of self consumption.

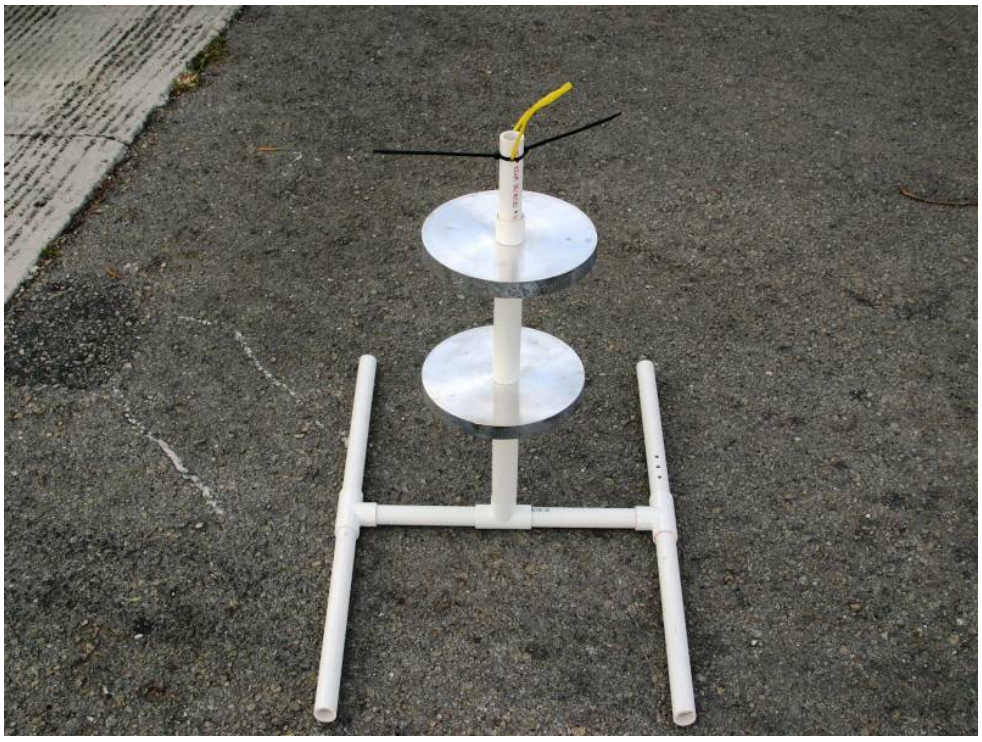

Figure 5.12 Magnesium specimens mounted on stand prior to submersion.

The study determined that the rate of self consumption for the 10.9 kg (24 lb) anodes at both bridge sites would be approximately 69 g/year (0.15 lbs/year) at Bridge 1, and 119 g/year (0.26 lbs/year) at Bridge 2 (full data can be found in appendix D). These values were then calculated to represent current densities of 0.87 mA/ft^2 and 1.51 mA/ft^2 respectively for the bridges, if this mass loss was equivalent to an anodic current being provided to the steel. The use of these values was then applied to the projected service lives based on observed current densities, and for Bridge 1, the lifetime of the anodes can be increased from 19 year to 37 using a 5 Ω resistor, while Bridge 2 can be increased

from 14 to 26 years for the same value (Sample Calculations can be found in Appendix E). While it is not feasible to utilize a 5 Ω resistor year round for the bridges, this evaluation suggests that regulation of the in-circuit resistance should have a respectable increase on the service life of the anodes.

5.9 Discussion

This chapter presents results from a field demonstration project in which a remote monitoring system was used to obtain data on the environmental conditions and performance of a sacrificial anode cathodic protection system. In addition, a circuit was designed to regulate the flow of current being provided to the pile by the anodes.

The results indicate that all of the sensors performed adequately and are therefore suitable for use in long term monitoring projects. There were no instances where the system lost power, suggesting that a solar powered unit would be capable of operating reliably in extremely remote areas.

As the measurements of the self consumption rate of the magnesium anodes indicated that the effect was relatively small, current regulation appears to be a feasible means of extending the anode service life.

5.10 Summary

This chapter discusses the successful implementation, monitoring and remote functionality of a system developed to operate in remote regions. The environmental conditions and effects on the performance of the cathodic protection were monitored, and a system for current regulation was successfully tested.

From the data presented, the following conclusions may be drawn:

(1) The remote monitoring and control system operated successfully over an extended period of time and under aggressive environmental conditions.

(2) The commercially available resistivity probe selected for the project preformed well. The only information processing problems encountered were with a faulty data logger and cellular modem. The data logger and modem were replaced and the cellular connection was enhanced by replacing the standard antenna with a high gain antenna. It is likely that the problems experienced with the faulty data logger were due to lightning damage.

(3) For the duration of the study, the water resistivity ranged from about 1000 to 2700 Ω-cm. Based on the US Army Corps of Engineers criteria in Table 5.1 and illustrated in Figure 5.5, magnesium anodes are suitable for about nine months of the year. However, this study showed that even in those months, the anodic current was in a range that could permit regulation using the remote switching circuit developed in this project. In the remaining three months, the water resistivity fell below the recommended usage range for magnesium anodes making circuit resistance regulation highly desirable to assure anode longevity. The same system also allows de-polarization tests to be performed remotely.

(4) Water resistivity was found to be lower when the water level decreased (Fig. 5.8), suggesting the possibility of estimating water resistivity from the water depth after an appropriate calibration period, as a separate verification measure.

(5) A limited study was conducted to determine the self-consumption rate of the magnesium anodes. For the period of lowest water resistivity it was estimated that the self-consumption rate of a typical 10.9 kg (24 lb) magnesium anode was 69 to 119 g/year (0.15 to 0.26 lb/year).

(6) A prototype resistance regulating circuit was designed, fabricated and tested on-site to improve the efficiency of sacrificial cathodic protection system by extending the life of the anodes. The circuit can also be used to conduct remote instant-off, depolarization, or polarization tests and also to vary the in-circuit resistance of the anodes to regulate the current draw. That approach resulted in the projected useful anode life of 19 to 37 years for Bridge 1 and 14 to 26 years for Bridge 2

(7) A logic decision criterion based on remotely acquired de-polarization data was established for when to change anodes or anode current resistance. This criterion states that the anodic current should be maintained at a density as close to 21.5 mA/m^2 (2 mA/ft^2) as feasibly possible without going below this threshold value. With current regulations, it is therefore possible to use magnesium anodes year round.

(8) The prototype circuits were also successfully used to conduct remote de-polarization tests for diagnostic purposes.

6 Computer Modeling for Improved Efficiency of a Hybrid FRP/CP System

A recently published report [6.1] provided evidence that the use of Fiber Reinforced Polymers (FRP) does have the ability to increase the efficiency of an embedded anode cathodic protection (CP) system. While a previous study has shown that FRP can restore corroded concrete sections to their original structural capacities [6.2], the combination of this with a means of arresting the ongoing corrosion have made it a more attractive option for pile repair in highly corrosive environments. One of the biggest issues with the system discussed in Chapter 4 is the labor involved in coring the concrete for placement of the embedded anodes. This, combined with the risk of coring through incorrectly spaced rebar, has hindered its acceptance as a repair system. The FRP wrap used in the hybrid system is installed without the used of a coffer dam and therefore the concrete is generally either submerged or still moist at the time of installation. This results in the wrapped region potentially having a lower resistivity than that of dry concrete. This theory lead to the idea of possibly using submerged bulk anodes alone or sub surface strip anodes parallel to the rebar to cathodically protect the wrapped region.

6.1 Introduction

Cathodic protection of steel in reinforced concrete is the only proven means of reducing/eliminating corrosion. This is of particular importance in the tidal zone of marine structures as this region tends to experience corrosion faster due to the increased

chloride concentration and availability of oxygen that results from daily cycles of wetting and drying [6.3].

Recently, a new system was developed which utilized embedded and submerged zinc anodes to provide cathodic protection for marine structural elements. This system also incorporated a fiber reinforced polymer (FRP) wrap to both restore the lost structural capacity of the element, as well as to provide a barrier layer [6.4] that limits the availability of oxygen – thereby reducing the ability of the steel reinforcement to corrode (Fig. 6.1) [6.5].

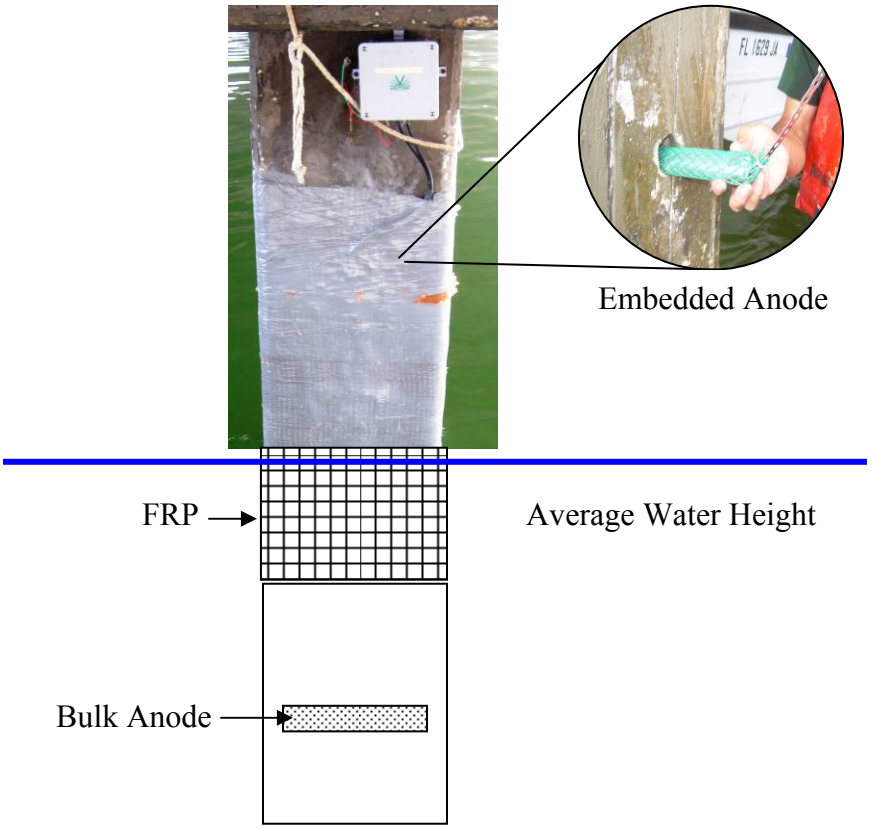

Figure 6.1 Schematic of present CP/FRP system.

Analysis of the system described in Chapter 4 suggests that bulk anodes alone might be capable of providing the minimum design current of 2.7 mA/m^2 (0.25 mA/ft^2)

throughout the entire tidal region which needs of cathodic protection - 1.83 m (6 ft) (Fig. 6.2). This is further supported by the data in Figure 6.3 that shows that piles wrapped with FRP have the potential to be polarized at a faster rate than unwrapped. It is theorized that in addition to limiting the ability of oxygen to diffuse through the concrete, the FRP also acts as a barrier to prevent moisture from exiting the concrete pores, thereby keeping the resistivity at levels which permit the bulk anode to generate this current density.

The systems labeled "Full CP" in Figure 6.2 comprise both bulk and embedded anodes, and the recorded current densities far exceeded the desired value of 2.7 mA/m^2 (0.25 mA/ft^2), suggesting that the embedded anodes might not be needed. The ability to provide CP protection solely with bulk anodes would enhance the speed with which the system is installed as well as reduce the overall cost of protection.

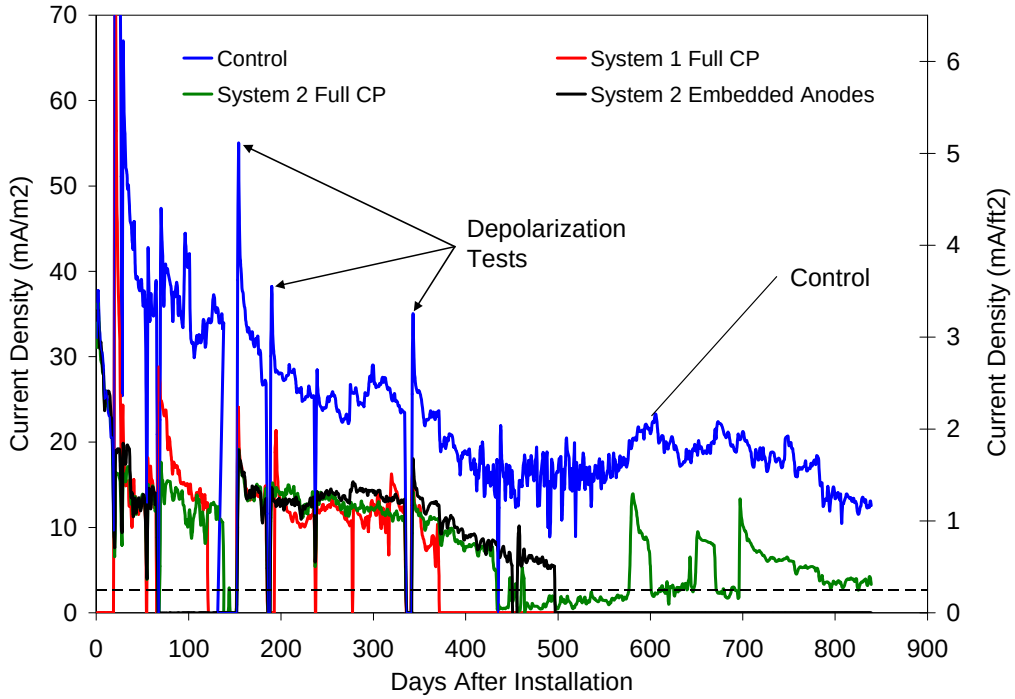

Figure 6.2 Cathodic current density for bulk and embedded anodes.

In evaluating the 24 hour decay values for the piles wrapped in the field study, it appears that the presence of the FRP wrap increased the ability of the anodes to polarize the reinforcement (Fig. 6.3a). The FRP also reduced the time after installation for the system to stabilize at potential values more negative than 100 mV relative to the depolarized potential (Fig 6.3b). One possible explanation for the effect which the FRP appears to have on the behavior of the CP system is that the FRP traps moisture inside the wrapped region, thereby reducing the resistivity of the concrete.

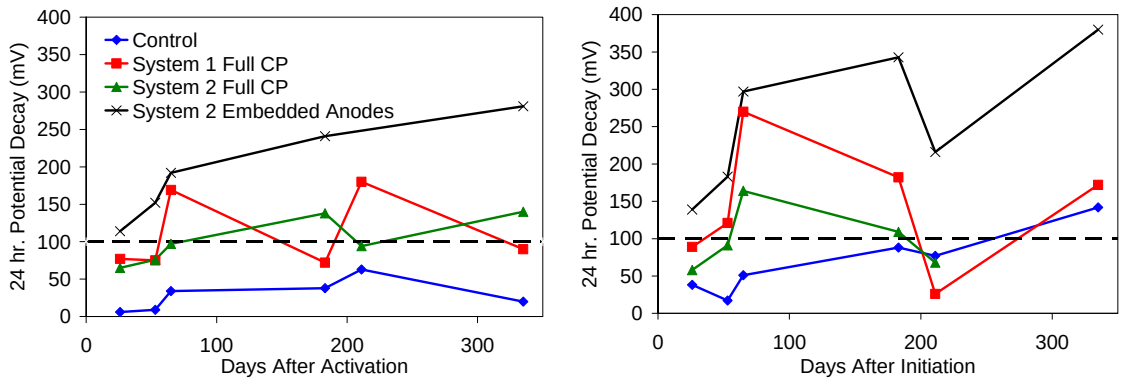

(a) (b)

Figure 6.3 24 hour depolarization values for (a) top and (b) bottom regions of piles.

6.2 Objective

The objective of this chapter is to assess the theoretical ability of FRP Wrapped piles to maintain concrete resistivity at levels low enough to facilitate the long-term cathodic protection of reinforced concrete elements solely by bulk anodes. Alternately, a system will be evaluated that utilizes a bulk anode and near surface embedded anodes in an attempt to provide the reinforcement with a level of protection equivalent to the embedded anode system.

6.3 One Dimensional Model

The piles assessed in this chapter are from the Friendship Trail Bridge Project (Chapter 4). A simple model was created based on theoretical and experimental values to attempt to predict the distance to which a bulk anode could protect the reinforcement.

6.3.1 Concrete Resistivity

Values for the resistivity of both piles were obtained using a Wenner Array Probe (Fig. 6.4) [6.6] connected to a Nilsson Meter [6.7]. The probe consisted of 4 discrete points through which current is either passed or recorded over a known distance. This allows the resistivity of a material/fluid to be calculated.

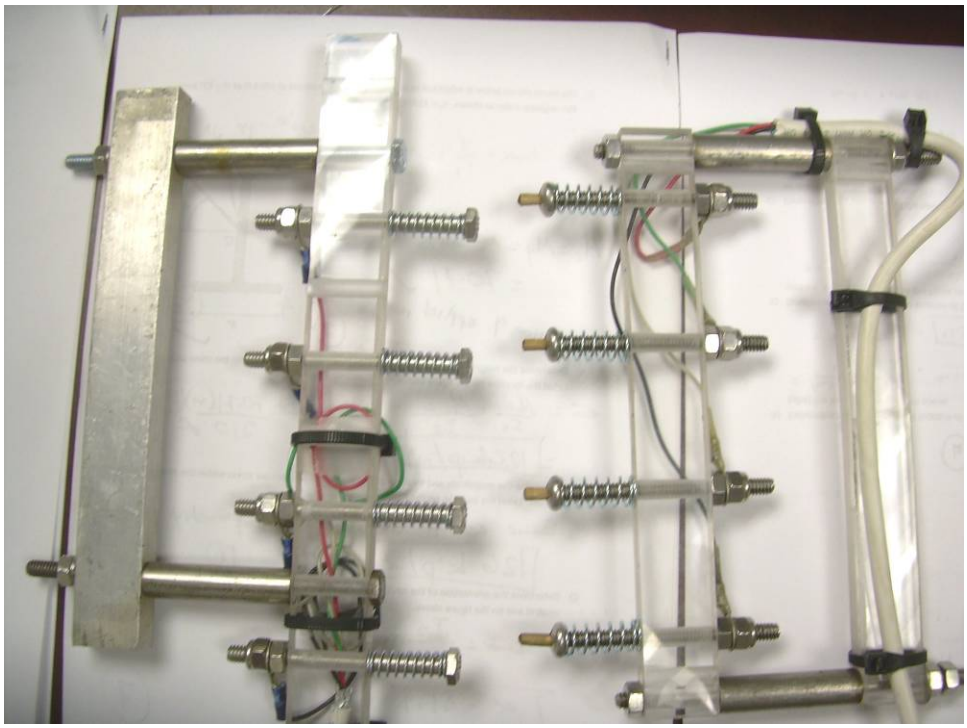

Figure 6.4 Wenner Array probes.

Four piles were used for assessment of the resistivity of the concrete piles; one was an unwrapped control, used as a baseline to represent typical concrete structures, and

the other three were piles wrapped with FRP. For the unwrapped pile, resistivity measurements were obtained simply by making contact between the probe and the concrete pile. However in the case of the FRP wrapped piles, the "barrier layer" was an insulator that prohibited reading from being obtained. To obtain readings on these piles, holes were drilled through the FRP to expose the concrete (1 set spaced 5 cm (2 in) on center). In addition to the piles wrapped during the FRP-CP study described in this chapter, another pile, wrapped in a previous study [6.8], was also compared in an attempt to see if there was any drastic change in the resistivity of the concrete with time. This pile had two set of holes drilled 40.6 cm (16 in) and 61 cm (24 in) from the top of the wrap (Fig. 6.5).

(a) (b)

Figure 6.5 (a) Drilling the FRP; (b) layout for measurement.

6.3.2 Calculations

To make a simple assessment of the distance that a bulk anode could polarize the steel reinforcement to at least 100 mV in accordance with the accepted NACE criterion [6.9], the resistivity was calculated from the measured resistance obtained by the Nilsson Meter, and the throwing distance calculated.

6.3.2.1 Resistivity

Resistivity calculations were performed using the following equation:

$$\rho = 2 \times \Pi \times a \times \frac{V}{I} \quad \{6.1\}$$

where: ρ = the resistivity of the pile in Ω-cm; a = the distance between probes in cm (5 cm for this device); V = the voltage in Volts; I = current in amps.

$$\frac{V}{I} = R \quad \{6.2\}$$

R is the measured resistance in Ω.

Therefore:

$$\rho = 2 \times \Pi \times 5 \times R \quad \{6.3\}$$

6.3.2.2 Throwing Distance

The throwing distance was estimated around the basic equation:

$$V = I \times R \quad \{6.3\}$$

where V = the difference in the polarized and depolarized potentials of the reinforcement; I equals the current required by the system; and R equals the resistance of the system. This equation was then modified to account for the resistivity of the concrete and the current density required by the reinforcement to become:

$$L = \sqrt{\frac{V \times A_c}{i \times S \times \rho}} \quad \{6.4\}$$

where L = the throwing distance in meters; V = the observed change in steel potential between polarized and depolarized state in Volts; A_c equals the area of concrete in cm^2; i

equals the current density in mA/m^2; S = the steel density in cm^2/cm; and ρ equals the resistivity of the concrete in Ω-cm.

6.3.3 Results

The results of the resistivity calculations are found in Tables 6.1 – 6.3. Table 6.1 contains the values for the piles wrapped during this project (Dec. 2008), while Table 6.2 contains the values for the pile wrapped in the previous project (Summer 2005). Table 6.3 contains resistivity values for an unwrapped concrete pile.

Table 6.1 Resistivity for Pile 103 B (unwrapped control).

16"		24"	
Probe Reading	Resistivity Ω-cm	Probe Reading	Resistivity Ω-cm
3600	115000	3600	115000
3200	102000	3600	115000
3400	109000	3800	121000
3600	115000	3800	121000
AVERAGE	110250	AVERAGE	118000
Std. Dev	6185	Std. Dev	3464

Table 6.2 Resistivity for Pile 104 A and 104 C (wrapped December 2008).

104 A		104 C	
Probe Reading	Resistivity Ω-cm	Probe Reading	Resistivity Ω-cm
480	15000	760	24000
450	14000	780	25000
470	15000	770	25000
450	14000	780	25000
AVERAGE	14500	AVERAGE	24750
Std. Dev	577	Std. Dev	500

Table 6.3 Resistivity for Pile 101 C (wrapped summer 2005).

16"		24"	
Probe Reading	Resistivity Ω-cm	Probe Reading	Resistivity Ω-cm
1500	48000	800	26000
1700	54000	780	25000
1600	51000	800	26000
1500	48000	790	25000
AVERAGE	50250	AVERAGE	25500
Std. Dev	2872	Std. Dev	577

The averaged values from Tables 6.1-6.3 were used in equation {4} along with the following constants in order to estimate the throwing distance of a bulk anode through concrete:

(1) V = 0.32V (averaged from the observed depolarization of the CP system)

(2) $A_c = 2580\ cm^2$

(3) $i = 2.70e\text{-}07\ A/cm^2$

(4) $S = 76.2\ cm^2/cm$

(5) ρ = average resistivity of the pile

The results of the calculations performed using equation {6.4} are found in Table 6.4. The furthest distance to which the steel could be polarized is 0.52 m (1.71 ft) in the case of Pile 104 A (wrapped 2008), with an average resistivity of 14768 Ω-cm. This value is just slightly less than three times the distance calculated for 103 B (control pile) at the same distance from the top of where the wrap would have been located on that pile, while Pile 101 C (wrapped 2005) had values between the control and the other wrapped piles. This confirms that the presence of the FRP does increase the throwing distance of a bulk anode, however not to the desired 1.83 m (6 ft) required for this project.

Table 6.4 Calculated throwing distance of a bulk anode based on resistivity.

Pile	L(m)	L (ft)
104 A [2008]	0.52	1.71
104 C [2008]	0.40	1.32
101 C - 40.6 cm (16 in) [2005]	0.28	0.93
101 C - 61 cm (24 in) [2005]	0.40	1.31
103 B - 40.6 cm (16 in) [Control]	0.19	0.63
103 B - 61 cm (24 in) [Control]	0.18	0.60

Table 6.4 values were used for verification of developing the 3D model prior to evaluation of the sub-surface mounted electrodes.

6.4 Three Dimensional Model

Due to the unique nature of the anode arrangement, a two dimensional model would not have properly represented the configuration and therefore a three dimensional model was used. The variables for the model were obtained based on previous work on concrete subjected to a saltwater environment. Three conditions that were analyzed:

(1) Bulk anode only

(2) Bulk and embedded anodes

(3) Bulk and eight near surface mounted anodes (two on each surface)

The three conditions were modeled using Comsol®. An axi-symmetric model was utilized to reduce computational needs. While all three scenarios have the same basic layout, only the presence/placement of the anodes differentiates them. For this reason, the layout with the most details (Condition 2) is shown for the schematic in Figure 6.6. In the case of the pile with no anodes and the one with near surface mounted anodes, all of the relevant data can be seen from a top view, as shown in Figure 6.7, However, this view would not facilitate viewing the embedded anodes. To show this,

Figure 6.8 is an isometric view of the embedded anode model. The full side profile of all three conditions can be seen in Figure 6.9.

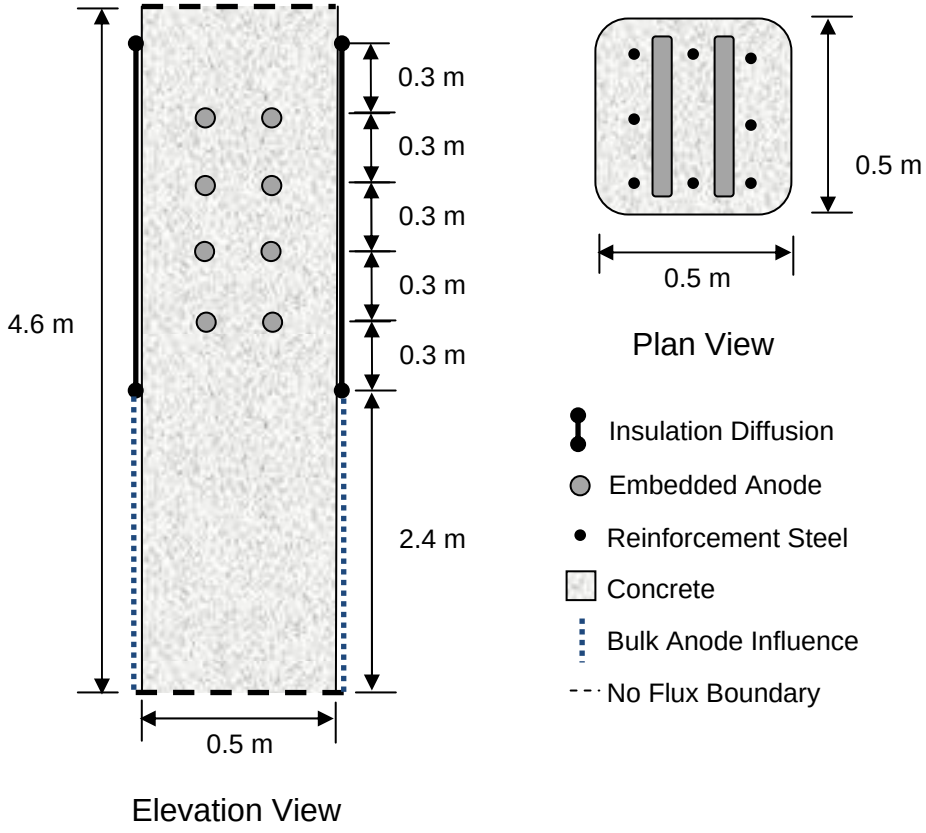

Figure 6.6 Pile schematic showing embedded anodes.

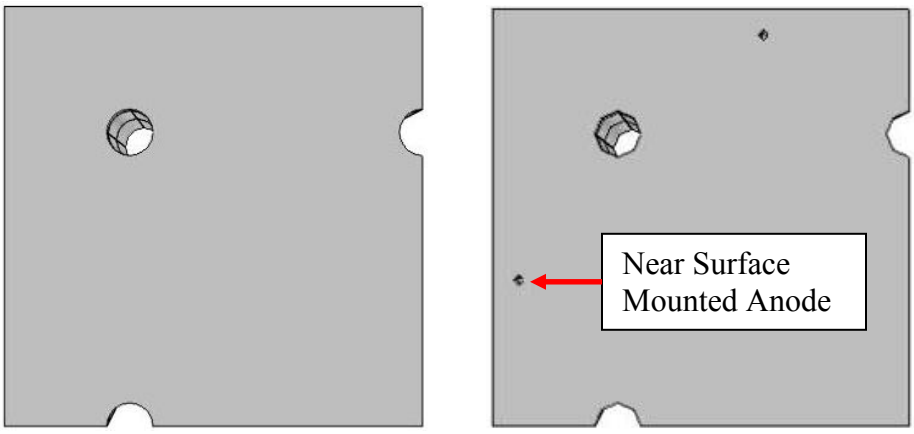

Figure 6.7 Plan view of (a) pile with no anodes; (b) pile with near surface anodes.

Figure 6.8 Isometric view of embedded anodes.

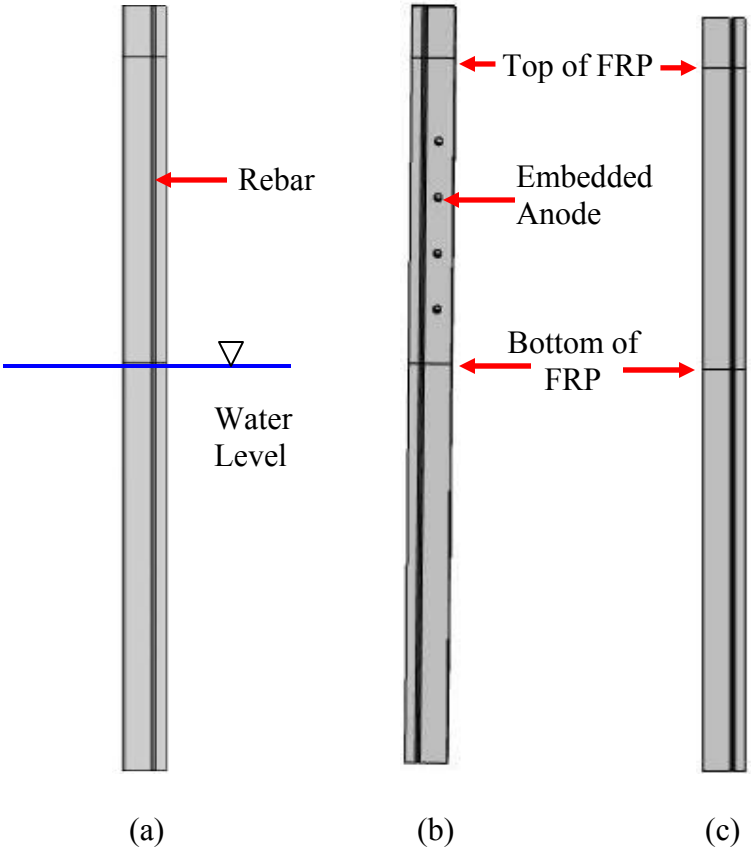

Figure 6.9 Side profiles for (a) no anodes; (b) embedded anodes; (c) near surface anodes.

6.4.1 Assumptions

The model used generalized assumptions as to the diffusivity and conductivity of concrete. As there was a need to attempt to minimize the error within the model, values from these parameters were not based on the data obtained for the 1D analysis, but were instead obtained from a paper in which extensive testing was performed. [6.10]

All three models were divided into 3 concrete sub domains that had varying properties. The zones represented the concrete exposed to air (Zone 1), the FRP wrapped region that was assumed to retain moisture (Zone 2) and the submerged region where the bulk anode was assumed to have influence over the entire surface (Zone 3). The sub domain properties for these zones can be seen in Figure 6.10.

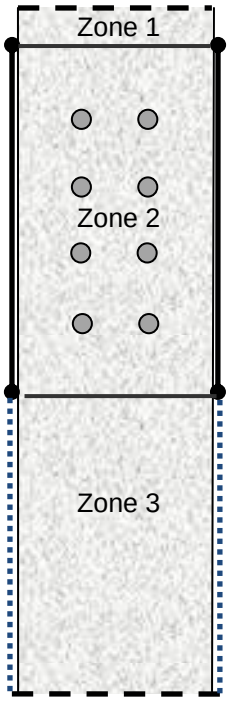

Zone	Conductivity (S/m)	Diffusion (m^2/s)
1	1.E-03	1.E-07
2	4.E-03	1.E-09
3	4.E-03	1.E-09

Figure 6.10 Sub domain concrete properties.

In addition to the assumptions made for the concrete in the three zones, others were also made, these included the following:

(1) Oxygen reduction at the anodes would obey the same potential dependence as that of the corroding reinforcement.

(2) Anodes were at a fixed potential and were non polarizable.

(3) The top and bottom of the pile were assumed to be electrically insulated.

(4) Anode consumption is ignored.

(5) The water would contain enough dissolved oxygen in equilibrium with the atmosphere, approximately 0.25 mol/m^3, so that value was used for the fixed surface concentration in both regions.

(6) The conductivity of the concrete within each zone was assumed to be uniform.

(7) The diameter of the bar was increase from 0.0254 m to 0.02794 m to account for the surface area of the stirrups.

The other input variables can be found in Table 6.5.

Table 6.5 Comsol® input variables.

Parameter	Value
β_a	0.06 V
io_a	3.0E-4 A/m^2
Eo_a	0.78 V
β_c	0.16 V
io_c	1.0E-5 A/m^2
Eo_c	-0.16 V
F	96500 C/mol
n	4
C_o	0.25 mol/m^3
Anode Voltage	-1.1 V

The cathodic current of the reinforcement was calculated using equation 6.5, and the corrosion current using equation 6.6.

$$icatFe = -io_c * c * 10^{(V-Eoc)/bc/Co} \quad \{6.5\}$$

$$i_{corr} = io_a * 10^{(Eoa-V)/ba} \quad \{6.6\}$$

These formulas were inputted into Comsol® to perform the necessary calculations.

6.4.2 Boundary Conditions

The model was made with the following boundary conditions:

(1) The top and bottom of the pile would be modeled as "Insulation/Symmetry"

(2) The corners where the pile was cut for symmetry were modeled as "Insulation/Symmetry"

(3) The FRP wrapped portion of the pile was modeled as "Insulation/Symmetry"

(4) The exposed concrete surfaces were modeled as fixed oxygen concentrations

(5) The exposed concrete surface below water was modeled as a fixed voltage to represent the influence of the bulk anode

(6) All anodes were modeled as a fixed voltage (-1.1 V)

(7) The rebar was modeled as "Inward Current Flow" and "Inward Flux"

6.4.3 Results

The tabulated values outputted from Comsol® were plotted next to the graphical output obtained from the software (Fig. 6.11). Analysis of the level of polarization on the corner and center bars yielded identical results, therefore only the values obtained for the polarization of the center bar in all three cases is reported in Figure 6.11. From this figure, the level of polarization drops off at the beginning of the wrapped region (~2.5 m) for the pile with no anodes. When comparing the embedded and near surface anodes, the same level of protection was provided through most of the wrapped region. The apparent increase in protection distance shown in Figure 6.11 is simply due to the fact that the near

surface anodes were extended throughout the entire length of the pile, while the embedded ones were restricted to the four locations reported.

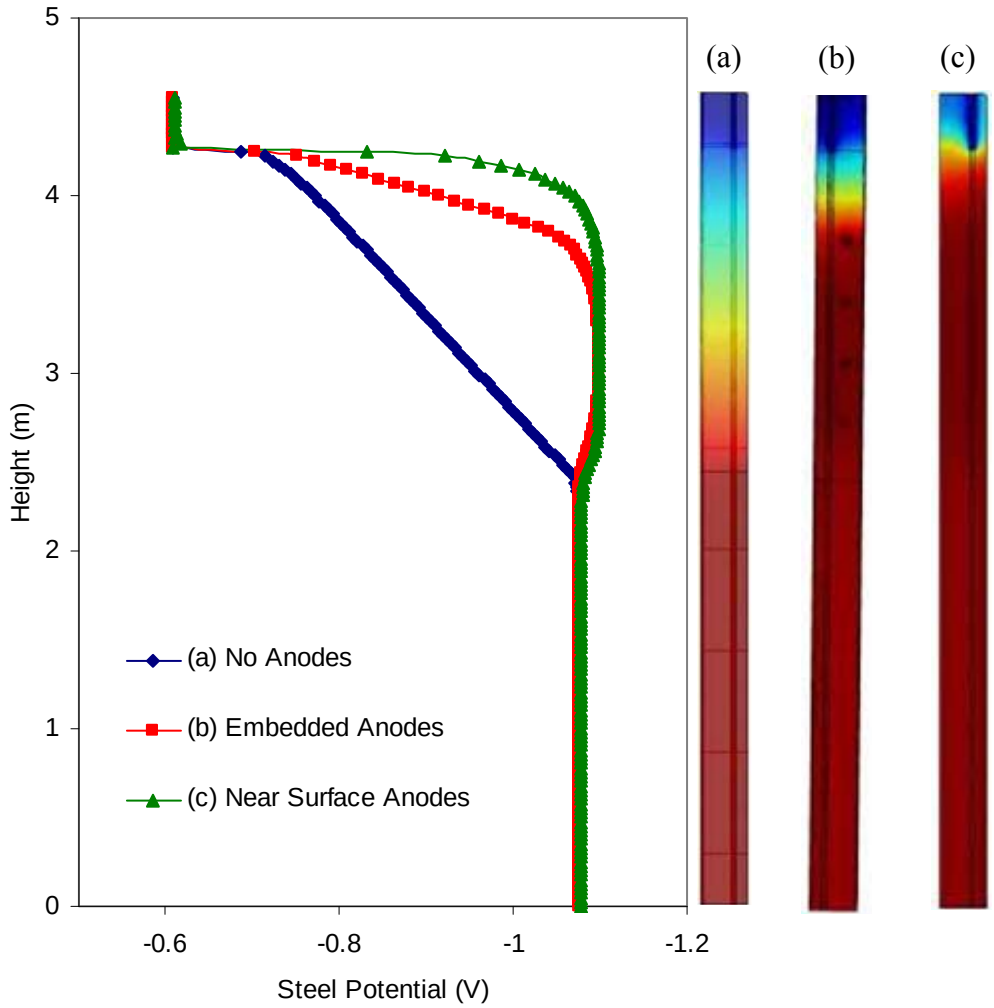

Figure 6.11 Results for (a) no anodes; (b) embedded anodes; (c) near surface anodes.

6.5 Discussion

Several generalized assumptions were made in the generation of this model. This included the assumption that the sub surface mounted and embedded anodes have the same potential as the bulk anode (-1.1 V), and there was no depletion of the anodes. In such an idealized case, the sub surface mounted anodes do appear to work. In an actual

situation, the size of the anodes would need to be adjusted to account for consumption. Also, the anodes used in the model were non-polarizable. I reality, the connection of dissimilar metals would alter the potential of both materials. Had this been incorporated into the model, the levels of polarization may have been lower. Although the values might not have been the same as those generated under ideal conditions, it is not certain that the anodes would not have been capable to provide the 100 mV change in potential required.

The sensitivity of the input variables also needs to be addressed prior to using this model for making polarization predictions. The model is effective when the specific variables are used; however, changing those values by as little as 1% may significantly alter the performance of the system. Further investigation is therefore needed by altering each variable independently to determine the effect that it has on the overall performance of the model.

The "Normal" mesh size was chosen for analyzing the reported data. The sensitivity of the mesh size should also be explored to ascertain the effect that element size will affect the output values.

6.6 Conclusion

The calculations presented here were exploratory in nature and should be confirmed by follow up work. Nevertheless, the results generated from the 3D model confirm the conclusions obtained from the 1D analysis that even with an assumed lower resistivity due to the presence of the FRP, a bulk anode alone will not be able to adequately protect the reinforcement throughout the wrapped region. In cases where the

resistivity would be lower or the wrapped region smaller, it could be possible for such a system to work, however, based on the specifications of the piles tested, that is not the case.

The 3D model did show that embedded the anodes as strips would allow a comparable level of protection, based on the limited study performed, however these strips would eventually have to be replaced (as with any sacrificial anode system). The fact that the system would work under ideal conditions suggests that an impressed current system with the same configuration should be investigated.

7 Contributions

This dissertation presents information from two unrelated research projects that are the subject of several peer-reviewed articles that have been published, or are in preparation. The specific conclusions from these studies are included at the last segments of Chapters 2-5. The intent of this chapter is not to reproduce these findings, but rather to highlight the most significant contributions from each research study.

7.1 Quantification of Bond Improvement Due to Pressure /Vacuum Bagging

A comprehensive test program convincingly demonstrated that the FRP-concrete bond is significantly improved for both wet and dry applications by pressure/vacuum bagging techniques.

7.2 Identifying Systems Where Bond was Improved by Pressure or Vacuum

The study showed that pressure worked best for the epoxy based system, while the urethane based system had better results with a vacuum. When no pressure was applied, transverse strips generated the best bond.

7.3 Proof-of-Concept for an Effective Hybrid FRP-CP System

Previous attempts at incorporating a cathodic protection system within a FRP wrap had replicated CP systems used for concrete in which a zinc mesh was bonded directly to the concrete surface. The new system, using embedded anodes, makes it

possible to combine FRP strengthening with cathodic protection. The results showed that the FRP appeared to reduce the anodic current and extend the lifetime of the anodes.

7.4 Remote Monitoring System for Cathodic Protection of Steel Piles

A system developed for remote monitoring and control was successfully tested as a means of monitoring the anodic current and steel potential of piles in a hostile environment. The system also proved capable of remotely regulating the current provided to the structure as well as performance testing that typically required an onsite technician. The system also monitored environmental conditions, and through these monitored values, suggested that current regulation would be a viable option without the sacrificial anodes suffering from excessive self consumption.

7.5 Corrosion Modeling

A 1-dimensional and preliminary 3-dimensional Finite Element Model were created to evaluate different means of improving the FRP-CP repair system. The theoretical model indicated that strip anodes embedded just below the surface of the concrete, could provide adequate protection when used in conjunction with bulk anodes.

The assumptions made in the model also suggest that an impressed current system may be preferred in future FRP-CP systems so that the anodes will not have to be replaced.

8 Future Work

Although most of the systems presented in this dissertation were successful in achieving their tasks, not all of them were as easy to use as initially expected. While the issues encountered while monitoring the CP performance were addressed by remote monitoring devices, refinements in the successfully implemented systems can aid in improving the overall system efficiency.

8.1 Alternative to Pressure Bagging

The goal of pressure bagging is to ensure that there is intimate contact between the resin-saturated FRP and the concrete substrate while the resin cures. This can be achieved by alternative means as follows.

8.1.1 Using Disposable Bubble Wrap

The FRP bond with concrete is always excellent at the rounded corners but poorer on flat surfaces. Pressure bagging overcomes this problem by artificially making the section more "circular" thereby exerting reasonably uniform pressure over the entire wrapped region. The drawbacks of the system are:

(1) The need to engineer the outer / inner bag for each different pile size so that they do not fail.

(2) The need for access to electrical power (in the tests and in the demonstration project, air compressors / vacuum pumps were run continuously in case there were leaks.

Disposable bubble wrap with horizontal cells provides a simpler alternative that can achieve the same objective, namely improving FRP-concrete bond. This type of bubble wrap widely used in packaging is inexpensive and can be tailored for this new application. This eliminates the need to design inner / outer bags for different pile sizes and their associated costs. More importantly, it can be easily integrated in current practice for installing FRP in vertical elements such as columns and piles.

A preliminary trial was conducted at USF to establish "proof of concept". The bubble wrap used was retrieved from packages received in which there were horizontal cells over the width as shown in Figure 8.1.

Figure 8.1 Bubble wrap with horizontal cell used in trial.

The bubble wrap from Novus Inflatable Plastic Packing was approximately 13 ½ in. wide and contained two inflated cells each 6 in. long and 2 in. wide with a ½ in. separation that was not inflated. The ends of the cells were tapered and the inflated depth was approximately one inch.

8.1.1.1 Test Procedure

The 12 in. piles used in Stage I laboratory testing were used in the trial. Two piles were tested, a "control" without the bubble wrap and a test specimen with the bubble wrap. In the testing, pressure sensitive paper was used. This paper records pressure by a change in color; the higher pressure, the darker the color. Thus, it can provide a qualitative basis for comparing pressure exerted on a wrap.

Since the test was used for comparison, no FRP wrapping was carried out. Instead, for the control, the pressure paper was directly placed on the pile surface and the blue shrink wrap applied normally in the transverse direction. For the test specimen, the bubble wrap was placed on the pressure sensitive paper with the cells in the transverse direction and wrapped over by the shrink wrap as shown in Figure 8.2 (a) and (b) in the same manner.

(a) (b)

Figure 8.2 (a) Shrinkwrap on pile; (b) Shrinkwrap with bubble wrap.

Figure 8.3 (a) is a scan of the results from the pile wrapped without the bubble wrap (Figure 8.2 a). The edges of the pile are clearly defined by dark color while the middle is distinguishable by its lighter shade of grey. This indicates that the distribution of the pressure resulting from the shrink wrap is uneven; it is higher at the edges than at the middle.

(a) **(b)**

Figure 8.3 (a) Results for control with shrinkwrap; (b) Results for bubble wrap.

The corresponding scan for the pile with the bubble wrap insert is shown in Figure 8.3 (b). As before, the edges are clearly defined, however the region in the middle

is darker in color compared to the pile without the bubble wrap. It may be seen that the scan plots the variation in pressure across the pile width and displays the profile of the bubble wrap containing two cells per row along the face of the pile. Clearly, there is a qualitative improvement.

The preliminary results are promising. By testing bubble wraps with a larger continuous bubbles that are large enough to encompass the entire pile width, it may be possible to develop a product that can provide the pressure needed to ensure good FRP-concrete bond both below and above the water line. Such a system can be readily implemented in the field.

8.2 Alternative Anode System

While Chapter 6 indicates that an idealized alternative sacrificial anode system would be capable of improving the ease of installation of the CP system, there are many issues which need to be considered. As the system assumed that the anodes would not be polarized and would never become exhausted, the results obtained do not reflect what might be experienced in a field application. There are two ways of rectifying this issue.

8.2.1 CP Model Refinement

The model used to generate the data in Chapter 6 did not consider effects such as the increased level of chlorides near the surface of the concrete. This issue was less significant for embedded anodes that were placed near the center of the pile, where the chloride content is lowest. The installation of the sub surface anodes in concrete with higher chloride contents might increase the rate at which the anodes are consumed.

Another issue not addressed is the variance of the concrete properties. Most of the structures for which the CP system is target were made more than twenty years ago. As quality assurance practices were more lax than those today, there may be issues where the concrete inspected at a particular elevation is completely different from that found only a short distance above or below that specific spot. The model must also be modified to consider the probability that the concrete of the pile is homogeneous, and if not, by how much it could potentially vary. These issues along others must be addressed thoroughly before the near surface mounted anodes can be recommended for common practice.

8.2.2 Solar Powered Impressed Current System

The present FRP-CP system uses the concept of preferential corrosion to protect the steel reinforcement. An alternative means of protection is through the use of impressed current. This system traditionally is a more expensive option due to the need to regulate the current applied to the reinforcement as well as need to monitor the system for faults.

For the initially proposed system, using the simple data loggers, impressed current would not be economically attractive. However, this would not be the case if the remote monitoring system described in Chapter 5 was used to monitor system performance. The remote monitoring system has demonstrated its ability to regulate current and monitor performance over an extended period of time, and therefore is the exact system that would be needed for an economical impressed current CP system.

In this system, a solar panel, similar to the one used for powering the remote monitoring system, could be used to charge a large direct current (DC) battery. That current could then be controlled using the regulating resistor circuit described in Chapter 5. Such a system would use inexhaustible anodes such as activated titanium, and would also eliminate the problems that might be encountered when the anodes covered by the wrapped region are consumed.

8.3 Summary

While the two topics discussed in this chapter do not have a significant effect on the overall performance of the hybrid FRP-CP system, they have the potential to increase the ease with which the system is accepted as a viable repair option. The elimination of the costs associated with fabrication of customized pressure bags along with the reduced labor costs associated with a CP system that requires less time to install could persuade more entities to use this system as their preferred means of reinforced concrete pile repair.

References

1.1 Koch, G., Brongers, M., Thompson, N., Virmani, Y., and Payer, J. (2001). "Corrosion Cost and Preventive Strategies in the United States." FHWA-RD-01-156, Springfield, VA: National Technical Information Service.

1.2 MnDOT, (2011). Economic Impacts of the I-35W Bridge Collapse, *Positively Minnesota*,http://www.dot.state.mn.us/i35wbridge/rebuild/municipal-consent/economic-impact.pdf , accessed October 3, 2011.

2.1 Kessler, R., Powers, R. and Lasa, I. (2006). "Case Studies of Impressed Current Cathodic Protection Systems for Marine Reinforced Concrete Structures in Florida," Paper No 06330, Corrosion NACE 2006.

2.2 Florida Department of Transportation. Item Average Unit Cost from 2008/05/01 to 2009/04/30, p. 16 ftp://ftp.dot.state.fl.us/LTS/CO/Estimates. Accessed August 5, 2009.

2.3 Sen, R., (2003). "Advances in the Application of FRP for Repairing Corrosion Damage," *Progress in Structural Engineering and Materials*, Vol. 5, No 2, pp. 99-113.

2.4 Sen, R. and Mullins, G. (2007). "Application of FRP for Underwater Pile Repair," *Composites Part B*, Vol. 38, No. 5-6, pp. 751-758.

2.5 Winters, D., Mullins, G., Sen, R., Schrader, A. and Stokes, M. (2008). "Bond Enhancement for FRP Pile Repair in Tidal Waters," ASCE, *Journal of Composites for Construction*, Vol. 12, No. 3, pp. 334-343.

2.6 Aguilar, J., Winters, D., Sen. R., Mullins, G. and Stokes, M. (2009). "Improvement in FRP-Concrete Bond by External Pressure," *Transportation Research Record, No. 2131,* pp. 145-154.

2.7 Aguilar, J., Winters, D., Sen. R., Mullins, G. and Stokes, M. (2010). "FRP-CP System for Pile Repair in Tidal Waters." *Transportation Research Record, No. 2150,* pp. 111-118.

2.8 Groves, W. G. "Tide," AccessScience@McGraw-Hill, DOI 10.1036/1097-8542.696900

2.9 Fyfe Co. LLC (2008). "Korea Chemical Plant Pier, Project Brief," San Diego, CA.

2.10 Bazinet, S., Cercone, L. and Worth, L., (2003). "Composite FRP Moves into Underwater Repair Applications," *SAMPE Journal*, V. 39, No. 3, May/June, pp.8-16.

2.11 Quakewrap Inc. (2007). Carbon FRP Repair of Underwater Bridge Pier, Fort Lauderdale, http://www.quakewrap.com/project_sheets/Carbon-FRP-Repair-of-Underwater-Bridge-Piers.pdf). Accessed May 26, 2010.

2.12 Sen, R. and Mullins, G. (2010). "Underwater FRP Repair of Corroding Piles Incorporating Cathodic Protection," Final Report NCHRP-IDEA 128, 28 pp.

2.13 Mullins, G., Sen, R., Suh, K and Winters, D. (2005). "Underwater FRP Repair of Prestressed Piles in the Allen Creek Bridge," *Journal of Composites for Construction*, Vol. 9, No. 2, Mar-April, pp. 136-146.

2.14 Mullins, G., Sen, R., Suh, K. and Winters, D. (2006). "A Demonstration of Underwater FRP Repair," *Concrete International,* Vol. 28, No. 1, pp 1-4.

2.15 Suh, K.S., Sen, R**,** Mullins, G. and Winters, D. (2008). "Corrosion Monitoring of FRP Repaired Piles in Tidal Waters," *ACI SP-252*, pp. 137-156.

2.16 Leng, D., (2002). "Zinc Mesh Cathodic Protection Systems," *Materials Performance*, V. 41, No. 8, Aug., pp. 28-33.

2.17 Harichandran, R. & Baiyasi, M. (2000). "Repair of Corrosion-Damaged Columns Using FRP Wraps," *Research Report RC-1386*, submitted to Michigan Department of Transportation, Lansing, MI.

2.18 ACI 546.3R-06 (2006). "Guide for the Selection of Materials for the Repair of Concrete," ACI, Farmington Hills, MI.

2.19 Concrete Repair Manual (2003). "Surface Preparation," Vol. 1, 2nd Edition, pp. 1539-1580, ACI International, Farmington Hills, MI.

2.20 Stallings, J., Tedesco, J., El-Mihilmy, M. and McCauley, M. (2000). "Field Performance of FRP Bridge Repairs," ASCE, *Journal of Bridge Engineering*, Vol. 5, No. 2, pp. 107-113.

2.21 Nazier, M., Giancaspro, J. and Balaguru, P. (2005). "Composite Jackets for Rehabilitation of Damaged Reinforced Concrete Pier Caps," *SAMPE '05 Proceedings*, Long Beach, CA, Vol. 50, pp. 1011-1024

2.22 Aguilar, J., Winters, D., Sen, R., Mullins, G. and Stokes, M. (2008). "Underwater FRP Repair of Corroding Piles Incorporating Cathodic Protection," Report on Stage 1 NCHRP-IDEA 128, 45 pp

2.23 SHRP-337 (1993). "Cathodic Protection of Reinforced Concrete Bridge Elements: A State-of-the-Art-Report," National Research Council, Washington, DC.

2.24 NACE (2005). "Sacrificial Cathodic Protection of Reinforced Concrete Elements – A State-of-the-Art-Report," Publication No 01105.

2.25 Bertolini,L., Elsener, B., Pedeferri, P. and Polder, R. (2004). *Corrosion of Steel in Concrete*, Wilet-VCH, Weinhem, Germany.

2.26 Fyfe & Co. (2003). "Tyfo Zinc Installation Procedure," San Diego, CA.

2.27 ASTM Standard C876 (2009). "Standard Test Method for Corrosion Potentials of Uncoated Reinforcing Steel in Concrete", ASTM International, West Conshohocken, PA.

3.1 Sheikh, S., Pantazoupoulou, S., Bonacci, J., Thomas, M. & Hearn. N. (1997). "Repair of Delaminated Circular Pier Columns with Advanced Composite Materials", Ontario Joint Transportation Research Report No 31902, Ministry of Transportation of Ontario, Toronto, Canada.

3.2 Berver, E., Jirsa, J., Fowler, D., Wheat, H. and Moon, T. (2001). "Effects of Wrapping Chloride Contaminated Concrete with Fiber Reinforced Plastics", FHWA/TX-03/1774-2, University of Texas, Austin.

3.3 Baiyasi, M. & Harichandran, R. (2001). "Corrosion and Wrap Strains in Concrete Bridge Columns Repaired with FRP Wraps". Paper No 01-2609, 80th Annual Meeting, Transportation Research Board, Washington, DC.

3.4 Bazinet, S., Cereone, L and Worth, F. (2003). "Composite FRP moves into underwater repair applications", SAMPE Journal, Vol. 39, No. 3, pp. 8-16.

3.5 Watson, R.J. (2003)."The Use of Composites in the Rehabilitation of Civil Engineering Structures", ACI SP – 215, Field Applications of FRP Reinforcement: Case Studies (Ed: S. Rizkalla, A. Nanni), Farmington Hills, MI, pp. 291-302.

3.6 Mullins, G., Sen, R., Suh, K and Winters, D. (2005). "Underwater FRP Repair of Prestressed Piles in the Allen Creek Bridge". ASCE, *Journal of Composites for Construction,* Vol. 9, Issue 2, pp. 136-146.

3.7 Mullins, G., Sen, R., Suh, K.S. and Winters, D. (2004). "Underwater FRP Pile Wrap of the Friendship Trail Bridge". Final Report submitted to Hillsborough County, FL, June, 32 pp.

3.8 Kessler, R. and Powers, R. (1990). "Zinc Metalizing for Galvanic Cathodic Protection of Steel Reinforced Concrete in a Marine Environment", Paper No 324, NACE, Corrosion Conference, Las Vegas, NV, 16 pp.

3.9 Kessler, R., Powers, R. and Lasa, I. (1991). "Cathodic Protection Using Scrap and Recycled Materials", Paper No 555, NACE, Corrosion Conference, Cincinnati, OH, 21pp.

3.10 Kessler, R., Powers, R. and Lasa, I. (2006). "Case Studies of Impressed Current Cathodic Protection Systems for Marine Reinforced Concrete Structures in Florida". Paper No 06330, NACE, Corrosion Conference, San Diego, CA; USA.

3.11 D.L. Leng (2000). "Zinc Mesh Cathodic Protection Systems", Materials Performance, Vol. 39, No. 8, pp. 28-33.

3.12 Aguilar, J., Winters, D., Sen. R., Mullins, G. and Stokes, M. (2009). "Improvement in FRP-Concrete Bond by External Pressure". To appear in *Transportation Research Record.*

3.13 Winters, D., Mullins, G., Sen, R., Schrader, A. and Stokes, M. (2008). "Bond Enhancement for FRP Pile Repair in Tidal Waters". ASCE, *Journal of Composites for Construction*, Vol. 12, No. 3, pp. 334-343.

3.14 NACE (2000) Standard RP0290-2000 Item No 21043. Impressed Current Cathodic Protection of Reinforcing Steel in Atmospherically Exposed Concrete Structures, Houston, TX.

3.15 NACE (2005). Sacrificial Cathodic Protection of Reinforced Concrete Elements – A State-of-the-Art-Report, Publication No 01105, Houston, TX.

3.16 SHRP-337 (1993). "Cathodic Protection of Reinforced Concrete Bridge Elements: A State-of-the-Art-Report", National Research Council, Washington, DC.

3.17 Whitmore, D. and Ball, C. (2005). "Galvanic Protection for Reinforced Concrete Structures", Concrete Repair Bulletin, Sept/Oct, pp. 20-22.

3.18 Suh, K.S., Sen, R**,** Mullins, G. and Winters, D. (2008). "Corrosion Monitoring of FRP Repaired Piles in Tidal Waters". *ACI SP-252*, pp. 137-156.

3.19 Mindess, S., Young, J. and Darwin, D. (2003). Concrete, 2nd Edition, Prentice-Hall, NJ, p. 497.

3.20 ASTM Standard C1152 (2004)."Standard Test Method for Acid-Soluble Chloride in Mortar and Concrete," ASTM International, West Conshohocken, PA.

3.21 Aguilar, J., Winters, D., Sen, R., Mullins, G. and Stokes, M. (2008). "Underwater FRP Repair of Corroding Piles Incorporating Cathodic Protection", Report on Stage 1 NCHRP-IDEA 128, 45 pp.

3.22 Bertolini, L., Gastaldi, M., Pedeferri, M. and Redaelli, E. (2002). "Prevention of Steel Corrosion in Concrete Exposed to Seawater with Submerged Sacrificial Anodes", Corrosion Science, Vol. 44, pp. 1497-1513.

3.23 Moreno, F. and Hartt, W. (2009). "Protection of Reinforced Concrete Bridge Substructures Using Submerged Bulk Anodes (BD 546-3)". Final Report submitted to Florida Department of Transportation, Tallahassee, FL.

4.1 Sheikh, S., Pantazoupoulou, S., Bonacci, J., Thomas, M. & Hearn. N. (1997). "Repair of Delaminated Circular Pier Columns with Advanced Composite Materials", Ontario Joint Transportation Research Report No 31902, Ministry of Transportation of Ontario, Toronto, Canada.

4.2 Berver, E., Jirsa, J., Fowler, D., Wheat, H. and Moon, T. (2001). "Effects of Wrapping Chloride Contaminated Concrete with Fiber Reinforced Plastics", FHWA/TX-03/1774-2, University of Texas, Austin.

4.3 Baiyasi, M. & Harichandran, R. (2001). "Corrosion and Wrap Strains in Concrete Bridge Columns Repaired with FRP Wraps". Paper No 01-2609, 80th Annual Meeting, Transportation Research Board, Washington, DC.

4.4 Bazinet, S., Cereone, L and Worth, F. (2003). "Composite FRP moves into underwater repair applications", SAMPE Journal, Vol. 39, No. 3, pp. 8-16.

4.5 Watson, R.J. (2003)."The Use of Composites in the Rehabilitation of Civil Engineering Structures", ACI SP – 215, Field Applications of FRP Reinforcement: Case Studies (Ed: S. Rizkalla, A. Nanni), Farmington Hills, MI, pp. 291-302.

4.6 Mullins, G., Sen, R., Suh, K and Winters, D. (2005). "Underwater FRP Repair of Prestressed Piles in the Allen Creek Bridge". ASCE, *Journal of Composites for Construction,* Vol. 9, Issue 2, pp. 136-146.

4.7 Mullins, G., Sen, R., Suh, K.S. and Winters, D. (2004). "Underwater FRP Pile Wrap of the Friendship Trails Bridge". Final Report submitted to Hillsborough County, FL, June, 32 pp.

4.8 Kessler, R. and Powers, R. (1990). "Zinc Metalizing for Galvanic Cathodic Protection of Steel Reinforced Concrete in a Marine Environment", Paper No 324, NACE, Corrosion Conference, Las Vegas, NV, 16 pp.

4.9 Kessler, R., Powers, R. and Lasa, I. (1991). "Cathodic Protection Using Scrap and Recycled Materials", Paper No 555, NACE, Corrosion Conference, Cincinnati, OH, 21pp.

4.10 Kessler, R., Powers, R. and Lasa, I. (2006). "Case Studies of Impressed Current Cathodic Protection Systems for Marine Reinforced Concrete Structures in Florida". Paper No 06330, NACE, Corrosion Conference, San Diego, CA; USA.

4.11 D.L. Leng (2000). "Zinc Mesh Cathodic Protection Systems", Materials Performance, Vol. 39, No. 8, pp. 28-33.

4.12 Aguilar, J., Winters, D., Sen. R., Mullins, G. and Stokes, M. (2009). "Improvement in FRP-Concrete Bond by External Pressure". To appear in *Transportation Research Record.*

4.13 Winters, D., Mullins, G., Sen, R., Schrader, A. and Stokes, M. (2008). "Bond Enhancement for FRP Pile Repair in Tidal Waters". ASCE, *Journal of Composites for Construction*, Vol. 12, No. 3, pp. 334-343.

4.14 NACE (2000) Standard RP0290-2000 Item No 21043. Impressed Current Cathodic Protection of Reinforcing Steel in Atmospherically Exposed Concrete Structures, Houston, TX.

4.15 SHRP-337 (1993). "Cathodic Protection of Reinforced Concrete Bridge Elements: A State-of-the-Art-Report", National Research Council, Washington, DC.

4.16 NACE (2005). Sacrificial Cathodic Protection of Reinforced Concrete Elements – A State-of-the-Art-Report, Publication No 01105, Houston, TX.

4.17 Whitmore, D. and Ball, C. (2005). "Galvanic Protection for Reinforced Concrete Structures", Concrete Repair Bulletin, Sept/Oct, pp. 20-22.

4.18 Suh, K.S., Sen, R**,** Mullins, G. and Winters, D. (2008). "Corrosion Monitoring of FRP Repaired Piles in Tidal Waters". *ACI SP-252*, pp. 137-156.

4.19 ASTM Standard C1152 (2004)."Standard Test Method for Acid-Soluble Chloride in Mortar and Concrete," ASTM International, West Conshohocken, PA.

4.20 Mindess, S., Young, J. and Darwin, D. (2003). Concrete, 2nd Edition, Prentice-Hall, NJ, p. 497.

4.21 ASTM Standard C876 (2009). "Standard Test Method for Corrosion Potentials of Uncoated Reinforcing Steel in Concrete", ASTM International, West Conshohocken, PA.

4.22 Aguilar, J., Winters, D., Sen, R., Mullins, G. and Stokes, M. (2008). "Underwater FRP Repair of Corroding Piles Incorporating Cathodic Protection", Report on Stage 1 NCHRP-IDEA 128, 45 pp.

4.23 Vector Corrosion Galvanode DAS, http://www.vector-corrosion.com/wordpress/wordpress/wp-content/uploads/2011/03/14000-2011Mar04-Galvanode-DAS-Datasheet1.pdf, accessed on November 7, 2011

4.24 Moreno, F. and Hartt, W. (2009). "Protection of Reinforced Concrete Bridge Substructures Using Submerged Bulk Anodes (BD 546-3)". Final Report submitted to Florida Department of Transportation, Tallahassee, FL.

5.1 Mickalonis, G., Hobbs, D., and Tshishiku, E. (2002). "A Corrosion Monitoring and Chemical Species Probe for the Savannah River Site". Department of Energy Contract DE-AC09-96SR18500, Westinghouse Savannah River Company.

5.2 Hughes, G., and Gittleman, M. (1995). "A Robotic End Effector for Inspection of Storage Tanks". Department of Energy Contract DE-AR21-93MC30363, Environmental Technology Development Through Industry Partnership Conference, Morgantown West Virginia, October 1995.

5.3 Edgemon, G, (1999). "Design of Multi-Function Hanford Tank Corrosion Monitoring System". Design description for Milestone B1 of FY 1999, Department of Energy Contract DE-AC06-96RL13200, 13 pp.

5.3 Ohl, P., Farwick, C., Douglas, D., and Cruz, E. (2003). "A Novel Approach to Drum Venting and Drum Monitoring", WM'03 Conference, Tucson, Az., February 2003.

5.5 Marietta, M, et al. (1993). "Intelligent Mobile Sensor System for Drum Inspection and Monitoring Phase 1". Topical Report to US Department of Energy, Contract DE-AC21-92MC29112.

5.6 Elder, J., Wiersma, B., and Sindelar, R. (2003). "Remote Inspection of a High level Radioactive Waste Storage Tank for Cracking, Thinning and Pitting". US Department of Energy, Contract DE-AC09-96SR18500.

5.7 Holcomb, G., Bullard, S., Covino, B., Cramer, S., Russell, J. and Ziomek-Moroz, M. (2002). "Electrochemical Noise Sensors for Detection of Localized and General Corrosion of Natural Gas Transmission Pipelines". Natural Gas Infrastructure Reliability Industry Forums, Morgantown West Virginia, September 2002.

5.8 Bullard, S., Covino, B., Russel, J., Holcomb, G., Cramer, S. and Ziomek-Moroz, M. (2002). "Electrochemical Noise Sensors for Detection of Localized and General Corrosion of Natural Gas Transmission Pipelines". Final Report Department of Energy Contract FE-01-06, 27 pp.

5.9 Braunling, R., and Christoffel, J. (2004). "Corrosion Monitoring System (CMS)" Final Report to the Department of Energy, Contract DE-FC36-00CH11017, 60 pp.

5.10 Sridhar, N., and Tormoen, G. (2005). "Remote Detection of Internal Pipeline Corrosion Using Fluidized Sensors." Report to the US Department of Energy, National Energy Technology Laboratory, NETL Project 42267, 54 pp.

5.11 Burkhardt, G., and Crouch, A. (2006). "Realtime Monitoring of Pipelines for Third-Party Contact". Report to US Department of Energy, Contract DE-FC26-03NT41878, 56 pp.

5.12 Vradis, G., and Leary, B. (2003). "Development of an Inspection Platform and a Suite of Sensors for Assessing Corrosion and Mechanical Damage of Unpiggable Transmission Mains". Quarterly Report to US Department of Energy, Contract DE-FC26-02NT41645

5.13 Garcia, K., and Porter, A. (1995). "Remote Measuring of Corrosion Using Ultrasonic Techniques". Us Department of Energy Contract DE-AC07-94ID3223

5.14 Mullins, G. (2009). "State of the Practice/Art for Structural Health Monitoring of Bridge Substructures", Final Report FHWA DTFH61-07-00033, 324 pp.

5.15 Mullins, G. (2010). "Instrumentation, Monitoring and Modeling of HVAC/Geothermal Wells", Draft Final Report to Coastal Caisson, 97 pp.

5.16 Sen, R., Mullins, G., and Sagues, A. (2011). "Remote Monitoring of Bridges", Final Report to Florida Department of Transportation, BDN23, 126 pp.

5.17 Mullins, G. (2009). "Attenuating Mass Concrete Effects in Drilled Shafts", Final Report to Florida Department of Transport, BD-544-39, 148 pp.

5.18 Sen, R. and Mullins, G. (2010). "Underwater FRP Repair of Corroding Piles Incorporating Cathodic Protection," Final Report NCHRP-IDEA 128, 28 pp.

5.19 Revie, R.W. (2006). "Uhlig's Corrosion Handbook", Second Edition, John Wiley & Sons Inc, Hoboken, NJ.

5.20 NACE (2007). "Standard Practice-Control of External Corrosion on Underground or Submerged Metallic Piping Systems", NACE SP0169-2007, NACE International, Houston TX.

5.21 US Army Corp of Engineers (2001). Cathodic Protection and Anode Selection, Public Works Technical Bulletin 420-29-37, Washington, DC, p. 8 and p.15.

5.22 Lenntech (2011). Water Treatment Solutions, http://www.lenntech.com/applications/ultrapure/conductivity/water-conductivity.htm, accessed on October 25, 2011.

5.23 Smalling, R. and Blankenstein, L. (2008). "Remote Monitoring and Computer Applications" in *Techniques for Corrosion Monitoring* (Edited by L. Yang). CRC Press LLC, Boca Raton, FL, pp. 476-498.

5.24 Nassif, H., Suksawang, N., Davis, J., Gindy, M. and Salama, T. (2010). "Monitoring of the Construction of the Doremus Avenue Bridge Structure". Final Report submitted to NJ Department of Transportation by Rutgers University, May.

5.25 Washer, G. (2010). "Long Term Remote Sensing System for Bridge Piers and Abutments". NCHRP IDEA Project 123. Draft Final Report, March.

6.1 Sen, R. and Mullins, G. (2010). "Underwater FRP Repair of Corroding Piles Incorporating Cathodic Protection," Final Report NCHRP-IDEA 128, 28 pp.

6.2 Mullins, G., Sen, R., Suh, K.S. and Winters D. (2004). "Underwater FRP Pile Wrap of the Friendship Trail Bridge." Final Report submitted to Hillsborough Country, FL, June, 32 pp.

6.3 Smith, J., and Virmani, Y. (2000). "Materials and Methods for Corrosion Control of Reinforced and Prestressed Concrete Structures in New Constuction." Final Report to Federal Highway Administration, August, 82 pp.

6.4 Khoe, C., Sen., R, and Bhethanabolta, V. (2011) "Oxygen Permeability of Fiber-Reinforced Polymers." ASCE, Journal of Composites for Construction, Vol 15, No. 4, pp. 513-521

6.5 Aguilar, J., Winters, D., Sen, R., Mullins, G. and Stokes, M. (2010). "FRP-CP System for Pile Repair in Tidal Waters." *Transportation Research Record, No. 2150,* pp. 111-118.

6.6 Morris, W., Moreno, E, and Sagues, A.(1996). "Practical Evaluation of Resistivity of Concrete in Test Cylinders Using a Wenner Array Probe", Cement and Concrete Research, Vol. 26, No. 12, pp. 1779-1787

6.7 Farwest Corrosion Control Compnay (2011). 4-pin Soil Resistance Meter, http://www.farwestcorrosion.com/fwst/instrum/nilss06.htm, accessed on October 4, 2011.

6.8 Winters, D., Mullins, G., Sen, R., Schrader, A. and Stokes, M. (2008). "Bond Enhancement for FRP Pile Repair in Tidal Waters". ASCE, *Journal of Composites for Construction*, Vol. 12, No. 3, pp. 334-343.

6.9 NACE (2007). "Standard Practice-Control of External Corrosion on Underground or Submerged Metallic Piping Systems", NACE SP0169-2007, NACE International, Houston TX.

6.10 Kranc, S. and Sagues. (1994). "Computation of Reinforcing Steel Corrosion Distribution on concrete Marine Bridge Substructures", Corrosion Vol. 50, No. 1, pp. 50-61.

Appendices

Appendix A Galvanic Anode Design

This appendix contains the calculations used to determine the number of anodes required for the field study. The design of the anode involves the following six steps:

A.1 Determination of the Steel Surface Area of Protected Pile

This was calculated from the original drawings showing the reinforcement layout and tie spacing. The piles 20 in. square piles with a 3 in. cover were reinforced by eight #8 bars. Horizontal ties consisted of ¼ in. spirals at a pitch of 9 in (Fig. A.1).

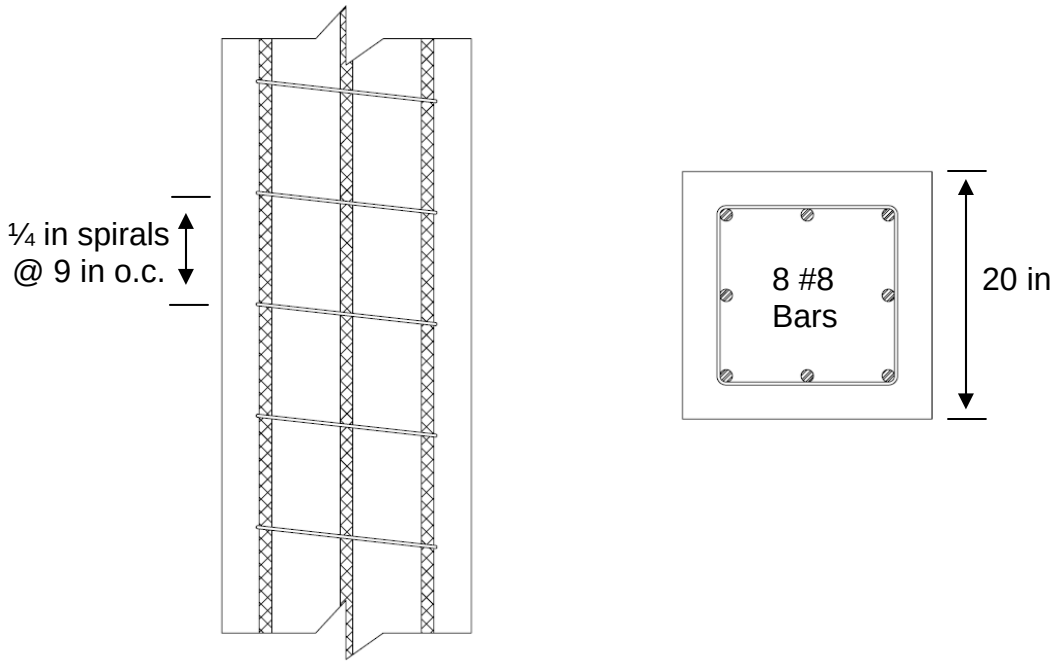

Figure A.1 Reinforcement layout.

(1) Vertical steel surface area/ft for n bars $= \pi \times d \times \ell \times n$
$= 3.14 \times 1 \times 12 \times 8$
$= 301.4 \text{ in}^2/\text{ft}$

(2) Tie steel surface area/ft $= \pi \times d \times \ell \times n$
$= 3.14 \times 0.25 \times (4 \times 14) \times 12/9$
$= 58.6 \text{ in}^2/\text{ft}$

Appendix A (Continued)

(3) Total steel surface area /ft = $301.4 + 58.6 = 360.1$ in^2/ft.

(4) Concrete surface area /ft = 20 x 12 x 4 sides = 960 in^2

(5) Steel to concrete surface area ratio = $360.1 \div 960 = 0.375$

(6) Steel surface over 5.5 ft. splash zone = 360.1 x 5.5
= 1,980.3 in^2
= 13.75 ft^2

A.2 Estimation of the Maximum Annual Average Anode Current Density

The anode design assumed a design current of **0.25 mA/ft^2**. This was lower than typical for chloride-contaminated atmospheric exposure; however, the overall corrosion rate was expected to be significantly reduced due to oxygen limitation at the cathodic sites (reinforcing steel) from the FRP system. This value was higher than the current output seen in some other galvanic jackets on similar projects.

A.3 Estimation of Anode Efficiency and Utilization

This accounted for the amount of the anode that would provide protective current following discussions with the manufacturer of the discrete system. Typical NACE recommendations for system evaluation [5.7] were incorporated. The manufacturer suggested factors were 0.9 for efficiency and 0.85 for utilization.

Appendix A (Continued)

A.4 Calculation of Required Anode Mass

The required anode mass was calculated using Faraday's law. Anode mass, $w = \frac{I \times L}{0.0424 \times E \times F}$, where w was the anode weight in pounds, I was the average current in amps, L was the duration of time in years, 0.0424 was the amp-years/lb of zinc, E was the anode efficiency, and F was the utilization factor.

Anode Current, I $= \text{Current Density} \times \text{Steel Surface}$
$= 0.25 \times 13.75 = 0.0034$ A

Zinc mass /pile $= \frac{0.0034 \times 35}{0.0424 \times 0.9 \times 0.85}$

$= 3.71$ lb

A.5 Anode Layout for Uniform Galvanic Current

The proposed scheme was developed taking into consideration:

(1) pile dimension

(2) reinforcement

(3) constructability

(4) need for symmetrical arrangement and

(5) individual anode size and

(6) hole dimension.

Zinc mass per anode $= \textit{Anode Length} \times \textit{mass / ft}$
$= 1.17 \text{ft.} \times 0.379 \text{ lbs.} = 0.46 \text{ lbs.}$

Appendix A (Continued)

$$\text{Number of anodes} = \frac{\textit{Required mass per pile}}{\textit{Mass per anode}}$$

$$= \frac{3.71}{0.46} = 8 \text{ Anodes Per Pile}$$

Each pile received eight (8) individual anodes with an approximate diameter of 1¼ in, and a length of 14 in (Fig. A.2), with a zinc mass of 0.47 lb (0.4 lb. per ft of anode). The hole concrete hole had a diameter of 2 in and a dept of 17 in.

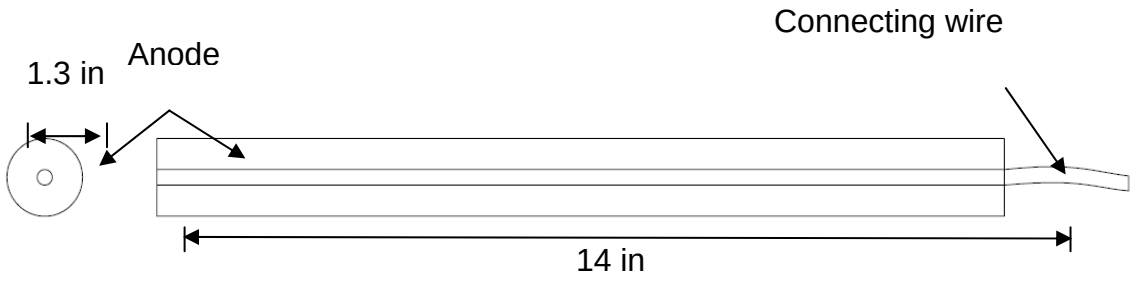

Figure A.2 Typical anode dimensions.

The anodes were placed on a 2 wide x 4 high grid pattern along one face of the pile. The vertical hole spacing was approximately 13.2" on center (Fig. A.3) and the horizontal spacing approximately 6.7" (between the vertical bars). After the holes were drilled, they were refilled using a low-resistivity grout. The embedded anodes were then inserted such that the grout encapsulated the anode without any voids.

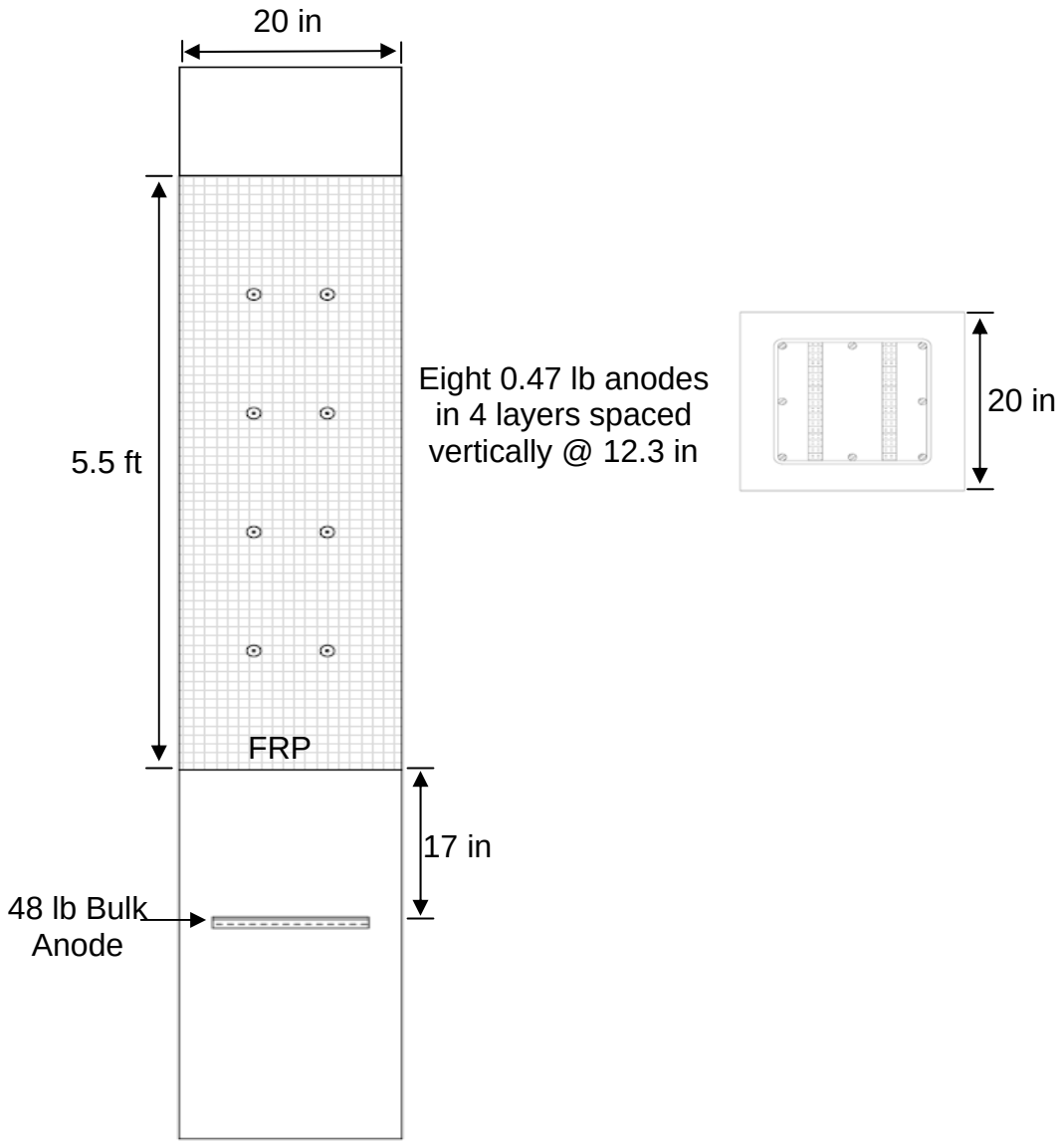

Figure A.3 Layout of anodes

A.6 Protection of Submerged Region

A bulk zinc anode weighing 48 lb was provided to cathodically protect the submerged region of two of the piles (one Fyfe and one Air Logistics) while the other two piles had the embedded anodes as the sole means of protection (one each for the Fyfe and Air Logistics FRP Systems).

Appendix B Bond Test Results

This appendix contains the tabulated tensile failure pressures of the regions tested during the laboratory bond improvement study.

Table B.1 Pile bond tensile values

Pile ID	System	Configuration	Pressure System	Position		Tensile Strength
				x (in)	y (in)	psi
A5	Urethane	Uni-Directional	Control	3	3	159
A5	Urethane	Uni-Directional	Control	6	3	129
A5	Urethane	Uni-Directional	Control	9	3	189
A5	Urethane	Uni-Directional	Control	3	6	387
A5	Urethane	Uni-Directional	Control	6	6	99
A5	Urethane	Uni-Directional	Control	9	6	119
A5	Urethane	Uni-Directional	Control	3	9	169
A5	Urethane	Uni-Directional	Control	6	9	129
A5	Urethane	Uni-Directional	Control	9	9	248
A5	Urethane	Uni-Directional	Control	3	12	119
A5	Urethane	Uni-Directional	Control	6	12	119
A5	Urethane	Uni-Directional	Control	9	12	89
A5	Urethane	Uni-Directional	Control	3	15	179
A5	Urethane	Uni-Directional	Control	6	15	129
A5	Urethane	Uni-Directional	Control	9	15	50
A5	Urethane	Uni-Directional	Control	3	18	159
A5	Urethane	Uni-Directional	Control	6	18	40
A5	Urethane	Uni-Directional	Control	9	18	79
A5	Urethane	Uni-Directional	Control	3	21	40
A5	Urethane	Uni-Directional	Control	6	21	69
A5	Urethane	Uni-Directional	Control	9	21	60
A5	Urethane	Uni-Directional	Control	3	24	37
A5	Urethane	Uni-Directional	Control	6	24	129
A5	Urethane	Uni-Directional	Control	9	24	50
A5	Urethane	Uni-Directional	Control	3	27	40
A5	Urethane	Uni-Directional	Control	6	27	40
A5	Urethane	Uni-Directional	Control	9	27	258
A5	Urethane	Uni-Directional	Control	3	30	40
A5	Urethane	Uni-Directional	Control	6	30	60
A5	Urethane	Uni-Directional	Control	9	30	357
A5	Urethane	Uni-Directional	Control	3	33	139
A5	Urethane	Uni-Directional	Control	6	33	69
A5	Urethane	Uni-Directional	Control	9	33	218
A5	Urethane	Uni-Directional	Control	3	36	40
A5	Urethane	Uni-Directional	Control	6	36	119
A5	Urethane	Uni-Directional	Control	9	36	327
A7	Urethane	Uni-Directional	Pressure	3	3	268
A7	Urethane	Uni-Directional	Pressure	6	3	198
A7	Urethane	Uni-Directional	Pressure	9	3	288

Appendix B (Continued)

Table B.1 (Continued)

Pile ID	System	Configuration	Pressure System	Position		Tensile Strength
				x (in)	y (in)	psi
A7	Urethane	Uni-Directional	Pressure	3	6	367
A7	Urethane	Uni-Directional	Pressure	6	6	228
A7	Urethane	Uni-Directional	Pressure	9	6	400
A7	Urethane	Uni-Directional	Pressure	3	9	407
A7	Urethane	Uni-Directional	Pressure	6	9	417
A7	Urethane	Uni-Directional	Pressure	9	9	258
A7	Urethane	Uni-Directional	Pressure	3	12	417
A7	Urethane	Uni-Directional	Pressure	6	12	268
A7	Urethane	Uni-Directional	Pressure	9	12	258
A7	Urethane	Uni-Directional	Pressure	3	15	308
A7	Urethane	Uni-Directional	Pressure	6	15	357
A7	Urethane	Uni-Directional	Pressure	9	15	407
A7	Urethane	Uni-Directional	Pressure	3	18	159
A7	Urethane	Uni-Directional	Pressure	6	18	218
A7	Urethane	Uni-Directional	Pressure	9	18	238
A7	Urethane	Uni-Directional	Pressure	3	21	169
A7	Urethane	Uni-Directional	Pressure	6	21	99
A7	Urethane	Uni-Directional	Pressure	9	21	129
A7	Urethane	Uni-Directional	Pressure	3	24	129
A7	Urethane	Uni-Directional	Pressure	6	24	30
A7	Urethane	Uni-Directional	Pressure	9	24	30
A7	Urethane	Uni-Directional	Pressure	3	27	89
A7	Urethane	Uni-Directional	Pressure	6	27	79
A7	Urethane	Uni-Directional	Pressure	9	27	50
A7	Urethane	Uni-Directional	Pressure	3	30	139
A7	Urethane	Uni-Directional	Pressure	6	30	37
A7	Urethane	Uni-Directional	Pressure	9	30	50
A7	Urethane	Uni-Directional	Pressure	3	33	109
A7	Urethane	Uni-Directional	Pressure	6	33	189
A7	Urethane	Uni-Directional	Pressure	9	33	228
A7	Urethane	Uni-Directional	Pressure	3	36	149
A7	Urethane	Uni-Directional	Pressure	6	36	238
A7	Urethane	Uni-Directional	Pressure	9	36	258
A6	Urethane	Uni-Directional	Vacuum	3	3	198
A6	Urethane	Uni-Directional	Vacuum	6	3	268
A6	Urethane	Uni-Directional	Vacuum	9	3	238
A6	Urethane	Uni-Directional	Vacuum	3	6	397
A6	Urethane	Uni-Directional	Vacuum	6	6	198
A6	Urethane	Uni-Directional	Vacuum	9	6	208
A6	Urethane	Uni-Directional	Vacuum	3	9	407
A6	Urethane	Uni-Directional	Vacuum	6	9	208
A6	Urethane	Uni-Directional	Vacuum	9	9	258
A6	Urethane	Uni-Directional	Vacuum	3	12	218

Appendix B (Continued)

Table B.1 (Continued)

Pile ID	System	Configuration	Pressure System	Position		Tensile Strength
				x (in)	y (in)	psi
A6	Urethane	Uni-Directional	Vacuum	6	12	238
A6	Urethane	Uni-Directional	Vacuum	9	12	218
A6	Urethane	Uni-Directional	Vacuum	3	15	258
A6	Urethane	Uni-Directional	Vacuum	6	15	318
A6	Urethane	Uni-Directional	Vacuum	9	15	318
A6	Urethane	Uni-Directional	Vacuum	3	18	258
A6	Urethane	Uni-Directional	Vacuum	6	18	400
A6	Urethane	Uni-Directional	Vacuum	9	18	119
A6	Urethane	Uni-Directional	Vacuum	3	21	79
A6	Urethane	Uni-Directional	Vacuum	6	21	89
A6	Urethane	Uni-Directional	Vacuum	9	21	258
A6	Urethane	Uni-Directional	Vacuum	3	24	109
A6	Urethane	Uni-Directional	Vacuum	6	24	169
A6	Urethane	Uni-Directional	Vacuum	9	24	327
A6	Urethane	Uni-Directional	Vacuum	3	27	40
A6	Urethane	Uni-Directional	Vacuum	6	27	159
A6	Urethane	Uni-Directional	Vacuum	9	27	208
A6	Urethane	Uni-Directional	Vacuum	3	30	169
A6	Urethane	Uni-Directional	Vacuum	6	30	357
A6	Urethane	Uni-Directional	Vacuum	9	30	119
A6	Urethane	Uni-Directional	Vacuum	3	33	159
A6	Urethane	Uni-Directional	Vacuum	6	33	60
A6	Urethane	Uni-Directional	Vacuum	9	33	119
A6	Urethane	Uni-Directional	Vacuum	3	36	79
A6	Urethane	Uni-Directional	Vacuum	6	36	298
A6	Urethane	Uni-Directional	Vacuum	9	36	238
A3	Urethane	Bi-Directional	Control	3	3	400
A3	Urethane	Bi-Directional	Control	6	3	159
A3	Urethane	Bi-Directional	Control	9	3	318
A3	Urethane	Bi-Directional	Control	3	6	119
A3	Urethane	Bi-Directional	Control	6	6	208
A3	Urethane	Bi-Directional	Control	9	6	318
A3	Urethane	Bi-Directional	Control	3	9	218
A3	Urethane	Bi-Directional	Control	6	9	218
A3	Urethane	Bi-Directional	Control	9	9	407
A3	Urethane	Bi-Directional	Control	3	12	268
A3	Urethane	Bi-Directional	Control	6	12	50
A3	Urethane	Bi-Directional	Control	9	12	407
A3	Urethane	Bi-Directional	Control	3	15	129
A3	Urethane	Bi-Directional	Control	6	15	99
A3	Urethane	Bi-Directional	Control	9	15	298
A3	Urethane	Bi-Directional	Control	3	18	169
A3	Urethane	Bi-Directional	Control	6	18	79

Appendix B (Continued)

Table B.1 (Continued)

Pile ID	System	Configuration	Pressure System	Position		Tensile Strength
				x (in)	y (in)	psi
A3	Urethane	Bi-Directional	Control	9	18	79
A3	Urethane	Bi-Directional	Control	3	21	69
A3	Urethane	Bi-Directional	Control	6	21	69
A3	Urethane	Bi-Directional	Control	9	21	99
A3	Urethane	Bi-Directional	Control	3	24	79
A3	Urethane	Bi-Directional	Control	6	24	79
A3	Urethane	Bi-Directional	Control	9	24	99
A3	Urethane	Bi-Directional	Control	3	27	40
A3	Urethane	Bi-Directional	Control	6	27	69
A3	Urethane	Bi-Directional	Control	9	27	238
A3	Urethane	Bi-Directional	Control	3	30	60
A3	Urethane	Bi-Directional	Control	6	30	89
A3	Urethane	Bi-Directional	Control	9	30	79
A3	Urethane	Bi-Directional	Control	3	33	109
A3	Urethane	Bi-Directional	Control	6	33	60
A3	Urethane	Bi-Directional	Control	9	33	79
A3	Urethane	Bi-Directional	Control	3	36	-
A3	Urethane	Bi-Directional	Control	6	36	-
A3	Urethane	Bi-Directional	Control	9	36	-
A8	Urethane	Bi-Directional	Pressure	3	3	218
A8	Urethane	Bi-Directional	Pressure	6	3	377
A8	Urethane	Bi-Directional	Pressure	9	3	258
A8	Urethane	Bi-Directional	Pressure	3	6	169
A8	Urethane	Bi-Directional	Pressure	6	6	387
A8	Urethane	Bi-Directional	Pressure	9	6	248
A8	Urethane	Bi-Directional	Pressure	3	9	198
A8	Urethane	Bi-Directional	Pressure	6	9	498
A8	Urethane	Bi-Directional	Pressure	9	9	208
A8	Urethane	Bi-Directional	Pressure	3	12	238
A8	Urethane	Bi-Directional	Pressure	6	12	159
A8	Urethane	Bi-Directional	Pressure	9	12	397
A8	Urethane	Bi-Directional	Pressure	3	15	278
A8	Urethane	Bi-Directional	Pressure	6	15	218
A8	Urethane	Bi-Directional	Pressure	9	15	238
A8	Urethane	Bi-Directional	Pressure	3	18	318
A8	Urethane	Bi-Directional	Pressure	6	18	228
A8	Urethane	Bi-Directional	Pressure	9	18	159
A8	Urethane	Bi-Directional	Pressure	3	21	50
A8	Urethane	Bi-Directional	Pressure	6	21	40
A8	Urethane	Bi-Directional	Pressure	9	21	198
A8	Urethane	Bi-Directional	Pressure	3	24	10
A8	Urethane	Bi-Directional	Pressure	6	24	119
A8	Urethane	Bi-Directional	Pressure	9	24	228

Appendix B (Continued)

Table B.1 (Continued)

Pile ID	System	Configuration	Pressure System	Position		Tensile Strength
				x (in)	y (in)	psi
A8	Urethane	Bi-Directional	Pressure	3	27	40
A8	Urethane	Bi-Directional	Pressure	6	27	40
A8	Urethane	Bi-Directional	Pressure	9	27	229
A8	Urethane	Bi-Directional	Pressure	3	30	20
A8	Urethane	Bi-Directional	Pressure	6	30	159
A8	Urethane	Bi-Directional	Pressure	9	30	99
A8	Urethane	Bi-Directional	Pressure	3	33	60
A8	Urethane	Bi-Directional	Pressure	6	33	119
A8	Urethane	Bi-Directional	Pressure	9	33	198
A8	Urethane	Bi-Directional	Pressure	3	36	40
A8	Urethane	Bi-Directional	Pressure	6	36	79
A8	Urethane	Bi-Directional	Pressure	9	36	337
A4	Urethane	Bi-Directional	Vacuum	3	3	268
A4	Urethane	Bi-Directional	Vacuum	6	3	238
A4	Urethane	Bi-Directional	Vacuum	9	3	258
A4	Urethane	Bi-Directional	Vacuum	3	6	400
A4	Urethane	Bi-Directional	Vacuum	6	6	228
A4	Urethane	Bi-Directional	Vacuum	9	6	180
A4	Urethane	Bi-Directional	Vacuum	3	9	407
A4	Urethane	Bi-Directional	Vacuum	6	9	400
A4	Urethane	Bi-Directional	Vacuum	9	9	228
A4	Urethane	Bi-Directional	Vacuum	3	12	342
A4	Urethane	Bi-Directional	Vacuum	6	12	337
A4	Urethane	Bi-Directional	Vacuum	9	12	228
A4	Urethane	Bi-Directional	Vacuum	3	15	179
A4	Urethane	Bi-Directional	Vacuum	6	15	159
A4	Urethane	Bi-Directional	Vacuum	9	15	248
A4	Urethane	Bi-Directional	Vacuum	3	18	228
A4	Urethane	Bi-Directional	Vacuum	6	18	258
A4	Urethane	Bi-Directional	Vacuum	9	18	159
A4	Urethane	Bi-Directional	Vacuum	3	21	89
A4	Urethane	Bi-Directional	Vacuum	6	21	119
A4	Urethane	Bi-Directional	Vacuum	9	21	119
A4	Urethane	Bi-Directional	Vacuum	3	24	69
A4	Urethane	Bi-Directional	Vacuum	6	24	100
A4	Urethane	Bi-Directional	Vacuum	9	24	119
A4	Urethane	Bi-Directional	Vacuum	3	27	69
A4	Urethane	Bi-Directional	Vacuum	6	27	218
A4	Urethane	Bi-Directional	Vacuum	9	27	49
A4	Urethane	Bi-Directional	Vacuum	3	30	40
A4	Urethane	Bi-Directional	Vacuum	6	30	397
A4	Urethane	Bi-Directional	Vacuum	9	30	337
A4	Urethane	Bi-Directional	Vacuum	3	33	139

Appendix B (Continued)

Table B.1 (Continued)

Pile ID	System	Configuration	Pressure System	Position		Tensile Strength
				x (in)	y (in)	psi
A4	Urethane	Bi-Directional	Vacuum	6	33	218
A4	Urethane	Bi-Directional	Vacuum	9	33	357
A4	Urethane	Bi-Directional	Vacuum	3	36	119
A4	Urethane	Bi-Directional	Vacuum	6	36	198
A4	Urethane	Bi-Directional	Vacuum	9	36	248
F8	Epoxy	Uni-Directional	Control	3	3	159
F8	Epoxy	Uni-Directional	Control	6	3	109
F8	Epoxy	Uni-Directional	Control	9	3	139
F8	Epoxy	Uni-Directional	Control	3	6	79
F8	Epoxy	Uni-Directional	Control	6	6	119
F8	Epoxy	Uni-Directional	Control	9	6	119
F8	Epoxy	Uni-Directional	Control	3	9	159
F8	Epoxy	Uni-Directional	Control	6	9	30
F8	Epoxy	Uni-Directional	Control	9	9	129
F8	Epoxy	Uni-Directional	Control	3	12	69
F8	Epoxy	Uni-Directional	Control	6	12	40
F8	Epoxy	Uni-Directional	Control	9	12	89
F8	Epoxy	Uni-Directional	Control	3	15	19
F8	Epoxy	Uni-Directional	Control	6	15	50
F8	Epoxy	Uni-Directional	Control	9	15	40
F8	Epoxy	Uni-Directional	Control	3	18	99
F8	Epoxy	Uni-Directional	Control	6	18	79
F8	Epoxy	Uni-Directional	Control	9	18	60
F8	Epoxy	Uni-Directional	Control	3	21	0
F8	Epoxy	Uni-Directional	Control	6	21	89
F8	Epoxy	Uni-Directional	Control	9	21	89
F8	Epoxy	Uni-Directional	Control	3	24	40
F8	Epoxy	Uni-Directional	Control	6	24	40
F8	Epoxy	Uni-Directional	Control	9	24	0
F8	Epoxy	Uni-Directional	Control	3	27	69
F8	Epoxy	Uni-Directional	Control	6	27	0
F8	Epoxy	Uni-Directional	Control	9	27	40
F8	Epoxy	Uni-Directional	Control	3	30	40
F8	Epoxy	Uni-Directional	Control	6	30	0
F8	Epoxy	Uni-Directional	Control	9	30	50
F8	Epoxy	Uni-Directional	Control	3	33	40
F8	Epoxy	Uni-Directional	Control	6	33	0
F8	Epoxy	Uni-Directional	Control	9	33	30
F8	Epoxy	Uni-Directional	Control	3	36	30
F8	Epoxy	Uni-Directional	Control	6	36	69
F8	Epoxy	Uni-Directional	Control	9	36	60
F3	Epoxy	Uni-Directional	Pressure	3	3	149
F3	Epoxy	Uni-Directional	Pressure	6	3	238

Appendix B (Continued)

Table B.1 (Continued)

Pile ID	System	Configuration	Pressure System	Position		Tensile Strength
				x (in)	y (in)	psi
F3	Epoxy	Uni-Directional	Pressure	9	3	397
F3	Epoxy	Uni-Directional	Pressure	3	6	337
F3	Epoxy	Uni-Directional	Pressure	6	6	238
F3	Epoxy	Uni-Directional	Pressure	9	6	367
F3	Epoxy	Uni-Directional	Pressure	3	9	258
F3	Epoxy	Uni-Directional	Pressure	6	9	397
F3	Epoxy	Uni-Directional	Pressure	9	9	198
F3	Epoxy	Uni-Directional	Pressure	3	12	337
F3	Epoxy	Uni-Directional	Pressure	6	12	397
F3	Epoxy	Uni-Directional	Pressure	9	12	258
F3	Epoxy	Uni-Directional	Pressure	3	15	129
F3	Epoxy	Uni-Directional	Pressure	6	15	198
F3	Epoxy	Uni-Directional	Pressure	9	15	189
F3	Epoxy	Uni-Directional	Pressure	3	18	397
F3	Epoxy	Uni-Directional	Pressure	6	18	119
F3	Epoxy	Uni-Directional	Pressure	9	18	357
F3	Epoxy	Uni-Directional	Pressure	3	21	248
F3	Epoxy	Uni-Directional	Pressure	6	21	179
F3	Epoxy	Uni-Directional	Pressure	9	21	218
F3	Epoxy	Uni-Directional	Pressure	3	24	208
F3	Epoxy	Uni-Directional	Pressure	6	24	159
F3	Epoxy	Uni-Directional	Pressure	9	24	218
F3	Epoxy	Uni-Directional	Pressure	3	27	298
F3	Epoxy	Uni-Directional	Pressure	6	27	278
F3	Epoxy	Uni-Directional	Pressure	9	27	318
F3	Epoxy	Uni-Directional	Pressure	3	30	181
F3	Epoxy	Uni-Directional	Pressure	6	30	308
F3	Epoxy	Uni-Directional	Pressure	9	30	238
F3	Epoxy	Uni-Directional	Pressure	3	33	218
F3	Epoxy	Uni-Directional	Pressure	6	33	298
F3	Epoxy	Uni-Directional	Pressure	9	33	238
F3	Epoxy	Uni-Directional	Pressure	3	36	318
F3	Epoxy	Uni-Directional	Pressure	6	36	198
F3	Epoxy	Uni-Directional	Pressure	9	36	298
F6	Epoxy	Uni-Directional	Vacuum	3	3	278
F6	Epoxy	Uni-Directional	Vacuum	6	3	258
F6	Epoxy	Uni-Directional	Vacuum	9	3	337
F6	Epoxy	Uni-Directional	Vacuum	3	6	149
F6	Epoxy	Uni-Directional	Vacuum	6	6	357
F6	Epoxy	Uni-Directional	Vacuum	9	6	179
F6	Epoxy	Uni-Directional	Vacuum	3	9	337
F6	Epoxy	Uni-Directional	Vacuum	6	9	258
F6	Epoxy	Uni-Directional	Vacuum	9	9	60

Appendix B (Continued)

Table B.1 (Continued)

Pile ID	System	Configuration	Pressure System	Position		Tensile Strength
				x (in)	y (in)	psi
F6	Epoxy	Uni-Directional	Vacuum	3	12	149
F6	Epoxy	Uni-Directional	Vacuum	6	12	400
F6	Epoxy	Uni-Directional	Vacuum	9	12	238
F6	Epoxy	Uni-Directional	Vacuum	3	15	208
F6	Epoxy	Uni-Directional	Vacuum	6	15	40
F6	Epoxy	Uni-Directional	Vacuum	9	15	397
F6	Epoxy	Uni-Directional	Vacuum	3	18	156
F6	Epoxy	Uni-Directional	Vacuum	6	18	179
F6	Epoxy	Uni-Directional	Vacuum	9	18	198
F6	Epoxy	Uni-Directional	Vacuum	3	21	99
F6	Epoxy	Uni-Directional	Vacuum	6	21	79
F6	Epoxy	Uni-Directional	Vacuum	9	21	158
F6	Epoxy	Uni-Directional	Vacuum	3	24	40
F6	Epoxy	Uni-Directional	Vacuum	6	24	50
F6	Epoxy	Uni-Directional	Vacuum	9	24	119
F6	Epoxy	Uni-Directional	Vacuum	3	27	69
F6	Epoxy	Uni-Directional	Vacuum	6	27	30
F6	Epoxy	Uni-Directional	Vacuum	9	27	139
F6	Epoxy	Uni-Directional	Vacuum	3	30	109
F6	Epoxy	Uni-Directional	Vacuum	6	30	60
F6	Epoxy	Uni-Directional	Vacuum	9	30	119
F6	Epoxy	Uni-Directional	Vacuum	3	33	119
F6	Epoxy	Uni-Directional	Vacuum	6	33	89
F6	Epoxy	Uni-Directional	Vacuum	9	33	119
F6	Epoxy	Uni-Directional	Vacuum	3	36	99
F6	Epoxy	Uni-Directional	Vacuum	6	36	129
F6	Epoxy	Uni-Directional	Vacuum	9	36	129
F5	Epoxy	Bi-Directional	Control	3	3	387
F5	Epoxy	Bi-Directional	Control	6	3	129
F5	Epoxy	Bi-Directional	Control	9	3	327
F5	Epoxy	Bi-Directional	Control	3	6	318
F5	Epoxy	Bi-Directional	Control	6	6	119
F5	Epoxy	Bi-Directional	Control	9	6	218
F5	Epoxy	Bi-Directional	Control	3	9	179
F5	Epoxy	Bi-Directional	Control	6	9	169
F5	Epoxy	Bi-Directional	Control	9	9	248
F5	Epoxy	Bi-Directional	Control	3	12	179
F5	Epoxy	Bi-Directional	Control	6	12	228
F5	Epoxy	Bi-Directional	Control	9	12	119
F5	Epoxy	Bi-Directional	Control	3	15	79
F5	Epoxy	Bi-Directional	Control	6	15	119
F5	Epoxy	Bi-Directional	Control	9	15	228
F5	Epoxy	Bi-Directional	Control	3	18	238

Appendix B (Continued)

Table B.1 (Continued)

Pile ID	System	Configuration	Pressure System	Position		Tensile Strength
				x (in)	y (in)	psi
F5	Epoxy	Bi-Directional	Control	6	18	0
F5	Epoxy	Bi-Directional	Control	9	18	50
F5	Epoxy	Bi-Directional	Control	3	21	298
F5	Epoxy	Bi-Directional	Control	6	21	60
F5	Epoxy	Bi-Directional	Control	9	21	119
F5	Epoxy	Bi-Directional	Control	3	24	169
F5	Epoxy	Bi-Directional	Control	6	24	99
F5	Epoxy	Bi-Directional	Control	9	24	179
F5	Epoxy	Bi-Directional	Control	3	27	268
F5	Epoxy	Bi-Directional	Control	6	27	139
F5	Epoxy	Bi-Directional	Control	9	27	298
F5	Epoxy	Bi-Directional	Control	3	30	238
F5	Epoxy	Bi-Directional	Control	6	30	218
F5	Epoxy	Bi-Directional	Control	9	30	129
F5	Epoxy	Bi-Directional	Control	3	33	248
F5	Epoxy	Bi-Directional	Control	6	33	0
F5	Epoxy	Bi-Directional	Control	9	33	149
F5	Epoxy	Bi-Directional	Control	3	36	-
F5	Epoxy	Bi-Directional	Control	6	36	-
F5	Epoxy	Bi-Directional	Control	9	36	-
F1	Epoxy	Bi-Directional	Pressure	3	3	298
F1	Epoxy	Bi-Directional	Pressure	6	3	268
F1	Epoxy	Bi-Directional	Pressure	9	3	318
F1	Epoxy	Bi-Directional	Pressure	3	6	278
F1	Epoxy	Bi-Directional	Pressure	6	6	238
F1	Epoxy	Bi-Directional	Pressure	9	6	337
F1	Epoxy	Bi-Directional	Pressure	3	9	298
F1	Epoxy	Bi-Directional	Pressure	6	9	288
F1	Epoxy	Bi-Directional	Pressure	9	9	208
F1	Epoxy	Bi-Directional	Pressure	3	12	228
F1	Epoxy	Bi-Directional	Pressure	6	12	169
F1	Epoxy	Bi-Directional	Pressure	9	12	119
F1	Epoxy	Bi-Directional	Pressure	3	15	367
F1	Epoxy	Bi-Directional	Pressure	6	15	367
F1	Epoxy	Bi-Directional	Pressure	9	15	327
F1	Epoxy	Bi-Directional	Pressure	3	18	179
F1	Epoxy	Bi-Directional	Pressure	6	18	228
F1	Epoxy	Bi-Directional	Pressure	9	18	228
F1	Epoxy	Bi-Directional	Pressure	3	21	397
F1	Epoxy	Bi-Directional	Pressure	6	21	129
F1	Epoxy	Bi-Directional	Pressure	9	21	377
F1	Epoxy	Bi-Directional	Pressure	3	24	149
F1	Epoxy	Bi-Directional	Pressure	6	24	119

Appendix B (Continued)

Table B.1 (Continued)

Pile ID	System	Configuration	Pressure System	Position		Tensile Strength
				x (in)	y (in)	psi
F1	Epoxy	Bi-Directional	Pressure	9	24	397
F1	Epoxy	Bi-Directional	Pressure	3	27	169
F1	Epoxy	Bi-Directional	Pressure	6	27	238
F1	Epoxy	Bi-Directional	Pressure	9	27	278
F1	Epoxy	Bi-Directional	Pressure	3	30	149
F1	Epoxy	Bi-Directional	Pressure	6	30	298
F1	Epoxy	Bi-Directional	Pressure	9	30	228
F1	Epoxy	Bi-Directional	Pressure	3	33	159
F1	Epoxy	Bi-Directional	Pressure	6	33	99
F1	Epoxy	Bi-Directional	Pressure	9	33	238
F1	Epoxy	Bi-Directional	Pressure	3	36	158
F1	Epoxy	Bi-Directional	Pressure	6	36	189
F1	Epoxy	Bi-Directional	Pressure	9	36	327
F4	Epoxy	Bi-Directional	Vacuum	3	3	238
F4	Epoxy	Bi-Directional	Vacuum	6	3	238
F4	Epoxy	Bi-Directional	Vacuum	9	3	278
F4	Epoxy	Bi-Directional	Vacuum	3	6	169
F4	Epoxy	Bi-Directional	Vacuum	6	6	357
F4	Epoxy	Bi-Directional	Vacuum	9	6	258
F4	Epoxy	Bi-Directional	Vacuum	3	9	119
F4	Epoxy	Bi-Directional	Vacuum	6	9	298
F4	Epoxy	Bi-Directional	Vacuum	9	9	258
F4	Epoxy	Bi-Directional	Vacuum	3	12	238
F4	Epoxy	Bi-Directional	Vacuum	6	12	400
F4	Epoxy	Bi-Directional	Vacuum	9	12	129
F4	Epoxy	Bi-Directional	Vacuum	3	15	400
F4	Epoxy	Bi-Directional	Vacuum	6	15	149
F4	Epoxy	Bi-Directional	Vacuum	9	15	208
F4	Epoxy	Bi-Directional	Vacuum	3	18	208
F4	Epoxy	Bi-Directional	Vacuum	6	18	228
F4	Epoxy	Bi-Directional	Vacuum	9	18	149
F4	Epoxy	Bi-Directional	Vacuum	3	21	119
F4	Epoxy	Bi-Directional	Vacuum	6	21	109
F4	Epoxy	Bi-Directional	Vacuum	9	21	0
F4	Epoxy	Bi-Directional	Vacuum	3	24	119
F4	Epoxy	Bi-Directional	Vacuum	6	24	60
F4	Epoxy	Bi-Directional	Vacuum	9	24	109
F4	Epoxy	Bi-Directional	Vacuum	3	27	60
F4	Epoxy	Bi-Directional	Vacuum	6	27	69
F4	Epoxy	Bi-Directional	Vacuum	9	27	189
F4	Epoxy	Bi-Directional	Vacuum	3	30	109
F4	Epoxy	Bi-Directional	Vacuum	6	30	79
F4	Epoxy	Bi-Directional	Vacuum	9	30	119

Appendix B (Continued)

Table B.1 (Continued)

Pile ID	System	Configuration	Pressure System	Position		Tensile Strength
				x (in)	y (in)	psi
F4	Epoxy	Bi-Directional	Vacuum	3	33	40
F4	Epoxy	Bi-Directional	Vacuum	6	33	109
F4	Epoxy	Bi-Directional	Vacuum	9	33	99
F4	Epoxy	Bi-Directional	Vacuum	3	36	-
F4	Epoxy	Bi-Directional	Vacuum	6	36	-
F4	Epoxy	Bi-Directional	Vacuum	9	36	-

Appendix C Pile Half Cell Potentials

This appendix contains the tabulated values obtained from the half cell potential measurements performed on piers 103 and 104.

Table C.1 Pier 103 surface potential readings (mV)

	103 – NE West Surface			103 – NE South Surface			103 - NE North Surface			103 - NE East Surface		
0.5ft	-226	-248	-165	-113	-156	-132	-207	-214	-241	-199	-201	-203
1.0ft	-130	-122	-111	-174	-157	-133	-234	-232	-240	-211	-215	-211
1.5ft	-133	-115	-113	-182	-155	-165	-250	-255	-255	-228	-228	-222
2.0ft	-147	-140	-135	-187	-204	-194	-270	-284	-312	-270	-268	-258
2.5ft	-212	-192	-200	-255	-258	-254	-389	-357	-368	-318	-312	-334
3.0ft	-234	-247	-268	-335	-339	-352	-413	-406	-405	-431	-408	-408
3.5ft	-286	-293	-415	-427	-418	-419	-472	-453	-458	-476	-462	-455
4.0ft	-440	-449	-488	-488	-442	-440	-502	-498	-513	-525	-507	-509
4.5ft	-515	-500	-502	-478	-456	-467	-564	-565	-575	-580	-570	-566
	103 – NI West Surface			**103 – NI South Surface**			**103 - NI North Surface**			**103 - NI East Surface**		
0.5ft	-206	-210	-210	-170	-170	-177	-176	-171	-173	-309	-320	-307
1.0ft	-213	-214	-213	-179	-180	-194	-190	-178	-181	-331	-354	-319
1.5ft	-228	-233	-232	-215	-205	-219	-210	-211	-219	-337	-340	-326
2.0ft	-258	-239	-239	-284	-242	-268	-254	-258	-256	-380	-354	-364
2.5ft	-297	-299	-312	-331	-332	-350	-313	-304	-303	-412	-405	-430
3.0ft	-371	-370	-367	-391	-392	-420	-394	-378	-388	-465	-468	-492
3.5ft	-418	-434	-435	-435	-454	-472	-441	-423	-422	-514	-505	-520
4.0ft	-464	-474	-460	-502	-501	-514	-472	-470	-470	-556	-561	-565
4.5ft	-541	-539	-540	-552	-540	-533	-504	-507	-511	-598	-599	-615
	103 – SI West Surface			**103 – SI South Surface**			**103 – SI North Surface**			**103 – SI East Surface**		
0.5ft	-198	-222	-202	-190	-185	-183	-200	-200	-197	-155	-169	-176
1.0ft	-214	-217	-210	-210	-215	-201	-197	-200	-201	-180	-182	-185
1.5ft	-222	-222	-224	-280	-268	-205	-201	-203	-206	-196	-191	-191
2.0ft	-240	-242	-241	-319	-321	-272	-236	-225	-239	-221	-217	-210
2.5ft	-256	-258	-257	-335	-339	-340	-287	-262	-277	-230	-255	-249
3.0ft	-309	-315	-315	-360	-379	-358	-339	-378	-376	-284	-281	-283
3.5ft	-371	-385	-372	-399	-402	-401	-425	-412	-414	-331	-355	-379
4.0ft	-453	-443	-446	-444	-444	-465	-482	-471	-528	-483	-523	-535
4.5ft	-514	-214	-497	-536	-534	-524	-561	-552	-545	-494	-512	-534
	103 - SE West Surface			**103 – SE South Surface**			**103 - SE North Surface**			**103 - SE East Surface**		
0.5ft	-180	-224	-145	-151	-148	-150	-149	-136	-168	-200	-209	-218
1.0ft	-169	-173	-163	-157	-152	-147	-165	-159	-167	-203	-196	-222
1.5ft	-187	-184	-173	-163	-161	-155	-184	-181	-184	-194	-228	-236
2.0ft	-204	-192	-193	-191	-185	-181	-239	-221	-239	-244	-231	-277
2.5ft	-266	-238	-221	-219	-220	-236	-290	-291	-292	-283	-270	-280
3.0ft	-289	-268	-284	-271	-282	-284	-312	-338	-326	-344	-321	-311
3.5ft	-335	-312	-338	-334	-344	-336	-360	-361	-359	-371	-368	-374
4.0ft	-393	-375	-389	-317	-323	-324	-406	-399	-404	-431	-436	-455
4.5ft	-413	-404	-409	-358	-371	-369	-443	-444	-439	-511	-508	-543

Appendix C (Continued)

Table C.2 Pier 104 surface potential readings (mV)

	104 – NE West Surface			104 – NE South Surface			104 - NE North Surface			104 - NE East Surface		
0.5ft	-285	-295	-287	-296	-340	-402	-290	-296	-286	-419	-397	-318
1.0ft	-309	-311	-334	-398	-408	-449	-332	-321	-303	-459	-416	-350
1.5ft	-325	-329	-343	-419	-455	-452	-361	-350	-331	-457	-445	-366
2.0ft	-382	-393	-382	-451	-462	-546	-462	-436	-401	-453	-451	-387
2.5ft	-430	-445	-435	-518	-544	-582	-513	-507	-504	-530	-511	-471
3.0ft	-500	-517	-533	-542	-554	-561	-560	-553	-546	-544	-508	-469
3.5ft	-529	-538	-548	-550	-555	-560	-582	-584	-575	-537	-535	-528
4.0ft	-	-	-	-574	-570	-584	-	-	-	-	-	-
4.5ft	-	-	-	-	-	-	-	-	-	-	-	-

	104 – NI West Surface			104 – NI South Surface			104 - NI North Surface			104 - NI East Surface		
0.5ft	-239	-238	-235	-225	-207	-217	-242	-235	-238	-288	-278	-278
1.0ft	-243	-249	-271	-269	-235	-233	-245	-233	-244	-319	-311	-322
1.5ft	-295	-292	-307	-309	-285	-283	-266	-253	-272	-321	-321	-304
2.0ft	-399	-396	-392	-355	-368	-354	-304	-314	-332	-433	-440	-438
2.5ft	-467	-464	-474	-481	-480	-481	-403	-415	-442	-522	-524	-523
3.0ft	-497	-500	-516	-544	-542	-544	-480	-473	-491	-546	-533	-534
3.5ft	-522	-532	-547	-576	-576	-577	-535	-528	-527	-602	-593	-565
4.0ft	-591	-599	-603	-607	-596	-600	-574	-567	-564	-	-	-
4.5ft	-	-	-	-	-	-	-	-	-	-	-	-

	104 – SI West Surface			104 – SI South Surface			104 - SI North Surface			104 - SI East Surface		
0.5ft	-280	-282	-255	-264	-250	-247	-247	-250	-261	-288	-286	-291
1.0ft	-251	-264	-249	-259	-256	-263	-250	-245	-259	-287	-287	-301
1.5ft	-300	-286	-300	-310	-295	-304	-286	-275	-300	-308	-311	-329
2.0ft	-354	-342	-366	-369	-364	-359	-326	-313	-352	-370	-356	-355
2.5ft	-465	-481	-482	-490	-470	-491	-359	-405	-396	-477	-479	-478
3.0ft	-553	-550	-547	-569	-562	-557	-495	-485	-484	-555	-558	-561
3.5ft	-572	-576	-580	-615	-609	-611	-551	-546	-550	-606	-605	-616
4.0ft	-624	-617	-610	-	-	-	-584	-582	-589	-	-	-
4.5ft	-	-	-	-	-	-	-	-	-	-	-	-

	104 – NE West Surface			104 – NE South Surface			104 - NE North Surface			104 - NE East Surface		
0.5ft	-472	-325	-305	-306	-296	-293	-402	-425	-462	-320	-381	-447
1.0ft	-476	-421	-322	-320	-321	-323	-471	-487	-514	-348	-407	-449
1.5ft	-512	-466	-362	-367	-380	-388	-485	-512	-532	-401	-437	-471
2.0ft	-518	-474	-420	-424	-417	-445	-544	-537	-552	-422	-436	-488
2.5ft	-544	-532	-511	-506	-476	-492	-574	-577	-579	-461	-471	-490
3.0ft	-589	-572	-544	-555	-539	-544	-601	-603	-610	-524	-532	-560
3.5ft	-613	-595	-534	-604	-596	-586	-609	-611	-629	-574	-570	-582
4.0ft	-	-	-	-	-	-	-	-	-	-	-	-
4.5ft	-	-	-	-	-	-	-	-	-	-	-	-

Appendix D Self Consumption Test Results

This appendix contains the tabulated values for the self consumption assessment study discussed in Chapter 5.

Table D.1 Self consumption rate for resistivity <1000 Ω-cm.

Br #	Specimen Identifier		Weight (Before)	Weight (After)	Mass Lost	Time Sub-merged	Consumption Rate
	Month	ID	grams	grams	grams	days	g/yr
1	I	1	1311.63	1309.61	2.02	38	19
	I	2	1274.47	1272.37	2.09	38	20
	II	1	1207.91	1203.80	4.11	104	14
	II	2	1165.76	1160.90	4.86	104	17
	III	1	1208.61	1202.60	6.01	128	17
	III	2	1188.07	1181.27	6.80	128	19
2	I	1	1750.85	1746.72	4.13	38	40
	I	2	1412.29	1408.42	3.87	38	37
	II	1	1459.28	1451.30	7.98	104	28
	II	2	1455.18	1447.80	7.38	104	26
	III	1	1347.37	Could not be recovered			
	III	2	1339.29				

*Note: Values shown are in metric for use in the formula for lifetime predictions.

Table D.2 Projected time for complete anode consumption for Bridge 1.

Resistance (Ω)	Anodic Current (mA)	Self Consumption (mA)	Time (years)
0.1	96	17.3	24
1	62	17.3	35
3	49	17.3	42
5	42	17.3	46
150	5.1*	17.3	123

*Note: this current is insufficient to adequately protect the piles; anodic current must be at least 40 mA to provide a minimum current density of 2mA/ft^2 per the criterion adopted here.

Table D.3 Projected time for complete anode consumption for Bridge 2.

Resistance (Ω)	Anodic Current (mA)	Self Consumption (mA)	Time (years)
0.1	132	30.2	17
1	72	30.2	27
3	60	30.2	30
5	53	30.2	33
150	4.7*	30.2	79

*See Note for Table D.2

Appendix D (Continued)

Table D.4 Projected time for complete anode consumption using a 0.5 efficiency factor.

	Bridge 1		Bridge 1	
Resistance (Ω)	Anodic Current (mA)	Time (years)	Anodic Current (mA)	Time (years)
0.1	96	14	132	10
1	62	22	72	19
3	49	28	60	23
5	42	33	53	26
150	5.1*	269	4.7*	292

*See Note for Table D.2

Table D.5 Expected anode lifetime using a 0.8 utilization factor.

Resistance (Ω)	Time (years)	
	Bridge 1	Bridge 2
0.1	19	14
1	28	21
3	33	24
5	37	26
150*	98*	63*

*See note on previous tables on applicability of this condition

Appendix E Anode Lifetime Calculations

E.1 General Properties

(1) Field Anode Weight = 24 lbs (10886 g)

(2) Magnesium Atomic Weight = 24.305 grams per mole

(3) Magnesium Density = 1.74 grams per cm^3

(4) n = 2 - number of electrons in the oxidation reaction assume formation of Mg^{+2})

(5) F = $9.65x10^4$ Coulombs per equiv. (Faraday's Constant)

E.2 Anode Dimensions

E.2.1 Field Specimens

(1) Length = 18 in (45.72 cm)

(2) Width = 9 in (22.86 cm)

(3) Thickness = 2.5 in (6.35 cm)

(4) Surface Area = 459 in^2 (2961 cm^2)

E.2.2 Coupon Specimens

(1) External Diameter = 8 in (20.32 cm)

(2) Internal Diameter = 1 in (2.54 cm)

(3) Average Thickness = 0.83 in (2.12 cm)

(4) Average Surface Area = 120 in^2 (773.5 cm^2)

Appendix E (Continued)

E.3 Projection for Bridge 1 for 3 Ω resistance (Using Field Self Consumption Data)

E.3.1 Self Consumption Rate

Specimen consumption rate: 17.91 grams per year

E.3.1.1 Convert to cm/year

(1) Divide consumption rate by the surface area of the specimen

$17.91\ g/yr \div 773.5\ cm^2 = 0.0231\ g/cm^2\ yr$

(2) Divide the rate in grams / cm^2 year by the density of magnesium

$0.0231\ g/cm^2yr \div 1.74\ g/cm^3 = 0.0133\ cm/yr$

E.3.1.2 Determine Consumption Rate for 24 lb Anode

(1) Multiply consumption rate in cm/year by the surface area of the 24 lb anode

$0.0133\ cm/yr \times 2961\ cm^2 = 39.38\ cm^3/yr$

(2) Multiply the rate in cm^3/year by the density of magnesium

$39.38\ cm^3/yr \times 1.74\ g/cm^3 = 68.52\ g/yr = 2.173 \times 10^{-6}\ g/sec$

Appendix E (Continued)

E3.2 Self Consumption Current

E3.2.1 Equivalent Anodic Current

Using the Faraday relationship (W = ItM/nF), determine an anodic current equivalent to the rate of self consumption. The modified formula will be (I = WnF/Mt), where W = weight loss per second, and t = 1 second.

$I = (2.173 \times 10^{-6} \times 2 \times 96500) / (24.305 \times 1) = 0.0173$ A (17.3 mA)

E3.2.2 Projection for Useful Anode Lifetime

(1) 3 Ω anodic current = 0.0490 A (49 mA)

(2) Add calculated Self consumption current to current for 3 Ω resistor

0.0490 A + 0.0173 A = 0.0663 A

Using the Faraday relationship (W = ItM/nF), determine the projected complete consumption time of the anodes. The modified formula is t = WnF/IM, $t = (10886 \text{ g} \times 2 \times 9.65\ 10^{4}) / (0.0663 \text{ A} \times 24.305 \text{ g}) = 1.31 \times 10^{9}$ sec = 41.3 yrs. Multiply calculated time by utilization factor of 0.8, Useful Lifetime = 41.3 yrs x 0.8 = 33 yrs. Expected anode lifetime using field self-consumption data for 3 Ω resistor on Bridge 1 = 33 yrs

Appendix E (Continued)

E.4 Projection for Bridge 1 for 3 Ω resistance (Using 0.5 Efficiency Factor)

3 Ω anodic current = 0.049 A (49 mA). Using the Faraday relationship and incorporating the efficiency factor (W = 0.5(ItM/nF)), determine the time for complete consumption of the anodes. The modified formula is t = 0.5 (WnF/IM)),t = 0.5 x (10886 g x 2 x 9.65 10^4) / (0.049 A x 24.305) = 8.82 x 10^8 sec = 28 yrs.Multiply calculated time by utilization factor of 0.8, Lifetime = 27 yrs x 0.8 = 22 yrs.

Time for complete consumption using 0.5 Efficiency Factor for 3 Ω resistor on Bridge 1 = 28 years. With the 0.8 utilization factor, the lifetime is 22 years.

About the Author

Julio Ivan Aguilar, the second son of David P. Aguilar Sr. and Carolice Skipton Aguilar was born in Belize on August 3, 1982. After earning an Associates Degree in Mathematics and Physics from St. John's College Junior College in Belize, he enrolled at the University of South Florida in 2002, where he joined his brother who at the time was pursuing a Ph.D. in Computer Science. Julio earned both his Bachelor's and Master's degrees from the University of South Florida, and in 2007 enrolled in the Ph.D. program. After graduation, Julio was hired by a company in Tampa, which enabled him to remain in close proximity to all of the friends that he made during his time in college.